



المملكة العربية السعودية

وزارة التعليم العالي

جامعة أم القرى

كلية العلوم التطبيقية

قسم الفيزياء

١٨٢١

الخواص الدوريمترية وبعض تطبيقات

لفلوريد الكالسيوم المشاب بالمنجنيز

رسالة مقدمة إلى قسم الفيزياء بكلية العلوم التطبيقية بجامعة أم القرى

كمطلب تكميلي لبرنامج درجة الماجستير في الفيزياء



٢٨٨١

إعداد الطالبة

فاطمة محمود جان

إشراف

د. وليد بن جميل الطف

أ.د. محمد سامي المنهراوي

الفصل الدراسي الأول

١٤٢١هـ - ٢٠٠٠م

١٠٧٢٨

بسم الله الرحمن الرحيم

في التعليم العالي  
أداء الفري  
العلوم التطبيقية

نموذج رقم ( ٨ )

إجازة أطروحة علمية في صيغتها النهائية بعد إجراء التعديلات

الاسم : صا طه محمد عبد البرهان كلية : العلوم التطبيقية قسم : الفيزياء  
درجة مقدمة قبل درجة : ماجستير العلوم في تخصص : الفيزياء  
نوع الأطروحة : المختصة التخصصية وتضمنت تطبيقات لنموذج الحاسوب لحساب باطنية

الحمد لله رب العالمين والصلاة والسلام على أشرف الأنبياء والمرسلين وعلى آله وصحبه أجمعين وبعد :

بناءً على توصية اللجنة المكلفة لمناقشة الأطروحة المذكورة أعلاه والتي تمت مناقشتها بتاريخ ١٠/٠٤/١٤٤٠هـ بقبولها بعد إجراء التعديلات المطروحة، وحيث لم يبق عمل لازم؛ فإن اللجنة توصي بإجازتها في صيغتها النهائية المرفقة للدرجة العلمية المذكورة أعلاه...

والله الموفق...

أعضاء اللجنة

المشرف

المناقش الداخلي

المناقش الخارجي

الاسم : د/ محمد سعيد بن محمد النوري الاسم : د/ نادر محمد عمار لغبري الاسم : د/ غالي بن محمد بن محمد النوري  
التوقيع : شاهين التوقيع : [موقع] التوقيع : [موقع]  
يتمتع

رئيس قسم

الاسم : د/ وليد عبد الحليم الطيف  
التوقيع : [موقع] ١٤٤٠/٠١/٢٥

يوضع هذا النموذج أمام الصفحة المقابلة لصفحة عنوان الأطروحة في كل نسخة من الرسالة.

## شكر وتقدير

الحمد لله الذي وفق بعض عباده \_ بعد البحث والتحري والتجارب والتحليل \_ إلى اكتشاف دقائق وأسرار كونه وأرضه التي استودعهم فيها للإفادة منها وعمارتهما بالعلم والإيمان " وَقُلْ أَعْمَلُوا فَيَسِيرَ اللَّهُ عَمَلَكُمْ وَرَسُولُهُ وَالْمُؤْمِنُونَ " .

أود أن أتقدم بخالص شكري وتقديري إلى سعادة الأستاذ الدكتور/ محمد سامي المنهراوي لإسهامه بالإشراف والتوجيه والتخطيط لهذا البحث، والذي أفاء وأفاد بجثي بعلمه ولم ييخل عليّ بوقته الثمين بالدعم والمساندة والمناقشة .

كما أتقدم أيضاً ببالغ الشكر والتقدير لسعادة الدكتور / وليد بن جميل ألطف المشرف الثاني على البحث ورئيس قسم الفيزياء لجهوده القيمة ومتابعته المستمرة للبحث سواء بتأمين الأجهزة اللازمة له أو المناقشة العلمية خلال مراحلها .

وشكري للمهندس/ محمد رضا سيد أحمد على جهوده القيمة في تحضير المادة الشمعية المستخدمة في الجزء التطبيقي من البحث بورشة قسم الفيزياء ، وتعرض العينات المستخدمة للإشعاع ومساعدته في بعض التجارب العملية وأعمال الحاسب الآلي . كما أتقدم بخالص شكري للأستاذ داود وترا على مساعداته الفنية.

وأخيراً الشاء الصادق والدعاء الخالص لزوجي الدكتور/ جميل أحمد ظفر على دعمه ومساندته وتوفير المناخ المناسب وحثه الدائم وتشجيعه المستمر .

وأود أن أنوه بالجهود الذي بذله شقيقي المهندس محمد محمود جان في توفير جملة من المراجع اللازمة للبحث من خارج المملكة فله مني جزيل الشكر .

وآخر دعوانا أن الحمد لله رب العالمين .

## إهداء

أهدي بحشي هذا إلى من كانت أعز إنسان وأغلاه عندي  
في الوجود .

إلى روح أُمي الحبيبة ، أسبغ الله عليها شآبيب الرحمة  
والرضوان وعوضها عن متاعب الحياة الدنيا بالخلد في جنات  
النعيم.



## الخواص الدوزيمترية وبعض تطبيقات لفلوريد الكالسيوم المشاب بالمنجنيز

### ملخص الرسالة

تعطي مادة فلوريد الكالسيوم المشابة بالمنجنيز ( $\text{CaF}_2:\text{Mn}$ ) في أشكالها المختلفة منحنيات اضاءة حرارية ذات شكل عام ثابت عند استثارتها بأي من أشعة جاما من الكوبالت- $^{60}\text{Co}$  أو الأشعة السينية، وتؤدي زيادة الجرعة المعطاة إلى زيادة مناظرة في كمية الاضاءة الحرارية.

يتكون منحنى الاضاءة الحرارية الناتج من قمة دوزيمترية رئيسه وأخرى صغيرة للغاية على جانبها وتعزى القمة الصغيرة إلى شوائب العناصر الأرضية النادرة الموجودة طبيعيا في المادة، أما الاضاءة الحرارية للقمة الرئيسية فهي ناتجة عن اتحاد مراكز  $\text{H}_A$  ,  $\text{F}_A$  التي تتكون أثناء تعريض المادة للإشعاع حيث مراكز  $\text{F}_A$  عبارة عن مركبات ( $\text{Mn}^{2+} - \text{F centre} - \text{Mn}^{2+}$ ) أما مراكز  $\text{H}_A$  فهي ذرات فلور مقحمة بينيا في النسق البلوري للمادة.

وقد اقترحت معالجة نظرية لبناء القمة الدوزيمترية، وبمقارنة القمة النظرية الناتجة بمثلاتها العملية تبين أن الأخيرة تتكون من قمتين مستقلتين متداخلتين ومتقاربتين في طاقة تنشيطهما. يؤيد ذلك ما لوحظ من اضمحلال ابتدائي عال نسبيا للاضاءة الحرارية خلال الأربع والعشرين ساعة التي تلي عملية التشعيع.

كما تبين أيضا أن ( $\text{CaF}_2:\text{Mn}$ ) له استجابة خطية لجرعات كل من أشعة جاما والأشعة السينية في مدى الجرعات التي تمت دراستها، كذلك وجد أن الحساسية المطلقة لرقائق المادة تفوق كثيرا حساسية أشكالها الأخرى، كما دلت حسابات دوال استجابة الجرعة المعيارية على أن ( $\text{CaF}_2:\text{Mn}$ ) يقترب في مواصفاته من مواصفات مقياس الجرعة المثالي.

وأخيرا أكدت الدراسة العملية صلاحية استخدام دوزيمتر ( $\text{CaF}_2:\text{Mn}$ ) ذي الانتفاخ الزجاجي في تمييز حقول الأشعة السينية المولدة حتى ١٥٠ كيلو فولت، وفي قياس النسب المئوية لجرعات العمق على طول المحور المركزي لهذه الحقول في مادة Mix D الشمعية. وقد تأكدت هذه الصلاحية من مقارنة النتائج التي أمكن الحصول عليها بنتائج قياسات مماثلة باستخدام غرفة التأين أجريت لهذا الغرض.

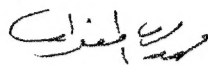
### عميد الكلية

د. عيسى بن محمد عيسى  
رواس



### إشراف

أ.د. محمد سامي توفيق  
المنهراوي



### اعداد الطالبة

فاطمة بنت محمود عبدالله جان



د. وليد بن جميل أحمد أطف



Kingdom of Saudi Arabia  
Ministry of Higher Education  
Umm Al Qura University

**DOSIMETRIC PROPERTIES  
AND SOME APPLICATIONS  
OF  $\text{CaF}_2 : \text{Mn}$**

By  
**Fatmah Mahmood Jan**

Supervised by  
Prof. M.S. Elmanharawy and Dr. W. J. Altaf

A thesis submitted in partial fulfillment  
of the requirements for the degree of  
Master of Science  
(Physics)

Physics Department  
Faculty of Applied Sciences  
Umm Al Qura University  
Holy Makkah – Saudi Arabia  
1421AH. – 2000G.

## **ACKNOWLEDGEMENTS**

I would like to express my deep gratitude to both Professor Mohamed Sami Elmanharawy and Dr. Waleed Jameel Altaf , Head of the Physics Department, for introducing me to the subject of this research and providing active continuous supervision during the course of this work. Their valuable guidance and discussions are highly appreciated.

I would also like to thank Mr. Mohamed Reda Sayed Ahmed for offering technical help , particularly in irradiating the dosimeters, and for assisting in some measurements and computer work.

Finally, the technical assistance of Mr. Dawood Watara is greatly acknowledged.

## CONTENTS

ABSTRACT .....	i
ACKNOWLEDGEMENTS.....	ii
<b>CHAPTER I</b>	
INTRODUCTION.....	1
1.1 The Thermoluminescence (TL) Phenomenon.....	2
1.2 TL Parameters And Their Determination.....	15
1.3 Applications Of TL Materials.....	19
1.3.1 Radiation Dosimetry.....	19
1.3.1.1 Stability.....	21
1.3.1.2 Dose Response.....	21
1.3.1.3 Energy Dependence.....	22
1.3.2 Personnel And Environmental Monitoring.....	23
1.3.3 Clinical Applications.....	24
1.3.4 Dating Of Archeological And Geological Materials.....	25
1.4 Review Of Past TLD Materials Research.....	26
1.5 Properties Of Manganese - Doped Calcium Fluoride	31
1.6 Scope Of The Present Work.....	33
<b>CHAPTER II</b>	
MATERIAL AND EXPERIMENTAL TECHNIQUES.....	35
2.1.TLD Material.....	35

2.2 Irradiation Facilities.....	36
2.2.1 The X - ray Machine And Its Calibration.....	36
2.2.2 The Gamma Irradiator And Its Calibration.....	39
2.3.Irradiation Of TL Dosimeters.....	43
2.4 Measurement Of Thermoluminescence (TL).....	44
2.5. Measurement Of The Quality Of X -Ray Beams.....	46
2.6 Measurement Of Central-Axis Percentage Depth Doses.....	48
<b>CHAPTER III</b>	
RESULTS AND DISCUSSION.....	51
3.1 Thermoluminescence Of Irradiated $\text{CaF}_2$ : Mn Dosimeters .....	51
3.2 Analysis Of The Main Dosimetric Peak Of $\text{CaF}_2$ :Mn..	62
3.3 Dosimetric Properties Of $\text{CaF}_2$ : Mn.....	71
<b>CHAPTER IV</b>	
SOME DOSIMETRIC APPLICATIONS OF $\text{CaF}_2$ : Mn....	77
4.1The Characterization Of X - Ray Beams.....	77
4.2 Central - Axis Percentage Depth Doses Of X-Ray Beams.....	84
CONCLUSIONS.....	93
REFERENCES.....	96

# CHAPTER I

## INTRODUCTION

Thermoluminescence (TL) is the light emission occurring during heating of a sample that has already absorbed some energy from radiation. TL is merely one of a large family of luminescence phenomena that are named after the type of radiation used to excite the emission, namely, photoluminescence (excitation by visible or ultraviolet light), cathodo-luminescence (by energetic electrons), electroluminescence (by electrical energy), radioluminescence (by  $\gamma$ -rays, X-rays,  $\beta$ -rays,) etc.. Thermoluminescence, in fact, is a misnomer in the conventional sense of the names of luminescence processes mentioned earlier as the heat radiation is only a stimulant and not an exciting agent.

While the observations of TL have been reported as early as the seventeenth century, Urbach [1] was the first to propose TL as an experimental technique for trap level distribution. It was only after the mathematical works of Randall and Wilkins [2] in 1945 and Garlick and Gibson [3] in 1948 that TL started receiving more attention.

Daniels et al [4] were the first to propose TL as a research tool in radiation dosimetry. They also suggested the determination of natural TL from rocks, which further led to the development of techniques for geological and archeological dating.

Considerable efforts have been made by numerous researchers to understand TL phenomenon, both physically and mathematically resulting in vast accumulation of data [5-26] in the form of books and about a dozen international conferences held regularly since 1965. Despite decades of research, the detailed processes involved in this complicated phenomenon are not yet sufficiently understood, though successfully applied.

### **1.1. The Thermoluminescence (TL) Phenomenon**

If we take a chunk of limestone, crush it and heat it at a constant rate to kitchen-stove temperatures under laboratory conditions, it will probably emit light, but only while the temperature is increasing. If we cool it back down again and repeat the process, nothing happens. This strange behaviour is an example of thermoluminescence, a powerful and valuable tool of use for solid - state research, nuclear safety, medical dosimetry, geological age determination and for archeological dating.

Thermoluminescence is the release of light in a crystalline material as it is heated at a constant rate. The light is proportional to the previous nuclear radiation dosage the material has received. Once the light is produced, the previous radiation history of the material is "erased" as the thermal cycling performs a destructive readout of the sample's past history.

Had we measured the output light produced by the limestone sample and made a few other measurements and assumptions, we could find out either "how old" the limestone is or else "how long" it has been since it had last been heated. Conversely, we could heat-cycle the piece of limestone to erase all the old radiation history. Any measurement made in the future on this sample would tell us how much new radiation the limestone had been exposed to since we last heat-cycled it.

Thermoluminescence is then a two-way street; it can either tell us how long it has been since a substance was last heated, if we make some assumptions about dosage rate; or it can tell us how much radiation has been picked up in a given time. The "how long" is of value to geologists and archeologists; the "how much" is important to medical doctors using radiation treatment and to nuclear and radiation scientists and other personnel exposed to



possibly dangerous radiation levels. Before looking further at the thermoluminescence field, we must note that thermoluminescence is a very specific effect. It should not be confused with incandescence or luminescence, the ordinary light we get when we heat something up red hot or hotter. The temperatures involved in thermoluminescence are far lower. While the maximum temperature involved is around 650 K, most of the light is obtained at much lower temperatures. In fact, ice can be made to thermoluminesce.

Crystals can suffer radiation damage which is a cumulative effect that can be picked up in a single blast of radiation, or over a very long time at very low radiation levels. Consider a crystalline substance that is an insulator or a semiconductor such as NaCl. Assume that it is initially a perfect crystal, without any impurities or mechanical problems. If we look down into the crystal, we would see a crystal lattice, a nice orderly arrangement of sodium and chlorine ions, one after the other, alternating in all three directions. Strong forces, called valence bonds, will try to hold all the ions in perfect alignment. Should we heat the crystal, thermal agitation will excite the individual ions. The higher the temperature, the greater the ion energy level, and the more likely

the valence bonds will be broken. If we provide too much heat, the bonds all break and the crystal melts.

If the NaCl crystal is exposed to some high energy radiation, an electron in one of the ions gets its own energy level raised so high that it cannot be recaptured by its own ion, and thus is free to wander through the crystal lattice. If more radiation strikes the crystal, more electrons get knocked loose and are free to roam around the crystal; they all have too much energy to get recaptured, and an electron cloud forms. The greater the radiation dose, or the longer the radiation dosage lasts, the bigger the electron cloud.

Electron clouds cannot thermoluminesce by themselves. If crystals were perfect, there would be no thermoluminescence. But crystals have imperfections. They can have impurities locked in their lattice structures, just like the n and p impurity doping in semiconductors. They can have mechanical structure defects. At higher temperatures, they can have "statistical" defects, caused by thermal agitation. Some of these defects can capture a loose electron. These are called "traps", and once an electron gets trapped, it is stuck there, at least for the time being. A trap that has caught an electron is called a filled trap. The greater the

radiation dosage, the more electrons get knocked loose, and the greater the number of filled traps.

Each trap can only supply so much holding energy to an electron. If we heat the material, the electrons can achieve enough additional thermal energy to surmount the potential barrier of the trap and the trap releases the electrons. Certain types of traps will also cause the electron to release its own excess energy in the form of light when the release temperature is reached. These traps produce thermoluminescence; they are also related to the mechanisms that determine the colour of the substance. Once the electron has released its excess energy, it is free to once again get captured by an ion with a missing electron, removing the effect of radiation dosage.

Some traps can very tenaciously hold onto an electron, while others can only retain one weakly. These are called high-energy or "deep" and low-energy or "shallow" traps. There are usually many more low-energy traps. A slight temperature increase can empty a low-energy trap, while a large temperature increase is needed to empty a high-energy trap. When long, uniform dosage rates are being used, the "equilibrium temperature" is defined as that temperature at which thermal

agitation is emptying the traps just as fast as incident radiation is filling them.

If we take some crystalline substance with imperfections and expose it to nuclear radiation, and then heat it at a constant rate, we would get a light - versus - temperature curve called a "glow" curve or a "thermoluminescence" curve. The glow curve can show one or more peaks that correspond to different energy - level traps that get progressively released as the increasing sample temperature provides more and more thermal energy. The shape of the glow curve depends upon the material selected, as does the position of the glow peaks and their number. The total area under the glow curve, or the total light produced, is proportional only to the received radiation dosage and nothing else. While the heating rate will affect the height of the glow peaks, it does not affect the total amount of light produced. The actual light output depends on how the material is prepared, the number of traps, the optics and photomultiplier in use and the electronic amplification.

It is of interest to mention that during early studies of luminescence emission in some materials, it was found that the material also exhibited photoconductivity during emission [27]. It became evident that photoconductivity occurred due to the release

of charge carriers during light emission. These observations led to establishing the "energy band model" for interpreting luminescence in many materials because of its usefulness in understanding processes involving the transport of electronic charges through the lattice. We describe here a modified form of the simple energy band model initially suggested by Johnson [28], Schon [29] and Klasens [30] and later modified by various others [31-33]. Figure (1.1) shows this modified model which represents various levels contributing to thermoluminescence and charge transportation; all types of centres being due to defects or impurities present in the TL material.

When the material is irradiated with a radiation of sufficient energy  $E_i$  greater than that of the band gap energy  $[E_c - E_v]$ , electrons are raised from the valence band to the conduction band leaving holes in the valence band (transition 1). A number of liberated electrons return immediately to the ground state accompanied / unaccompanied by light emission causing phosphorescence or giving radiationless transitions causing internal heating. Some of them get trapped in the electron trapping states T with the corresponding holes at hole traps H (transitions 3 and 7). Electrons and holes have also the option to recombine via luminescent centres C (transitions 4 and 6). Apart from transition

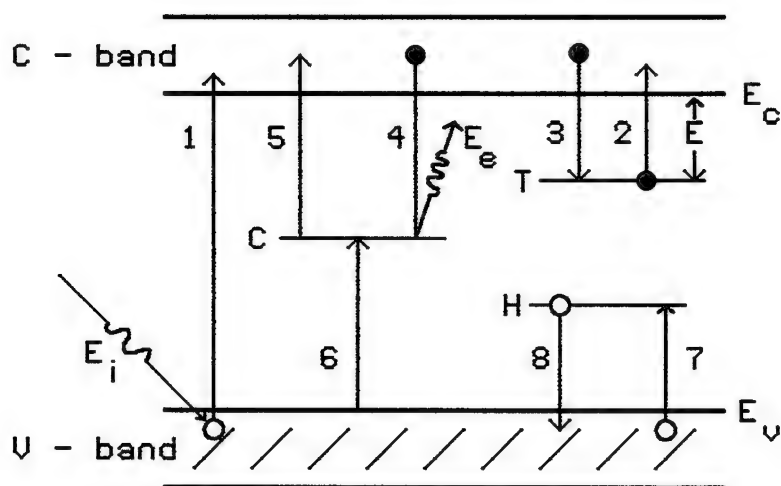


Figure (1.1) Modified band model representing various levels contributing to TL and charge transportation.

1, electrons can also be freed from the recombination centres C by radiation of energy greater than the energy difference of  $E_c$  and C ( transition 5 ).

Other possible electronic processes (e.g. band - to - band recombination) have not been considered in figure (1.1) , because direct recombination of free electrons and holes across the band gap is a less likely process than indirect, especially in wide gap semiconductors and insulators [34]. Thus, in order for recombination to take place, holes first become trapped at centres C ( transition 6 ) .

These trapped holes recombine with free electrons via the process of annihilation (transition 4) and the emission occurs if this transition is radiative. Other transitions (e.g. trap to recombination centers [35] and trap to valence band [36] are not shown in the figure because of their end result being equivalent to radiative recombination transition [29-37] ) .

If the traps are not very deep, detrapping and recombination may already occur at a substantial rate around room temperature (at which the material is irradiated ) resulting in a short half-life of stored energy. This is called phosphorescence, usually but strictly it is room temperature thermoluminescence.

If the traps are deep enough, the carriers will be retained in these traps for a long period of time even after the removal of the irradiation. The probability  $p$  per unit time of the release of an electron from the trap depth  $E$  given by :

$$p = s \exp ( - E / kT ) \quad (1.1)$$

(where  $s$  is the frequency factor and  $T$  the temperature) will be slow. A state of nonequilibrium will exist for an indefinite period, governed by the rate parameters  $E$  and  $s$ . Detrapping probability  $p$  will increase and equilibrium will be restored by raising the temperature of the specimen above the temperature of irradiation such that  $kT \geq E$ . Electrons will now be released from the traps to the conduction band resulting in their recombination with the trapped holes at the luminescent centres  $C$  giving rise to thermoluminescence (TL) .

The TL intensity  $I(t)$  at any time during heating is proportional to the rate of recombination of holes and electrons at level  $C$ . The intensity will first increase and further start decreasing as more and more traps are emptied and hence a characteristic TL peak will be produced. The TL glow peak temperature  $T_m$  is a measure of the depth of electron traps or hole traps. The position of the TL peak will, however, depend on the



values of  $E$  and  $s$ . For a given value of  $s$ , the peak position of the glow curve will occur at higher temperatures for deep traps. If the traps are distributed in depth, the TL curve will show more than one peak. The position of the luminescent centres  $C$  below the lower edge of the conduction band (i.e.  $E_c - C$ ) can be known by measuring TL spectra of the material. The energy of the emitted TL light  $E_e$  is equal to  $(E_c - C)$ .

In practice, an electron when released from the trap will possess a finite probability of getting retrapped. When this probability of retrapping is dominant, the shape of the glow curve is different from the case when it is absent.

During TL process, the charge carriers move through the lattice during irradiation of the specimen. These charge carriers travel in conduction / valence band before recombination and the processes of trap filling (during excitation) and trap emptying (during thermal excitation) take place. Each process can be described by a set of simultaneous differential rate equations which describe the traffic of charge carriers between conduction band, valence band, traps and recombination centres.

٣ ٨ ٨١



If the luminescent centre has a metastable state at a position  $E$  in energy below its first excited state, the phosphorescence intensity  $I(t)$  at any time  $t$  is given by:

$$I(t) = I_0 \exp(-pt) \quad (1.2)$$

where  $p = s \exp(-E/kT)$ , such that:

$$I(t) = I_0 \exp \left[ -s \exp \frac{-E}{kT} t \right] \quad (1.3)$$

where  $I_0$  is the initial intensity at  $t = t_0$ . This means that the rate of decay increases exponentially with temperature.

Similarly, if the electrons released on heating are not retrapped but all of them go to the recombination centres resulting in TL, the TL intensity is proportional to the rate of release of electrons from the traps, that is:

$$\begin{aligned} I_{TL} &\propto (dn/dt) = -c p n \\ &= -c n s \exp \left( \frac{-E}{kT} \right) \end{aligned} \quad (1.4)$$

where  $n$  is the number of trapped electrons and  $c$  is a constant.

Thus:

$$(dn/n) = -cs \exp \left( \frac{-E}{kT} \right) \frac{dt}{dT} \cdot dT$$

or :

$$(dn/n) = -c \frac{s}{\beta} \exp(-E/kT) dT$$

where the heating rate  $\beta = (dT / dt)$

By integrating on both sides and substituting in equation (1.4), an equation for the TL intensity  $I_{TL}$  can be derived as:

$$I_{TL} = n_0 c s \exp\left(\frac{-E}{kT}\right) \exp\left[-\int_0^T \frac{s}{\beta} \exp\frac{-E}{kT'} dT'\right] \quad (1.5)$$

where  $n_0$  is the initial number of trapped electrons.

Equation (1.5) gives an expression for the variation of TL intensity with temperature.

At a fixed temperature  $T$ ,  $[cs \exp\left(\frac{-E}{kT}\right)]$  is a constant and is taken as  $A$ . Equation (1.4) can be written as  $[dn/n] = -A dt$ , which on integration gives:

$$n = n_0 s \exp(-At)$$

or :

$$I(t) = I_0 s \exp(-At)$$

where  $I_0 = An_0$ .

Thus, at a fixed temperature  $T$ , the TL intensity decays exponentially and the TL process is said to follow first - order kinetics. Bohn and Scharmann [38] have shown that exactly the same equation can be obtained when thermally disconnected traps are included.

It is easily seen that the intensity builds up as  $T$  increases, reaches a maximum for a particular value of  $T_m$  and falls off for any further increase of temperature. By setting  $(dI_{TL} / dT) = 0$  at  $T = T_m$ , one obtains:

$$\frac{\beta E}{kT_m^2} = s \exp\left(\frac{-E}{kT_m}\right) \quad (1.7)$$

A few interesting results are apparent from the mentioned Randall and Wilkins formalism:

1. for a given trap [i.e.  $E$  and  $s$  values being constant],  $T_m$  shifts to higher temperatures as  $\beta$  is increased [40],
2. for a given value of  $\beta$ ,  $T_m$  shifts toward higher temperatures as  $E$  increases or  $s$  decreases,
3. the area under the glow curve for given  $s$ ,  $\beta$  and  $E$  values, is independent of  $n_0$  as is the temperature of maximum emission  $T_m$ , and
4. at low temperatures, we have:

$$I_{TL} = n_0 s \exp(-E / kT)$$

so the value of  $E$  can be obtained from the initial portion of the thermoluminescence curve without determining  $s$ .

This theory was also extended by Randall and Wilkins for the case where a distribution of activation energies was involved

[27] ( i.e. uniform, quasiuniform and exponential distribution of energies) .

## 1.2 TL Parameters And Their Determination

TL characteristics of a material are expressed by two trapping parameters which are the activation energy  $E$  and the frequency factor  $s$ . A knowledge of these two parameters is essential for the understanding of the TL process occurring in a material. Various methods have been developed for this purpose based on the glow curve shape, heating rate and area measurements; these methods have been reviewed by many authors [11,39-48] . There is hardly any method that takes into account the full shape of the glow peak and also no single method is yet available that is applicable to all the cases of TL peaks for all materials.

The initial rise method [3,49-52] is applicable subject to the condition that  $s$  is independent of temperature and the glow peak is well defined without any overlapping with other peaks. For the initial rising part of the glow curve, the TL intensity is proportional to  $\exp(-E/kT)$  . By plotting the natural logarithm of the TL intensity versus  $(1/T)$  over the initial rising region of the

glow peak, a straight line of slope  $(-E / k)$  is obtained from which the activation energy  $E$  is easily calculated.

Glow curve shape methods are dependent on the order of kinetics and are based on the shape of the peak that is strongly affected by the kinetic order. Two of three points from the glow curve, that is, the temperature of the peak  $T_m$  and either or both the low - and high - temperature half heights at  $T_1$  and  $T_2$  are utilized. The simplest type of glow curve to analyze is that for a material in which retrapping is absent, a single-valued trap depth is involved, radiationless transitions are negligible and a monomolecular process is involved. These assumptions are possibly not rigorously valid for any real material; however, under certain conditions they may be approximately valid for some materials.

Grossweiner [52] has presented a fairly simple method for approximating the values of  $E$  and  $s$  for a material for which the glow peaks do not overlap and for which the above assumptions apply. He developed an explicit expression for  $E$  in terms of  $T_m$ , the temperature at which the maximum in the glow curve occurs, and  $T_1$ , the temperature at which the glow curve reaches half its

peak value on the low temperature side of the glow peak. This expression is given as follows:

$$E = (1.51) k T_m T_1 / (T_m - T_1) \quad (1.8)$$

and is correct to within  $\pm 5\%$  when  $(E / kT) > 20$  and  $(s / \beta) > 10^7$  where  $\beta$  is the heating rate.

Further, Grossweiner gave a method of obtaining an estimate of the value of  $s$  which leads to an expression of the form:

$$s = \frac{e^{E/kT_m} .3 T_1 \beta}{2 T_m (T_m - T_1)} \quad (1.9)$$

The values of  $E$  and  $s$  thus calculated may then be used with equation (1.5) to determine a theoretical glow curve for comparison with the experimental curve.

For the same case, but using only the high - temperature half - height,  $T_2$ , of the glow peak, Lushchik [53] showed that the activation energy can be given by:

$$E = k T_m^2 / (T_2 - T_m) \quad (1.10)$$

Using the value of  $E$  and equation (1.7), the expression for  $s$  has the form:

$$s = \left( \frac{\beta}{(T_2 - T_m)} \right) \cdot \exp \left( \frac{T_m}{(T_2 - T_m)} \right) \quad (1.11)$$

Another method for calculating E was given by Keating [54] for first - order kinetics as:

$$(kT_m / E) = (1.2 \gamma - 0.54) \frac{w}{T_m} + 0.0055 - \left[ \frac{1}{2} (\gamma - 0.75) \right]^2 \quad (1.12)$$

where  $\gamma = (T_2 - T_m) / (T_m - T_1)$  , and  $w = (T_2 - T_1)$ .

The expression is valid for  $0.75 < \gamma < 0.9$  and  $10 < (E/kT_m) < 35$ .

Chen [42] gave a method for calculating the activation energy E and the frequency factor s using the total half-width  $w = [T_2 - T_1]$  of the glow peak. For a first - order peak with a frequency factor s independent of temperature, the activation energy E is given by:

$$E = 2 K T_m ( 1.26 T_m / w) \quad (1.13)$$

and the frequency factor s is found to be:

$$s = [ 2 \beta (1.26 T_m / w) / (e^2 T_m) ] \cdot \exp (2.52 T_m / w) \quad (1.14)$$

where  $e = 2.718$  .

The activation energy E can also be calculated [55,56] by using two different heating rates  $\beta_1$  and  $\beta_2$  , finding their corresponding peak temperatures  $T_{m1}$  and  $T_{m2}$  and applying the equation:

$$E = \left( \frac{kT_{m1} T_{m2}}{T_{m1} - T_{m2}} \right) \ln \left[ \frac{\beta_1 \left( \frac{T_{m2}}{T_{m1}} \right)^2}{\beta_2} \right] \quad (1.15)$$



Heating rate methods are useful because the only data required is the temperatures of the peak maximum that can be reasonably and accurately determined from the glow curves. Also, the calculation of  $E$  is not affected by problems due to thermal quenching as with the initial rise method. This technique is, however, not reliable for overlapping peaks where  $T_m$  is affected when glow peaks are separated by the cleaning process.

### **1.3 Applications Of TL Materials**

Apart from determining the trapping parameters and defect studies in solids, TL is widely used in the detection of UV and ionizing radiations, for example, in safety monitoring of x - ray machines in health care centres and in monitoring the radiations around power plants. TL phenomenon can be used to establish the ages of certain archeological samples, especially pottery, and of geological formations. Thus, it has played a decisive role in detecting forgeries and for the authenticity of artifacts and ancient art works.

#### **1.3.1 Radiation Dosimetry**

Radiation dosimetry, which is one of the major applications of TL, needs accurate detection and measurement of ionizing radiations. Environmental and personnel monitoring, radiation

therapy dosimetry, and diagnostic radiology dosimetry are the areas of applications of TL dosimetry. These applications have been discussed in a number of books as well as the proceedings of several international conferences held since 1965 [18-26]. The published proceedings of these conferences present a detailed view of the development of TL dosimetry, which is being preferred as a method of radiation dose measurement to the more traditional techniques of darkening of films and of ionization chambers.

Materials for measuring doses of different kinds of radiation so-called " Thermoluminescent Dosimeters " [TLDs] are commercially available. They are quite sensitive, highly economical and possess reasonably accurate and linear response over a wide range of dose. Quick and on the spot dose evaluation are possible. They can be made in extremely small sizes and desired shapes. The limitations of their use, however, being that the repeat reading with them is not feasible and the evidence value for later verification is almost nil compared to photographic films.

When choosing a material as a dosimeter, several properties must be examined [16,17]. These include dose response, usable

dose range, linearity, energy dependence, sensitivity, reproducibility of results, stability over a period of time of the stored information, effect of environment on dosimeter performance, and difference in performance from batch to batch. The selection also requires a precise knowledge of a particular application such as personnel dosimetry (dose estimate in body tissue) and environmental monitoring (dose estimate in air) . Some of the properties are being mentioned in the following discussion.

#### **1.3.1.1 Stability**

Stability of a TLD is determined by the temperature at which the maximum intensity of the glow peak occurs, that is, it should have high glow peak temperature ( above about 400 K but below 600 K ) so that the black - body radiation does not swamp the TL signal. Stability must be maintained in an unusual temperature or humid atmospheric conditions, which can also enhance fading and corrosive effects.

#### **1.3.1.2 Dose Response**

A good TLD should exhibit a linear relationship between the dose received and the subsequent TL output. The dosimeter should also be most sensitive in the dose range of interest and its

response be dependent on dose rate (100 $\mu$ Gy to 1 Gy for personnel dosimetry) and must not show any signs of saturation within this range. Many TL materials show a nonlinear growth of TL intensity with absorbed dose (superlinear and sublinear behaviour) over certain dose ranges. The mechanism of sensitization (increase in TL sensitivity) following the absorption of radiation is exhibited by many materials and is closely related to the superlinearity. The problems of sensitization and superlinearity are overcome by annealing the material after each irradiation re-establishing, thereby, the defect equilibrium and allowing the material ready for reuse. A uniform cooling is also used after many annealings.

#### **1.3.1.3 Energy Dependence**

Since the TL intensity emitted from a material is proportional to the amount of energy absorbed initially by the material, it is desirable to have a detector which exhibits a constant response over a wide range of energies. If the dose is to be delivered to the body tissue, the so-called "tissue - equivalent" dosimeters are required. Lithium borate, for example, is one such material with  $Z_{\text{eff}} = 7.4$ , equal to that of tissue. Energy response, if necessary, can be modified by use of filters [57] whose optimum characteristics can be calculated beforehand [58].

### 1.3.2 Personnel and Environmental Monitoring

TLDs can be used in personnel monitoring and safety of people working with reactors, particle accelerators, x-ray machines, and radioactive sources [59] . Since accidental exposures can range from a few roentgens (R) to thousands of R and different energies of radiation are likely to be encountered in personnel dosimetry, the dosimeter should give a response that reflects the actual dose to tissue regardless of the energy of radiation. The International Commission on Radiation Protection (ICRP) recommended limit, which corresponds to the maximum dose equivalent value and not expected to cause injury during a person's working life time, amounts to about 10 mR per month.

The tissues that are at risk during irradiation of an individual include the skin and deeper lying material such as gonads, lungs, thyroid, bone surface and bone marrow stem cells, and the breasts in females. TLDs can be classified into skin - dosimeters and body - dosimeters depending on their ability to assess the dose delivered to a depth of 5 to 10 mg cm<sup>-2</sup> (to skin) and 300 to 1000 mg cm<sup>-2</sup> (to the male gonads), respectively.

Environmental monitoring is concerned with the natural radioactivity arising from radioactive materials present in the surroundings and from cosmic rays, radiation released from nuclear power stations, and background radioactivity in space. Environmental dosimeters require different sets of performance characteristics from those used in personnel dosimetry. The dose levels to be measured are much lower, the measurement periods are much longer, and the dosimeter often spends considerable periods exposed in the open requiring high moisture and chemical resistance. Thus, a dosimeter needs to be durable, easily identifiable and easily detectable in the field. Calibration and measurement procedure for environmental assessment using TLD has been suggested by Piesch [60].

### **1.3.3 Clinical Applications**

TLDs can be used to estimate the dose given to a patient during radiotherapy and diagnostic radiology. Moreover, the radiation output of therapy machines, beam uniformity checks and measurement of absorbed dose in phantoms and so on can be performed with the help of TLDs which have become part of the standard equipment of a radiation therapy clinical setting. The small physical size of TLDs is especially utilized to use them in

body cavities, or to monitor particular small regions such as the cornea of the eye. TLDs are being used to measure the radiation exposure for various diagnostic examinations such as mammography, chest, dental and so on. Dosimetry of energetic beta particles and accelerator-produced electrons, which are not very different from that for x and gamma rays, can be performed.

#### **1.3.4 Dating of Archeological and Geological Materials**

The age of archeological or geological samples using TL phenomenon can be determined utilizing the already established relation between TL intensity and absorbed dose. Natural TL occurring in minerals and rocks is directly related to the nuclear radiations absorbed from radioactive U, K, or Th elements present within the material, which the material has received over a long period. By knowing the irradiation rate from the radioactive minerals, the geological age of the sample can be estimated to be equal to the ratio of the absorbed dose to the irradiation dose rate. Archeological dating of an ancient pottery (i.e. fired clay), copper and bronze slags, bones, and shells, and similarly, the geological age determination of volcanic events and ocean deposits can be determined using TL phenomenon [61-63]. TL dating, by now, is a well established process of age determination and a great



deal of literature is available [64-67]. TL has also been used in the study of lunar materials [8,68,69] and meteorites [70,71].

#### **1.4 Review of Past TLD Materials Research**

It is now more than 40 years since Daniels and his research group at the university of Wisconsin (USA) first suggested the use of thermoluminescence (TL) as a technique in radiation dosimetry [4,7]. The group has appreciated that irradiated material contains stored energy which could be thermally released. Since photomultiplier tubes can detect very low light levels, the overall process of TL offers a sensitive method of detection of radiation history for the crystals. Daniels' first successful application of LiF to radiation dosimetry during atomic bomb testing in the early 1950 s [7] used a form of this material which is almost identical to the TLD-100 of today [72]. It is of historical interest to note that the relationship between the emitted TL and the impurities present within LiF samples used at that time was not fully appreciated by Daniels' research team. The late nineteenth - early twentieth century witnessed an increased interest in the phosphorescence properties of materials and their connection with absorbed radiation [73]. The ability of materials to emit TL upon warming after being exposed to x - rays, beta



particles, electron beams and gamma rays was being investigated in detail. Marie Curie [74] was influential in this effort when she reported on the ability of natural  $\text{CaF}_2$  to re-emit TL after being exposed to a radiation source. Studies of the induced TL from natural  $\text{CaF}_2$  continued through the 1920s with Lind and Bardwell[75] and several of their colleagues [67,77], examining the x - ray induced TL from this material. The study of the TL properties of synthetic materials also gained momentum at this time with  $\text{CaSO}_4 : \text{Mn}$  being of particular interest, since manganese was recognized to be an excellent activator of luminescence [78]. The use of TL in UV dosimetry using  $\text{CaSO}_4 : \text{Mn}$  was actively being examined in this era [79].

When researching through the literature for the first mention of various TLD materials, it is very difficult to pinpoint when many of them made their first appearance - that is, when their TL properties were first studied in depth and the data subsequently published. Equally, it is difficult to define exactly when the transition occurred to mark these materials as firm candidates for TL applications. In what follows a rather coarse history of those TLD materials which find popular use today is presented.

Perhaps the first serious study of the TL properties of synthetic materials was by Weidemann and Schmidt [80], as long

ago as 1895.  $\text{CaSO}_4$  doped with Mn was of particular interest but the purpose of the study was not dosimetry since this period merely marks the dawn of research into radiation. Over 50 years went by before  $\text{CaSO}_4 : \text{Mn}$  was first studied as a possible TL dosimetric material by Watanabe in 1951 [81]. Similarly, although the ability of natural  $\text{CaF}_2$  was well known as early as 1898 [82], the first serious suggestion to use this material as the basis of a TL dosimeter was not made until the early 1960s [83].

Serious efforts to find materials for specific applications as TL dosimeters only started in the early 1950s with Daniels and his colleagues [4,84]. The most promising material to emerge at this time was LiF. Only later was it to become evident that the desirable properties of the material were the result of the interplay between the complex defects present within the material resulting from the presence of Mg and Ti impurities. This realization emerged with the work of Cameron and colleagues [7,85] and this work led eventually to the patenting of TLD - 100 by the Harshaw Chemical Company (USA) in 1963.

Daniels' group soon despaired of the unpredictable properties of LiF and turned their attention to the next material to arrive on the TLD scene, namely  $\text{Al}_2\text{O}_3$  [86,87].  $\text{Al}_2\text{O}_3$  appeared to fit the requirements of reliable dosimetric materials for a time,

but due to lack of sensitivity, lost favour in preference to other newer materials.

Beryllium oxide appeared in a study of its dosimetric properties by Moore in 1957 [88]. However, the next material to have major impact was  $\text{CaF}_2 : \text{Mn}$ , reported first by Ginther and Kirk in the same year as Moore's work on  $\text{BeO}$  [89]. The luminescence properties of the activator Mn gave this material excellent sensitivity.  $\text{CaF}_2 : \text{Mn}$  was the first TLD material to arrive in the field and stay up to the present day without any periods of disillusionment and rejection.

The 1960s witnessed the arrival of several new TLD materials and the re-emergence of old ones.  $\text{CaSO}_4 : \text{Sm}$  appeared in 1961 [90],  $\text{Li}_2\text{B}_4\text{O}_7 : \text{Mn}$  in 1965 [91],  $\text{CaF}_2 : \text{Dy}$  in 1968 [92] and both  $\text{CaSO}_4 : \text{Tm}$  and  $\text{CaSO}_4 : \text{Dy}$  also in 1968 [93]. In addition, about this time both natural  $\text{CaF}_2$  [94] and  $\text{LiF} : \text{Mg, Ti}$  [7,85] came back into the limelight, the latter in part because of its close equivalence in radiation response to that of human tissue.

The 1970s saw the re-birth of another previously studied but prematurely abandoned TLD material.  $\text{Al}_2\text{O}_3$  reappeared in the TLD literature in the form of  $\text{Al}_2\text{O}_3 : \text{Mg, Y}$  [95] and  $\text{Al}_2\text{O}_3 : \text{Si, Ti}$  [96]. Another form of  $\text{CaF}_2$ , namely  $\text{CaF}_2 : \text{Tm}$  was reported the

following year at the 5<sup>th</sup> international conference on Luminescence Dosimetry at Sao Paulo [97]. This particular series of conferences has been a popular forum for the announcement of new TLD materials and the trend continued at the 6<sup>th</sup> conference in the series at Toulouse when both  $\text{Li}_2\text{B}_4\text{O}_7 : \text{Cu}$  [98] and  $\text{MgB}_4\text{O}_7 : \text{Dy}$  or  $\text{Tm}$  [99] were reported for the first time. A related material,  $\text{MgB}_4\text{O}_7 : \text{Mn}$ , has also very recently been introduced [100].

Two years before the publication of the Toulouse conference, there appeared in the literature a paper by Nakajima and colleagues describing the TL properties of a variety of  $\text{LiF}$ -based materials, among which was  $\text{LiF} : \text{Mg, Cu, P}$  [101]. The paper went relatively unnoticed until the group at the Solid Dosimetric and Detector Laboratory in Beijing reported the manufacture of a  $\text{LiF} : \text{Mg, Cu, P}$  TLD material, known as GR-200 in 1986 [102]. This material was the latest "ultrasensitive" TLD material, with reported sensitivities as high as 50 times that of TLD-100. This was followed some years later by a more sensitive material, and another in the  $\text{Al}_2\text{O}_3$  family. This was  $\text{Al}_2\text{O}_3 : \text{C}$ , described as "anion defective"  $\text{Al}_2\text{O}_3$  by the authors, Akselrod and colleagues [103]. These two compounds currently mark the vanguard of TLD materials research.

One should note that historically radiation dosimetry has centred on monitoring personnel exposure to radiation. This is only one topic in a much wider field and dosimetry methods are applied over wide dynamic ranges of irradiation level and timescale (between irradiation and measurement). Applications of TL occur in medicine, nuclear reactor environments, in spacecraft, and for archeological and geological dating, mineral prospecting, food irradiation and even in recording the fire resistance of brick. This wide range of applications covers factors of  $10^6$  or more in total dose, dose rate and storage time. New and improved dosimeters are desirable in all these areas and their development will be aided by the knowledge gained from the study of personnel TLDs.

### **1.5 Properties of Manganese-Doped Calcium Fluoride**

$\text{CaF}_2 : \text{Mn}$  is one of the best known dosimeters. It is synthesized by following the procedure of Ginther [104].  $\text{CaF}_2 : \text{Mn}$  dosimeters may be obtained as single crystals, extruded rods, powder and hot pressed chips. The primary sources of these dosimeters are Bicron - NE (Harshaw), USA and Victoreen Inc. , USA. Other suppliers include Jozef Stefan Institute, Slovenia. Single crystals can be obtained from Optovac Inc. , USA.

The emission of  $\text{Mn}^{2+}$  in  $\text{CaF}_2$  is quite interesting. The characteristic emission under x-ray excitation peaks at 495 nm [104]. Another emission band is found at 280 nm under x-ray excitation and is attributed to electron-hole recombination [105].

The concentration of manganese has profound effects on the thermoluminescence of  $\text{CaF}_2 : \text{Mn}$  [89]. The TL curve for low concentration ( $< 1$  mol%) of manganese has some low-temperature peaks at 60, 90 and 140 C. At higher concentrations ( $> 1$  mol%) of Mn, the lower temperature peaks are suppressed and a well-defined single high-temperature peak at 250 to 260 C is observed. The optimum Mn content for this peak was found to be 3 mol%. The Mn concentrations quoted here refer to the mol% added to firing charge. However, the actual amount of Mn incorporated in the host lattice is generally less than this amount [106]. The TL mechanism in  $\text{CaF}_2 : \text{Mn}$  has been subjected to several discussions and disputes. Several mechanisms have been suggested and each mechanism results finally in the de-excitation of the  $\text{Mn}^{2+}$  ion to the ground state:  ${}^6\text{A}_{1g} ({}^6\text{S})$ .

The main TL peak of  $\text{CaF}_2 : \text{Mn}$  (3 mol%) has a linear response over a dose range of about 5 mrad to  $10^5$  rad. The initial large fading of the main peak during the first 24 hours after

irradiation is not properly understood despite the explanation forwarded by Schulman et al [107].

CaF<sub>2</sub>: Mn is not a tissue equivalent material; the effective atomic number of CaF<sub>2</sub> is 16.57 ( $Z_{\text{eff}}$  for tissue is 7.4). The material exhibits an energy dependent response. It is several times more sensitive to 30 KeV photons, than the cobalt - 60 photon irradiation [108].

CaF<sub>2</sub> : Mn has been employed to monitor the proton radiation with energies up to 137 MeV in the space [109]. Dose linearity measurements for 100 MeV protons showed results similar to cobalt - 60 in the dose range from 10 to 10<sup>4</sup> rad. CaF<sub>2</sub> : Mn dosimeters have been found quite suitable for environmental dosimetry due to their good performance and noticeably small dispersion [110]. Compared to LiF, the sensitivity of CaF<sub>2</sub> : Mn to 2 - 5 MeV  $\alpha$ -particles is a factor of two higher. CaF<sub>2</sub> : Mn has a very poor sensitivity to fast neutrons [111].

## 1.6 Scope Of The Present Work

The present work is designed to investigate the dosimetric properties of calcium fluoride doped with manganese; the material being supplied by two different manufacturers in various physical configurations. Thermoluminescence is measured and

analyzed following irradiation with cobalt - 60 gamma rays and orthovoltage x-rays. Theoretical analysis of the glow curves is attempted; the results are compared with the experimental curves. The dosimetric properties of the material are investigated in detail.

Finally, the possible use of  $\text{CaF}_2 : \text{Mn}$  in clinical dosimetry is studied. Interest is focussed on the characterization of orthovoltage x-ray beams of different qualities and the measurements of their central - axis percentage depth doses in a tissue - equivalent material prepared especially for this purpose. Factors affecting these depth doses are investigated. The results are compared with those of measurements made with a fixed -volume ionization chamber.



## CHAPTER II

### MATERIAL AND EXPERIMENTAL TECHNIQUES

#### 2.1 TLD Material

The Mn - doped calcium fluoride ( $\text{CaF}_2 : \text{Mn}$ ) dosimeters used in the present work were in a variety of physical configurations. They were obtained in a factory - synthesized form from two different suppliers : Victoreen Inc., USA and Bicron - NE (Harshaw) , USA. The Victoreen dosimeters included hot pressed square chips ( 3.2 mm x 3.2 mm x 0.9 mm ; supplied as 2600 - 14) , extruded square rods ( 1 mm x 1 mm x 6 mm ; supplied as 2600 - 50) and bulbs ( supplied as 2600 - 49) . The Harshaw samples were in two different forms: hot pressed square chips of the same dimensions as those of Victoreen Inc., and a polycrystalline powder ; both forms being supplied as TLD - 400.

The bulb dosimeter consisted of two pieces of the TL material mechanically bound to a heater strip and encapsulated in glass. When an electric current is passed through the heater strip, the irradiated material is heated and light is emitted. The glass encapsulation protects the TL sample from environmental

contamination and breakage; and the use of nitrogen gas flow during measurements of glow curves is not necessary in this case.

The basic preparation technique of  $\text{CaF}_2 : \text{Mn}$  has been described in the literature [89-112]. It consists of co-precipitating  $\text{MnF}_2$  and  $\text{CaF}_2$  from a solution of  $\text{CaCl}_2$  and  $\text{MnCl}_2$  in  $\text{NH}_4\text{F}$ , drying and firing up to 1200 C in an inert atmosphere. The material is then ground to the required particle size ( about 100  $\mu\text{m}$ ) and formed into extruded chips or rods. Generally, the manganese doping level in the final dosimetric material is claimed to be less than 1.5 mol% [106].

## **2.2 Irradiation Facilities**

Two sources of irradiation were employed in dosing the TL dosimeters; an x - ray therapy machine and a cobalt - 60 gamma-ray irradiator.

### **2.2.1 The X - Ray Machine And Its Calibration**

The x- ray machine was a therapy type ( Therapex 150K ) manufactured by Pantak Ltd., U.K. and is shown in figure (2.1). It is one of the most reliable x- ray machines used for radiotherapy in the kilovoltage range and has been running trouble - free for more than fifteen years since its installation in 1984. A potential difference up

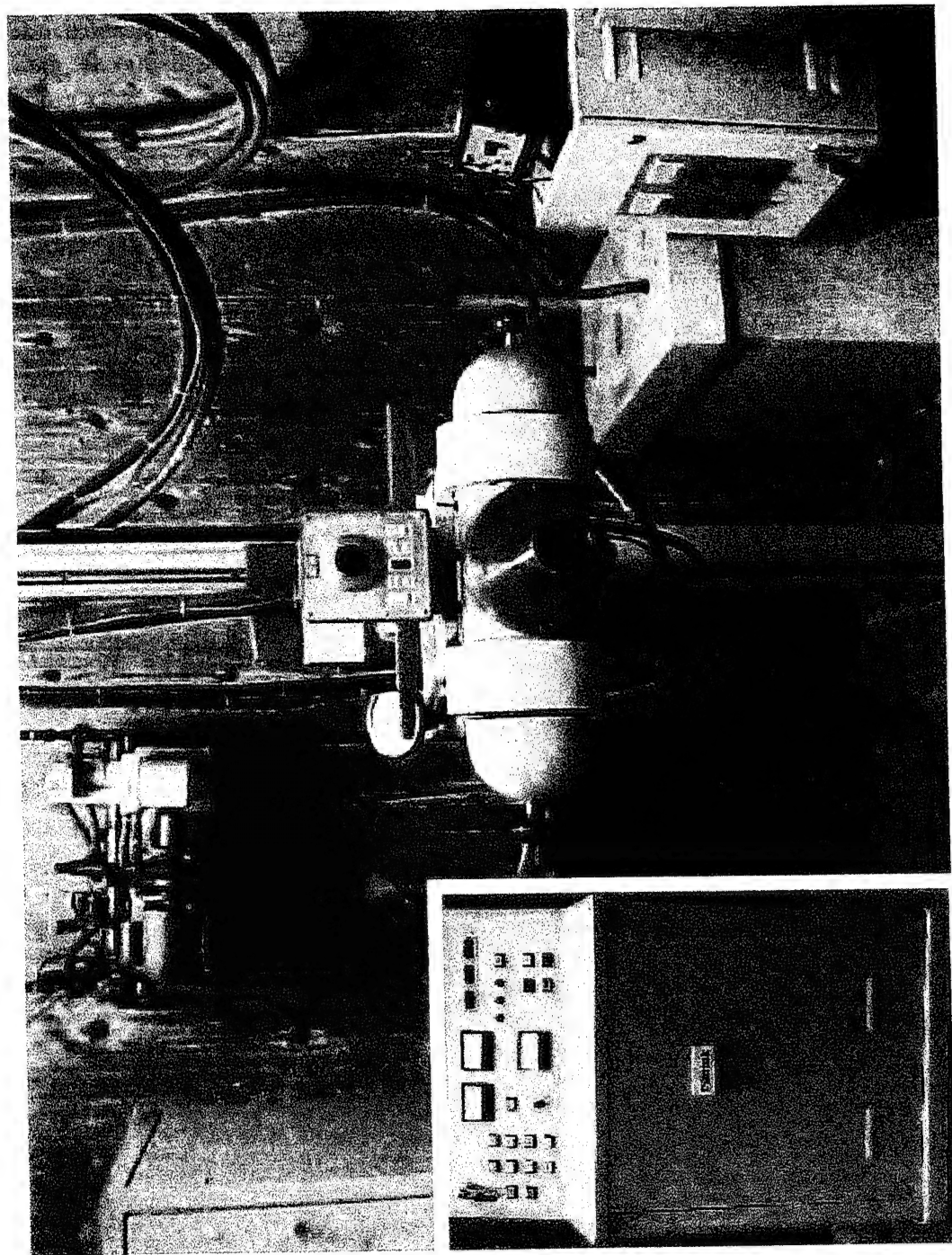


Figure (2.1) . The X-ray machine (Therapex 150K) and its control panel.

to 150 KVP can be applied to the x - ray tube while the tube current can be varied up to 20 mA. The machine is operated by means of a control panel located outside the radiation room. Four filters were supplied with the machine and are used to obtain x - ray beams of different qualities (i.e. HVL) ; each filter operates within specific applied kilovoltage and tube current ranges. Three of these filters are made of aluminum while the fourth is an aluminum filter backed with copper. The x - ray focal spot is 1 cm in diameter while the target angle is about  $30^0$  . The x-ray machine can be operated at various source - to - surface distances ( SSD ) . Cooling of the target is essential to remove the excessive heat generated during electron bombardment of the target and this is performed by means of circulating oil which is , in turn, cooled by cold water.

The x-ray machine can be fitted with any of several stainless -steel collimators of various shapes and sizes. Thus, radiation beams of specified shapes and dimensions can be easily obtained.

The output of the x-ray machine was measured in air using a Farmer dosimeter (type 2570/1B) connected to a thimble ionization chamber (type 2581); both dosimeter and chamber were manufactured and supplied by NE Technology Ltd. , U.K. and are shown in figure (2.2).

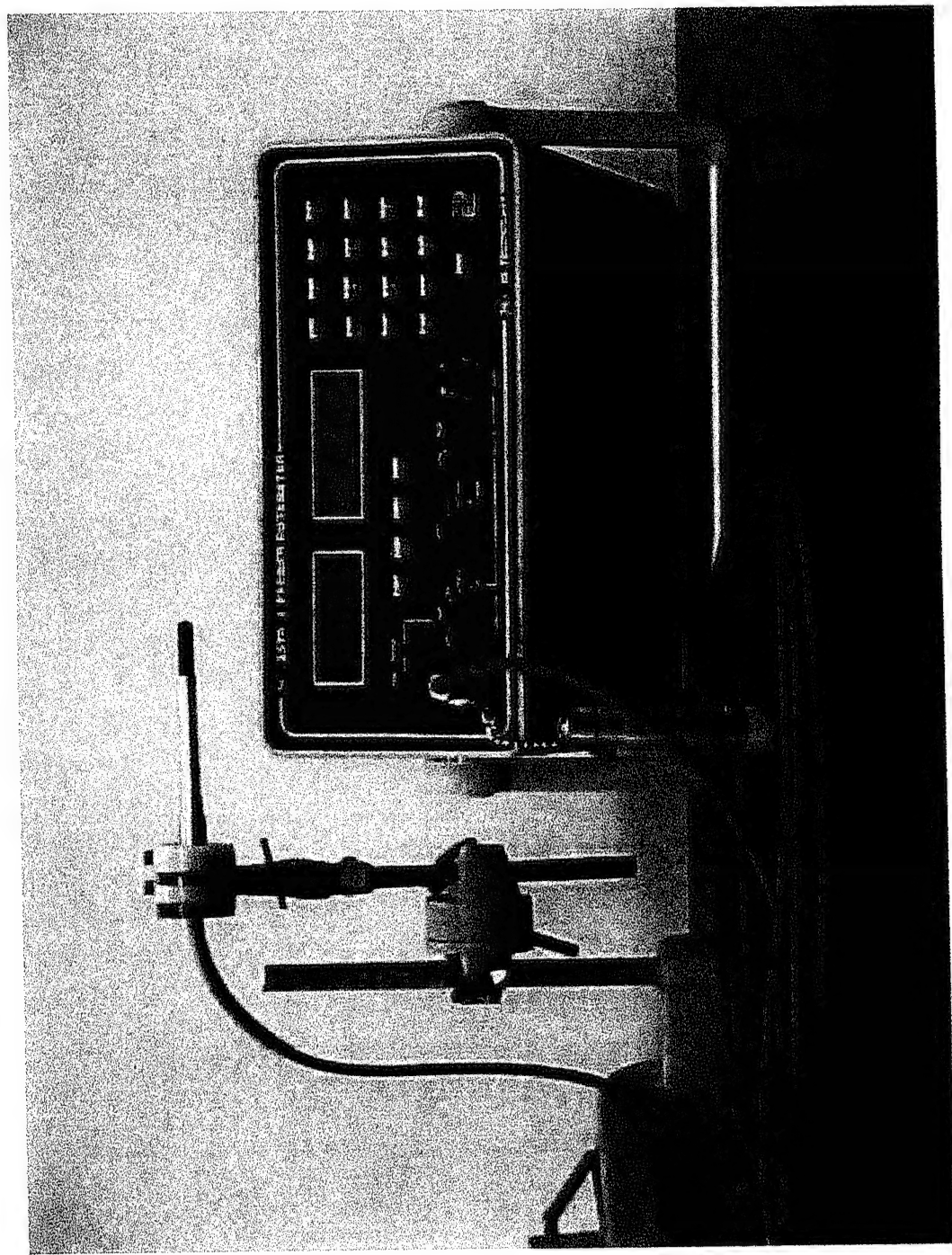


Figure (2.2) . The Farmer dosemeter and its ionization chamber.

The Farmer dosimeter is a portable battery - operated instrument designed for accurate field dosimetry of x - and gamma - rays as well as electron beams. The instrument is based on the "Townsend Balance" principle and measures the quantity of charge produced in its ionization chamber. The charge collected is due to the ionization produced in the air cavity of the chamber by electrons liberated from its walls and is expressed in grays (Gy) on a digital display. The display also indicates the units and all correction factors which have been taken into account. Normal corrections are performed by keying in the ambient temperature , the air pressure and the calibration factor of the ionization chamber. This can be done either before or after the dose measurement has been conducted. The ionization chamber consists of a thin air - equivalent walled thimble and a central electrode supported by a thin aluminum stem.

To calibrate the output of the x- ray machine; i.e. to measure the dose rate, the ionization chamber was positioned in air at a fixed SSD and adjusted so that its centre coincided with the centre of the radiation beam selected by means of the appropriate collimator. The ambient temperature, air pressure inside the radiation room as well as the calibration factor of the ionization chamber were keyed in the



dosimeter. Several readings of the output were taken at the selected KV and SSD and the average was calculated. A typical result of this calibration at 70 KV<sub>p</sub>, a tube current of 9.6 mA and 1.1 mm Al filtration gave an average dose rate of  $2.54 \pm 0.01$  Gy per minute at 15 cm SSD ; the corresponding value at 30 cm SSD amounted to  $643.0 \pm 0.01$  mGy per minute.

### **2.2.2 The Gamma Irradiator And Its Calibration**

The cobalt-60 gamma irradiator used in dosing the TL samples was installed in the Physics Department , Umm Al-Qura University in 1984. It contains two cobalt - 60 sources ; cobalt-60 emits gamma -rays of energies 1.17 MeV and 1.33 MeV. At that time, the activity of each source , as quoted by the supplier, amounted to  $1.2 \times 10^9$  MBq ; i.e. 3245 Ci. The calculated activity in october 1998, after correction for the decay of the source, was found to be  $1.93 \times 10^7$  MBq . i.e. 520.2 Ci.

The lead housing of the irradiator was designed and manufactured by Nuclear Division, Von Gahlen Nederland B.V., Holland while the cobalt - 60 sources were supplied by Amersham International, U.K. The irradiator consists of a huge lead housing fitted with a rotating carrousel. The carrousel has a chamber which

accommodates the samples to be irradiated. It also has two stop - positions:

- (a) The load / unload position in which the samples can be placed inside the chamber or removed out after irradiation ceases.
- (b) The irradiation position in which an open connection exists between the two cobalt-60 sources and the irradiation chamber.

Both the load / unload, and irradiation positions are indicated with indicating lamps on the control panel which controls all functions of the irradiator; the control panel being mounted on the front side of the irradiator as shown in figure (2.3).

The cobalt - 60 irradiator was designed to ensure uniform irradiation of samples placed inside its chamber. The requirement of uniform dosage was fulfilled by mounting two cobalt - 60 sources inside the irradiator instead of the traditional single source usually employed in other irradiators. Both sources were mounted in the lead shielding such that the upper source irradiates the chamber from its top while the lower source irradiates its bottom at the same time. The design of the irradiator also allows both sources to remain in their shielded positions inside the irradiator and it is impossible to





Figure (2.3) . The Cobalt-60 gamma-ray irradiator.

have access to the irradiation chamber except in the load / unload position.

The dose rate within the irradiation chamber was determined by chemical dosimetry. Here, the energy absorbed from gamma radiation produces a chemical change in the absorbing medium and the amount of this may be used to measure the absorbed dose [113] . One of the most useful and reliable chemical dosimeters is the Fricke dosimeter which can be used accurately for absorbed dose determination in the range from 50 Gy to 500 Gy. It depends on the oxidation of an acidic aqueous solution of ferrous sulphate to ferric sulphate. The amount of ferric ion produced by radiation can be easily measured by absorption spectroscopy, since ultraviolet light at 304 nm is strongly absorbed by the ferric ion. No effect on the accuracy of the measurement of radiation dose is observed with dose rates between 0.2 Gy/s and  $10^7$  Gy/s. The reliability of the dosimeter is not significantly influenced by a variation of the temperature of the system between 1.0 and 60 °C during irradiation. The response of the system, defined as the change in absorbance per unit absorbed dose, has been shown to be energy independent in the range from 0.1 to 16 MeV.

In calibrating the gamma irradiator, the American Society for Testing Materials (ASTM) Standard No. D 1671-72 has been followed [114]. While there are other procedures for use of the ferrous sulphate dosimetry system, the standard method has been carefully researched and tested to include the best techniques available. The other techniques differ only in minor detail.

A 500 ml fresh solution of the Fricke dosimeter was prepared and consisted of:

0.001 M       $\text{Fe}(\text{NH}_4)_2 (\text{SO}_4)_2$ ,  
0.8 N       $\text{H}_2\text{SO}_4$ , air saturated

and 0.001 M      NaCl.

A thoroughly - cleaned glass container was filled with 200 ml of this solution and exposed to gamma rays for 4 hours inside the irradiator. Samples of this irradiated solution were placed in a quartz cuvette of 1.0 cm path length and their absorbance measured against the stock solution at 304 nm using a Varian DM5 100S spectrophotometer. Extreme care was always taken not to contaminate the solutions with any foreign particles or ions as the technique is very sensitive to contamination.

The doses were calculated by the following equation [113] :

$$\text{Dose to FeSO}_4 = \frac{\Delta A_\lambda}{E_\lambda \cdot l \cdot \rho \cdot G} (9.65 \times 10^9) \text{ Gy}$$

Where:  $\Delta A_\lambda$  is the measured absorbance,  $l$  is the optical path length (1.0 cm) ,  $\rho$  is the density of the solution ( 1024 kg/m<sup>3</sup>),  $E_\lambda$  is the molar extinction coefficient (2196 moles<sup>-1</sup> cm<sup>2</sup>), and  $G$  is the number of molecules of Fe<sup>+3</sup> ions produced per 100 eV of absorbed energy (15.5 for cobalt - 60 gamma-rays ).

Using this procedure, the dose rate inside the chamber of the gamma irradiator was estimated as  $168.90 \pm 0.34$  Gy/hour.

### 2.3 Irradiation Of TL Dosimeters

TL dosimeters were dosed with x - rays directly in air and in complete darkness. In this case, the 100% dose occurs at the surface of the irradiated material. To avoid any unnecessary excessive heating of the x - ray target which could cause its damage, short exposure times were used and dosage was restricted to a dose range from 0.5 Gy to 12 Gy . After termination of exposure, the samples were kept in light - tight containers ready for TL measurements in the laboratory.

The situation is however, different when dosage with cobalt - 60 gamma - rays is being considered. Here, the 100% dose exists at

0.5 cm below the surface of the irradiated specimen due to the known build-up phenomenon. For this reason, dosage of TL chips, rods and powder samples with cobalt - 60 gamma -rays was conducted on samples mounted in grooves engraved in a perspex sheet of 0.5 cm thickness and covered by another sheet of the same thickness. TL bulbs were irradiated while being mounted inside a cylindrical perspex capsule of 0.5 cm wall thickness. Again, all irradiated samples were kept in complete darkness ready for assessment in the laboratory.

## **2.4 Measurement Of Thermoluminescence (TL)**

Thermoluminescence of dosed TL dosimeters was measured using a Victoreen thermoluminescence dosimeter reader ( Model 2800 M) . This model is a microprocessor based system designed to meet the application needs of health, medical and experimental physics as well as mixed field and environmental dosimetry. The reader head is designed to accommodate a variety of TLD configurations including chips, rods, bulbs and powders. A photograph of the TL reader is shown in figure (2.4) .

The basic function of the TL reader is to heat the irradiated specimen using a reproducible controlled temperature cycle ( 20 - 400 C°) at a linear heating rate (10 C/s) and to detect the light

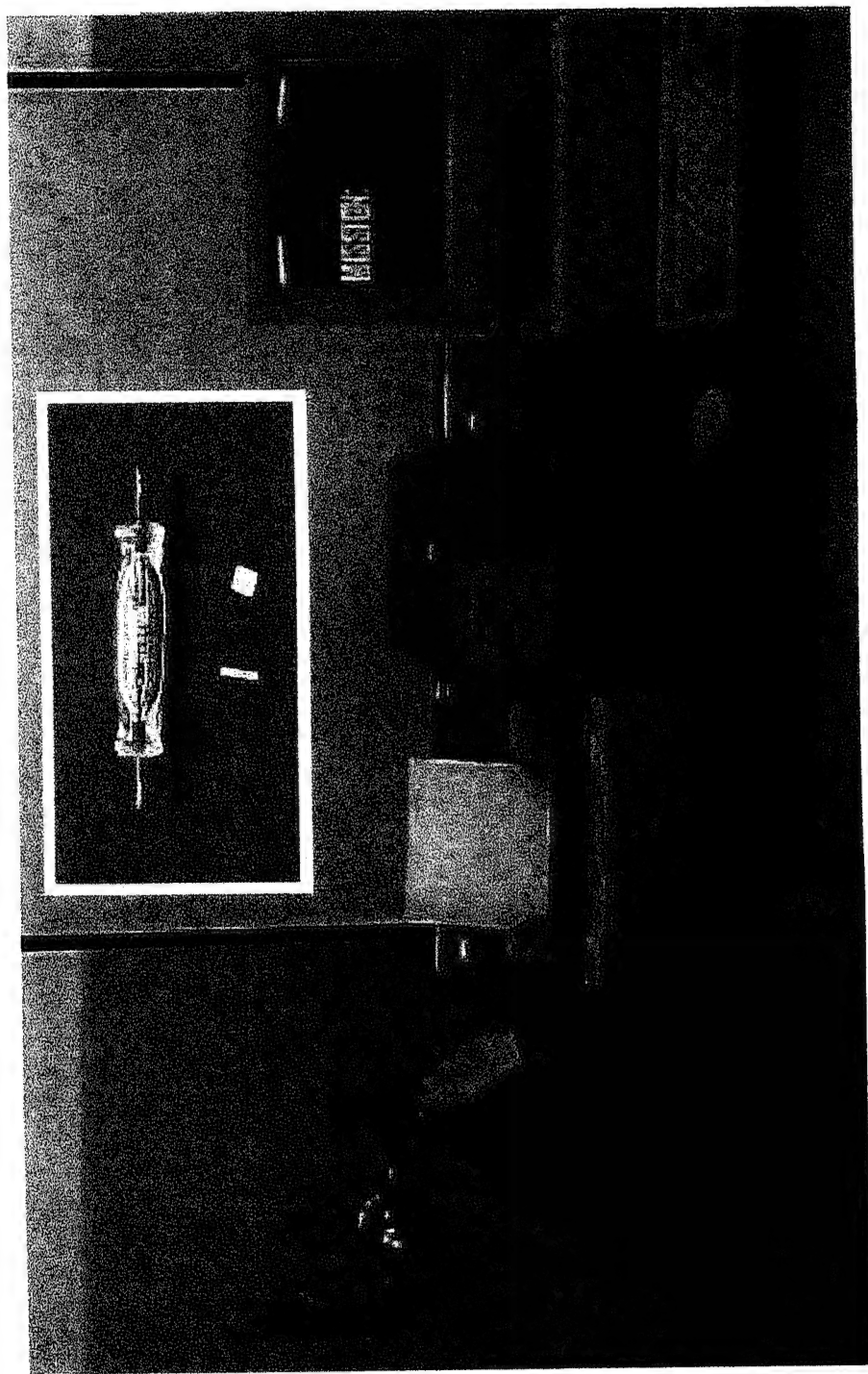


Figure (2.4) .The Victoreen TLD reader (Model 2800M). The Chip,rod and bulb dosimeters are shown in top of the figure.



emitted by means of a low noise and high gain photomultiplier converting it to a current signal which is amplified, integrated and displayed as a charge signal on a CRT display.

The model 2800 M reader can be easily calibrated in terms of Coulombs , Roentgens or Grays. Digitized glow curves, integral TL data and identification can be printed or transferred to a computer for analysis and evaluation.

In measuring thermoluminescence, the following precautions were always taken into consideration:

- (a) The TL dosimeters were never touched by bare fingers. Teflon and vacuum tweezers were used in handling the TLDs .
- (b) Powder samples of fixed weight were employed. The fixed weight was obtained by using a Harshaw magnetic dispenser which poured 100 mg of powder each time it was pressed.
- (c) Irradiated samples were transferred quickly to the TLD Reader after termination of irradiation. This proved necessary in order to avoid any possible fading.
- (d) To prevent oxidation of the heater pan and reduce the heat signal from the hot heater pan and sample, a steady flow

of nitrogen gas was passed over the heater pan during TL measurements.

- (e) Since the counting electronics of the TLD reader were limited to a total integral measurement of 45 microcoulomb, TL signals exceeding this value and displayed on the instrument were considered meaningless.
- (f) It is known that exposure of TL dosimeters to light can mimic an exposure to ionizing radiation in an unexposed TLD. Also, exposure to light of a TLD after exposure to ionizing radiation can cause loss of TL signal, greater than that attributable to the normal fading phenomenon. Since TL dosimeters are sensitive to wavelengths of light in the ultraviolet range, care was ensured not to expose them to direct sunlight or to fluorescent light by keeping them in a black box and using incandescent light bulbs in the laboratory.

## **2.5 Measurement Of The Quality Of X -Ray Beams**

The quality of a primary x - ray beam incident on a patient or a phantom is controlled by the applied KVp and the filtration. The quality is satisfactorily stated in terms of the half thickness (HVT or HVL) for x - rays generated at voltages below 400 KVp [115]. Since



the HVL used for the specification of an x - ray beam is that for a narrow beam of radiation, only one determination of the HVL for each radiation quality (i.e.. KVp plus filtration) used is needed.

The HVL needs to be known only to an accuracy of about 0.2 mm [115] and measurement to this accuracy poses no serious experimental problems. The HVL is the thickness (in mm) of the stated material (aluminum up to about 150 KVp , copper above 150 KVp ) which reduces the exposure rate of radiation beam to one half of its unattenuated value . Its determination is conveniently made by measuring and plotting on a graph the reduction in exposure rate as successive thicknesses of the attenuating material (Al) are inserted into the x- ray beam. The HVL is then determined by graphic interpolation.

Figure (2.5) illustrates the experimental arrangement used for measuring qualities (i.e HVLs). The practical aspects followed were as follows:

- (a) The x-ray tube was directed towards a TL bulb dosimeter which was held in air inside a hole engraved in a perspex sheet of 1.0 mm thickness and at a fixed distance of 1.0 m from the x - ray target.

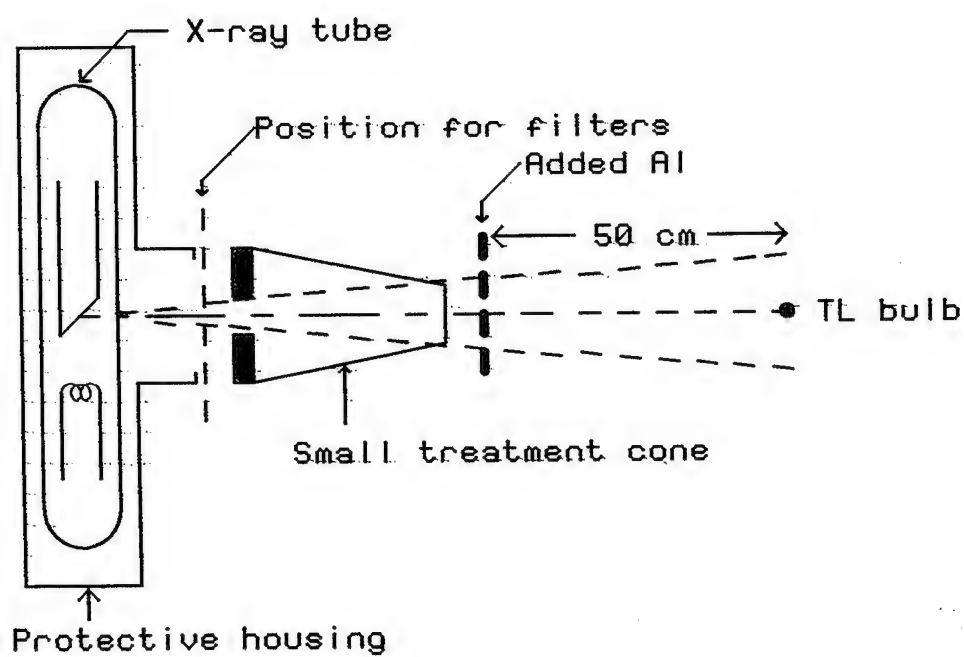


Figure (2.5) Experimental arrangement for measuring quality of x - ray beams.

- (b) A narrow circular x - ray beam ( 1.0 cm in diameter) was selected by a treatment cone ; the centre of the beam was adjusted to coincide with the centre of the TL bulb dosimeter. Care was taken to ensure that a space of at least 50 cm existed between the TLD and any structure behind it in the x-ray room that could be coincidentally irradiated during the measurement.
- (c) Readings of exposure rate were first taken for the normal beam with no added attenuator then with sheets of aluminum positioned midway between the x - ray tube target and the TL detector.
- (d) The values of measured transmitted radiation that are to be plotted as the ordinate of the graph refer to the situation where the radiation incident on the attenuator is constant . This was achieved by keeping the KVp, mA and exposure time the same for each separate exposure.

## **2.6 Measurement Of Central-Axis Percentage Depth Doses**

A solid phantom of Mix D wax was constructed for this purpose. Mix D is a mixture first proposed by Jones and Rain [116] as a tissue - equivalent material. It has a density of  $0.99 \text{ g/cm}^3$  and consists of 60% (by weight) paraffin wax ( $\text{C}_{25}\text{H}_{52}$ ), 30.4%

polyethylene [n(CH)] , 6.4% MgO and 2.4% TiO<sub>2</sub> . The tissue - equivalence of Mix D had been theoretically and experimentally confirmed [117,118]. It was found to possess an effective (Z/A) value of 0.555 ; Z being the atomic number and A the atomic weight. The corresponding value for water , regarded as soft tissue - equivalent , is 0.556.

The preparation technique adopted for the Mix D phantom consisted of melting together the exact amounts of the constituents while being stirred continuously and leaving the liquid mixture to solidify while being cooled down to room temperature. The resulting bulk sample was machined into circular discs of varying thicknesses; all discs being of the same diameter (12 cm) . The thicknesses ranged from 0.9 cm to 5.0 cm . Each disc was then fixed inside a hollow circular groove cut in a perspex sheet (20 cm x 20 cm) of the same thickness as the Mix D disc. Like Mix D , perspex is also considered tissue-equivalent.

Figure (2.6) shows the experimental arrangement used to measure percentage depth doses along the central - axis of the x-ray beam. The area of the x - ray beam was first defined by fitting the appropriate treatment cone ( collimator) to the x - ray tube. The KVp to be applied and the corresponding filtration were selected. The radiation beam was directed towards a TL bulb dosimeter which was

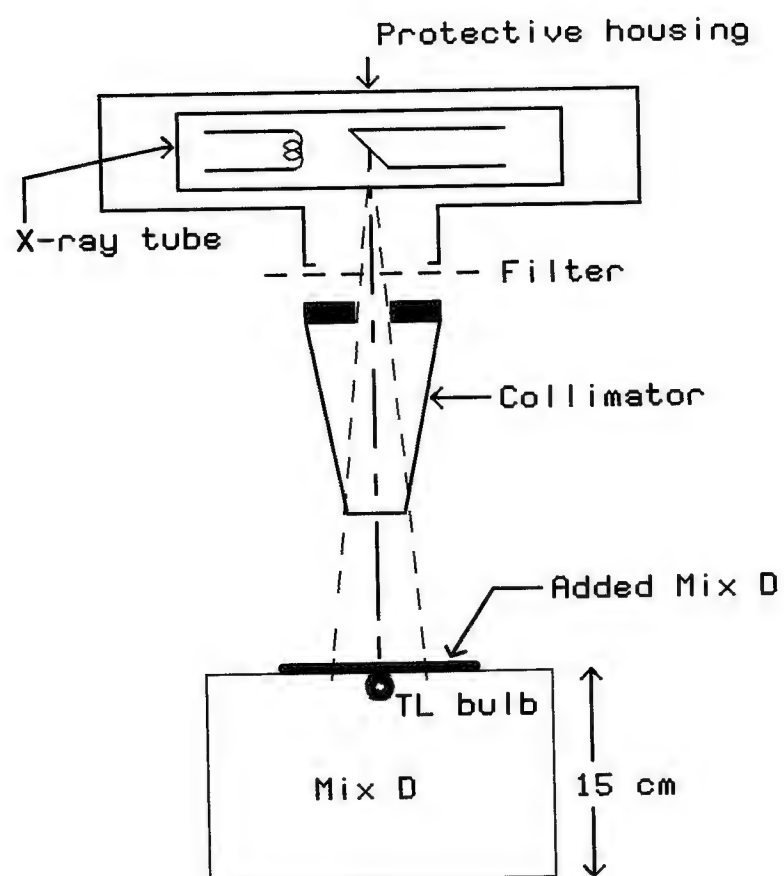


Figure (2.6) Experimental arrangement for measuring percentage depth doses.

embedded inside a groove in a Mix D sheet. The TL bulb was backed with more sheets of Mix D (15 cm thick) to ensure full backscattering. The centre of the TL bulb was adjusted to coincide with the centre of the radiation beam. Two exposures, each lasting for one minute, were made for each added thickness of Mix D ; the first conducted for the normal beam with no added attenuator then with the sheet of Mix D positioned directly on top of the TL bulb dosimeter. The corresponding glow curve was measured immediately after termination of exposure.

Percentage depth dose at any point in an irradiated medium has been defined as the ratio (expressed as a percentage) of the exposure rate at that point to the exposure rate at the dosage reference point. The reference point usually varies with the radiation energy and in case of kilovoltage radiations, this point is normally taken on the surface of the irradiated medium at the centre of the radiation beam . In terms of TL measurements, where the glow curve area is directly proportional to the exposure delivered to the TL dosimeter, percentage depth dose at any depth in Mix D can be expressed as the ratio ( taken as a percentage) of the glow curve area measured for the depth in question to the glow curve area measured at the reference point with no added Mix D. Using this definition, it is now possible to determine percentage depth doses in Mix D with TLDs as radiation detectors.

## **CHAPTER III**

### **RESULTS AND DISCUSSION**

#### **3.1 Thermoluminescence Of Irradiated $\text{CaF}_2\text{:Mn}$ Dosimeters**

The  $\text{CaF}_2$  : Mn dosimeters used in the current work consisted of hot pressed chips , extruded rods , bulbs and a polycrystalline powder supplied by two different manufacturers. A cobalt - 60 gamma - ray irradiator as well as an orthovoltage therapeutic X-ray machine were used to irradiate the dosimeters at room temperature to known doses; the given doses ranged from 0.5 Gy to 10 Gy. Thermoluminescence (TL) curves were immediately measured after termination of the irradiation process in order to avoid any fading of TL by the irradiated sample. An initial large fading of 6% has been observed in the first 24 hours of storage but the rate of fading decreased with storage time and it was only 12% for a period of one year. With the exception of bulb dosimeters, the irradiated specimens were heated in the TL reader in the presence of a nitrogen gas flow and a linear heating rate of 10 K/s was employed for all forms of dosimeters. Reasons for using this gas flow have been given in the experimental part of this work.

The general features of TL curves recorded for  $\text{CaF}_2 : \text{Mn}$  are illustrated in figures (3.1) to (3.5) after dosage with cobalt - 60 gamma rays . The corresponding curves for the same dosimeter configurations dosed with orthovoltage x - rays are shown in figures (3.6) to (3.10). At first sight, each TL curve appears to subsume a main glow peak , usually termed as the dosimetric peak, and a small satellite one appearing on the low temperature side of the main TL signal. The given dose,  $D$  , as well as the temperatures  $T_m$  of maximum TL intensity ,  $T_1$  of 50% of maximum intensity on the rising side of the peak and  $T_2$  of 50% maximum intensity on the descending side of the peak are quoted on each figure.

It is obvious that the general shape of the TL curve seems to be independent of the dosimeter physical configuration , the type of exciting radiation source and the given radiation dose. The only effect which is worthy noting is the increase in TL intensity and hence in the glow peak area with increasing radiation dose. This is due to the increased population of electron traps during the irradiation process. Published work [106] on TL of  $\text{CaF}_2 : \text{Mn}$  containing low concentrations of Mn showed this material to exhibit a glow curve with a number of peaks appearing above room temperature . When the dopant concentration was increased, a single



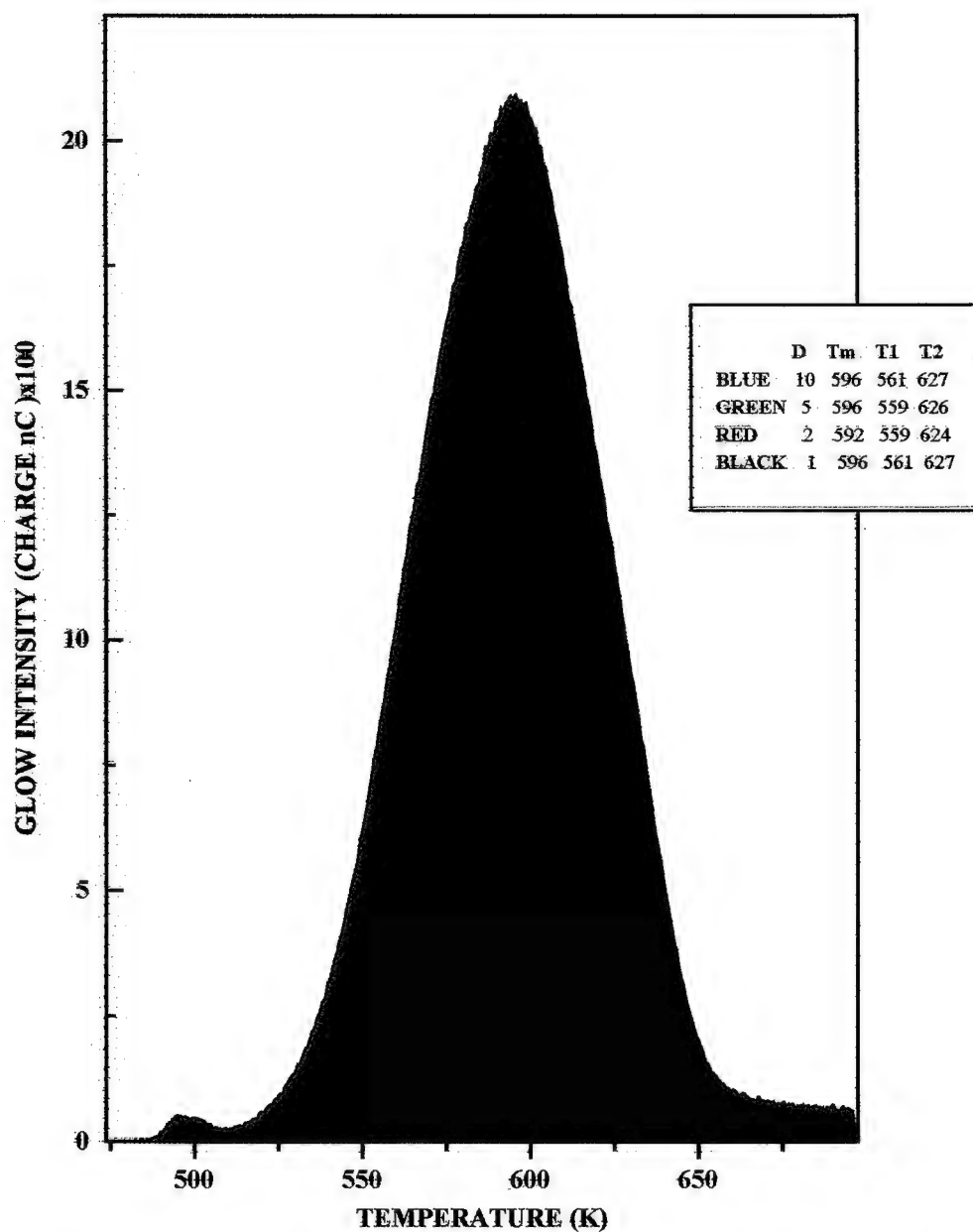


**Fig.3.1** Glow curves for a Victoreen Mn-doped Calcium Fluoride chip dosed with Cobalt-60 gamma rays.

**D** Given dose in Gy.

**T<sub>m</sub>** Temp. of glow peak max intensity in (K).

**T<sub>1</sub>** Temp. of 50% intensity (rising side).

**T<sub>2</sub>** Temp. of 50% intensity (falling side).

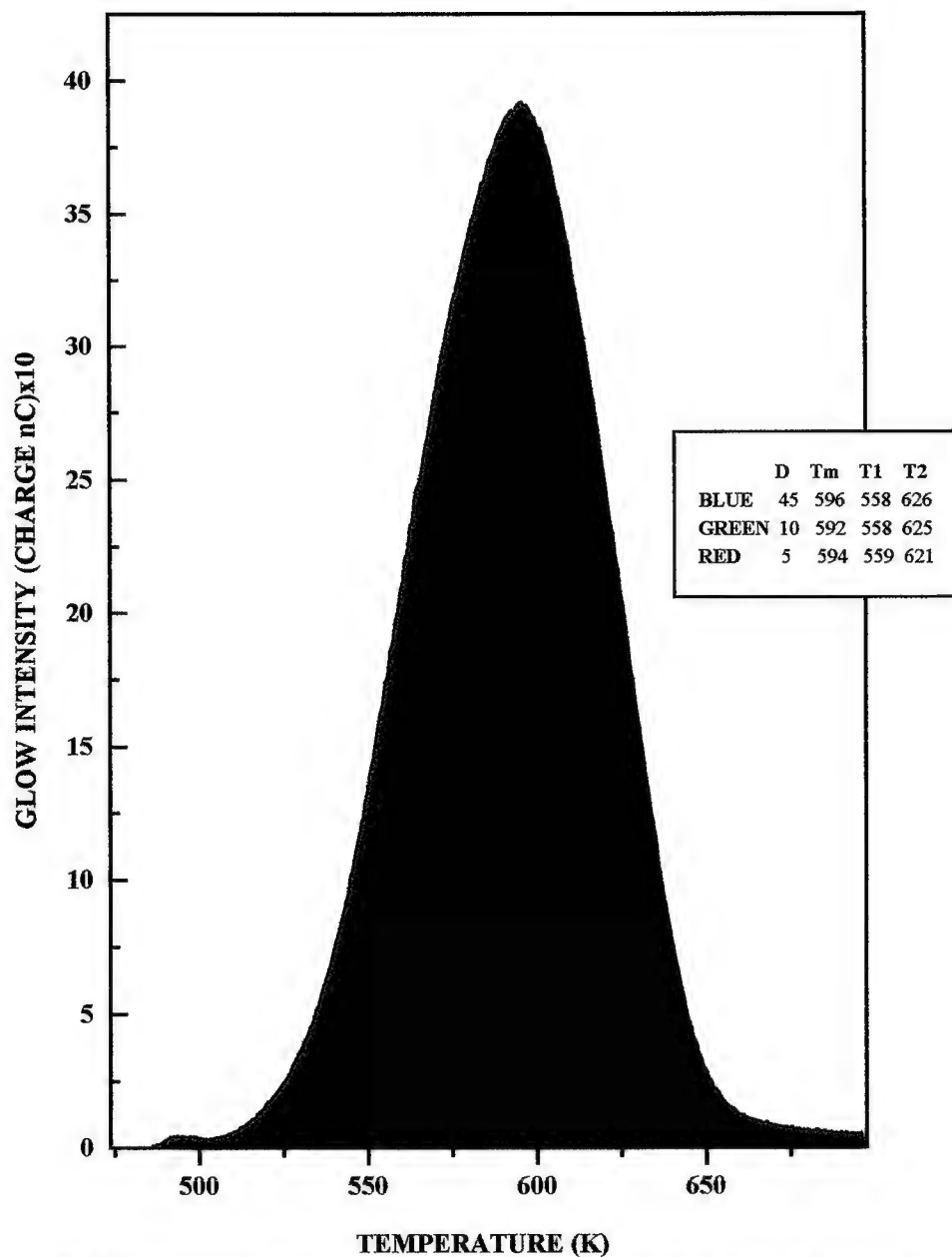


**Fig.3.2** Glow curves for a Victoreen Mn-doped Calcium Fluoride rod dosed with

Cobalt-60 gamma rays.

**D** Given dose in Gy.

**T<sub>m</sub>** Temp. of glow peak max intensity in (K).

**T<sub>1</sub>** Temp. of 50% intensity (rising side).

**T<sub>2</sub>** Temp. of 50% intensity (falling side).

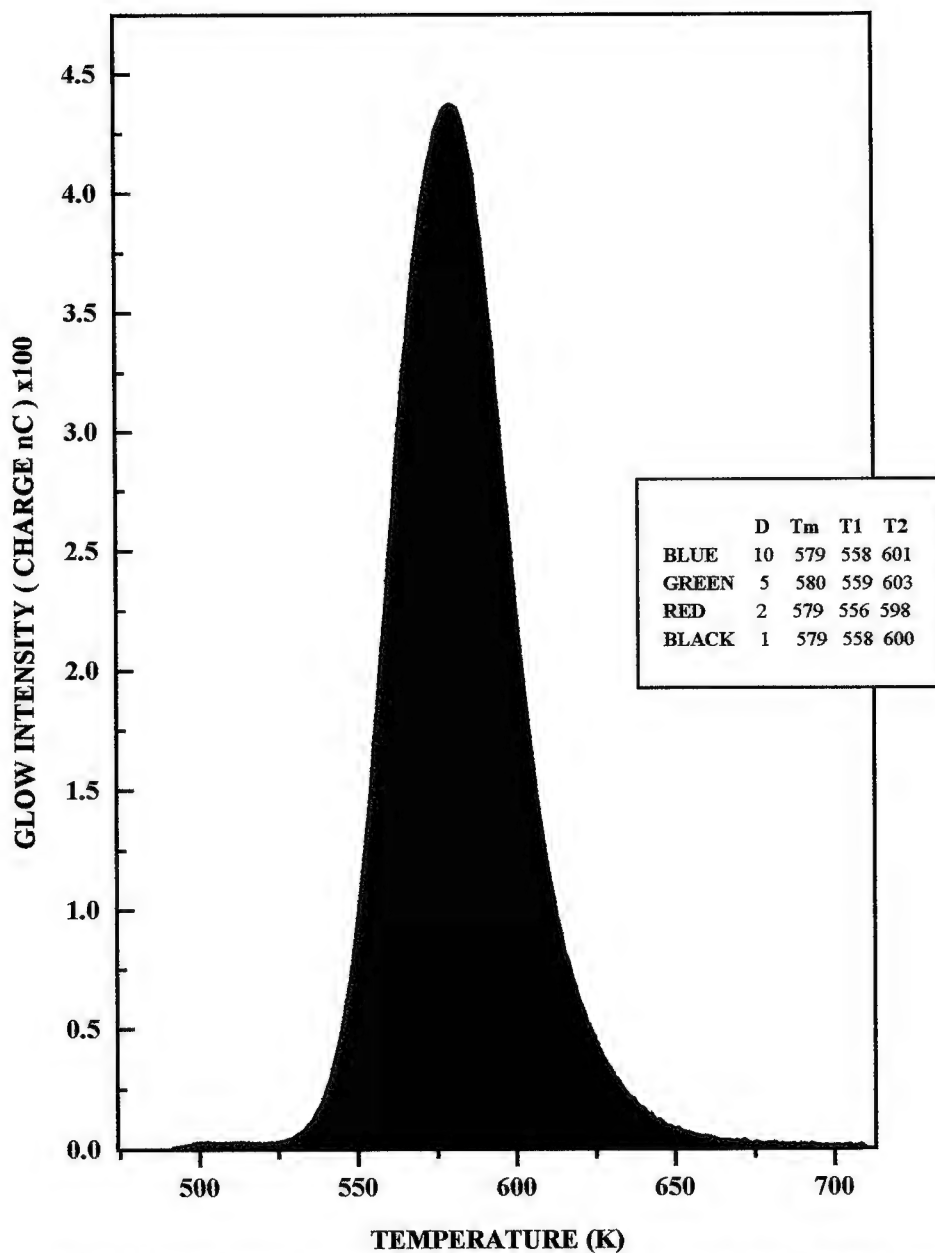


**Fig.3.3** Glow curves for a Victoreen Mn-doped Calcium Fluoride bulb dosed with Cobalt-60 gamma rays.

**D** Given dose in Gy.

**T<sub>m</sub>** Temp. of glow peak max intensity in (K).

**T<sub>1</sub>** Temp. of 50% intensity (rising side).

**T<sub>2</sub>** Temp. of 50% intensity (falling side).

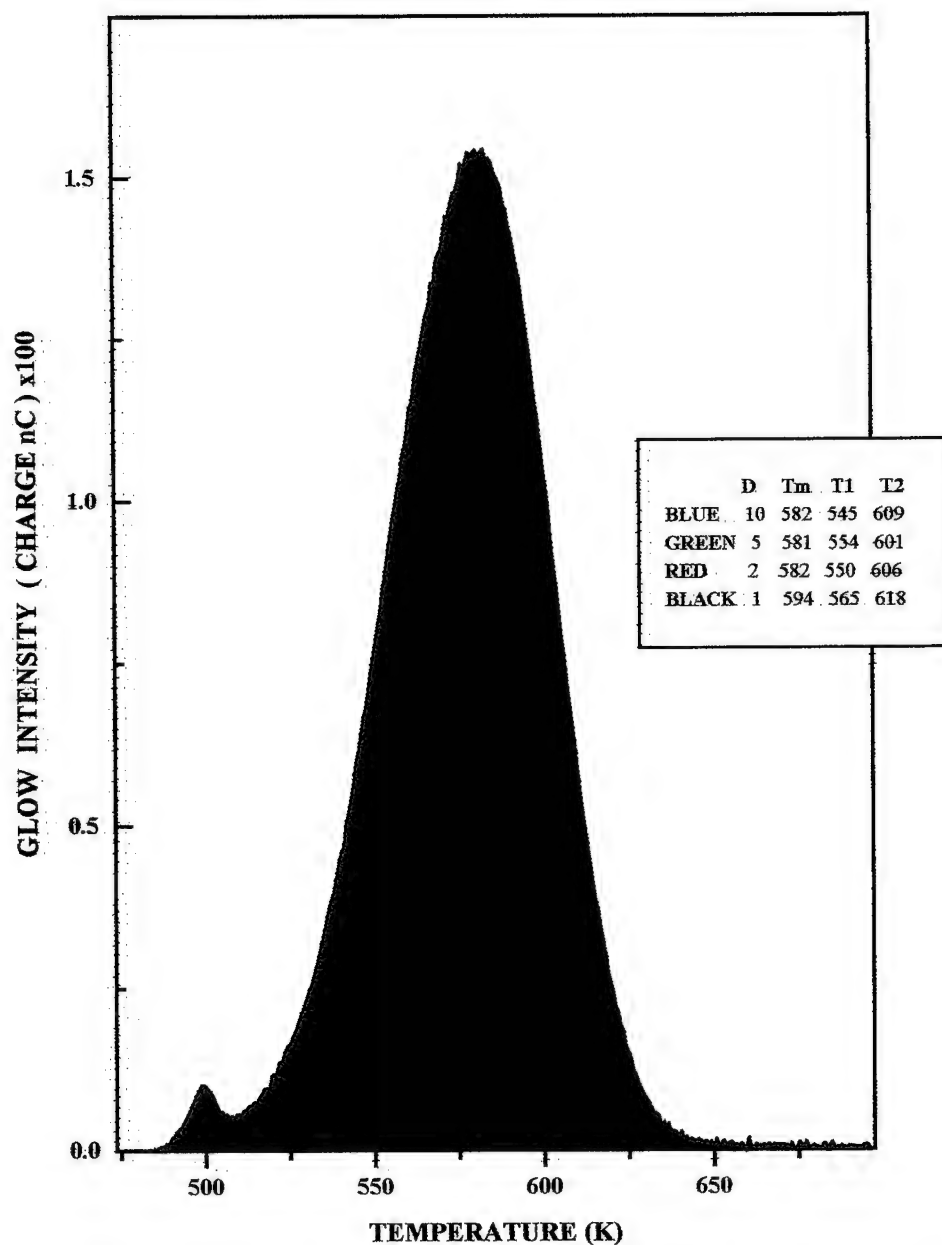


**Fig.3.4** Glow curves for a Harshow Mn-doped Calcium Fluoride chip dosed with Cobalt-60 gamma rays.

**D** Given dose in Gy.

**Tm** Temp. of glow peak max intensity in (K).

**T1** Temp. of 50% intensity (rising side).

**T2** Temp. of 50% intensity (falling side).

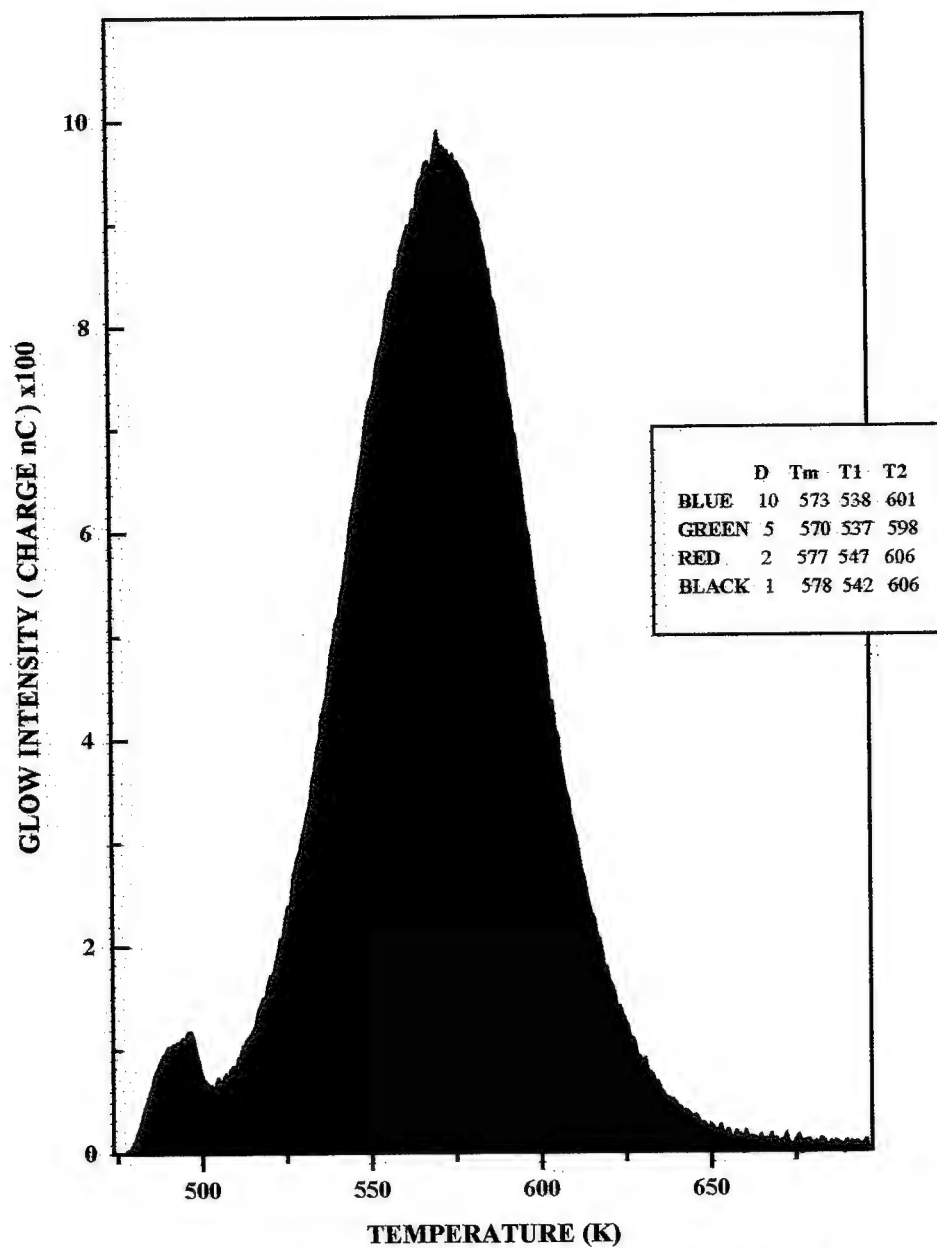


**Fig.3.5** Glow curves for a Harshaw Mn-doped Calcium Fluoride powder dosed with Cobalt-60 gamma rays.

**D** Given dose in Gy.

**Tm** Temp. of glow peak max intensity in (K).

**T1** Temp. of 50% intensity (rising side).

**T2** Temp. of 50% intensity (falling side).

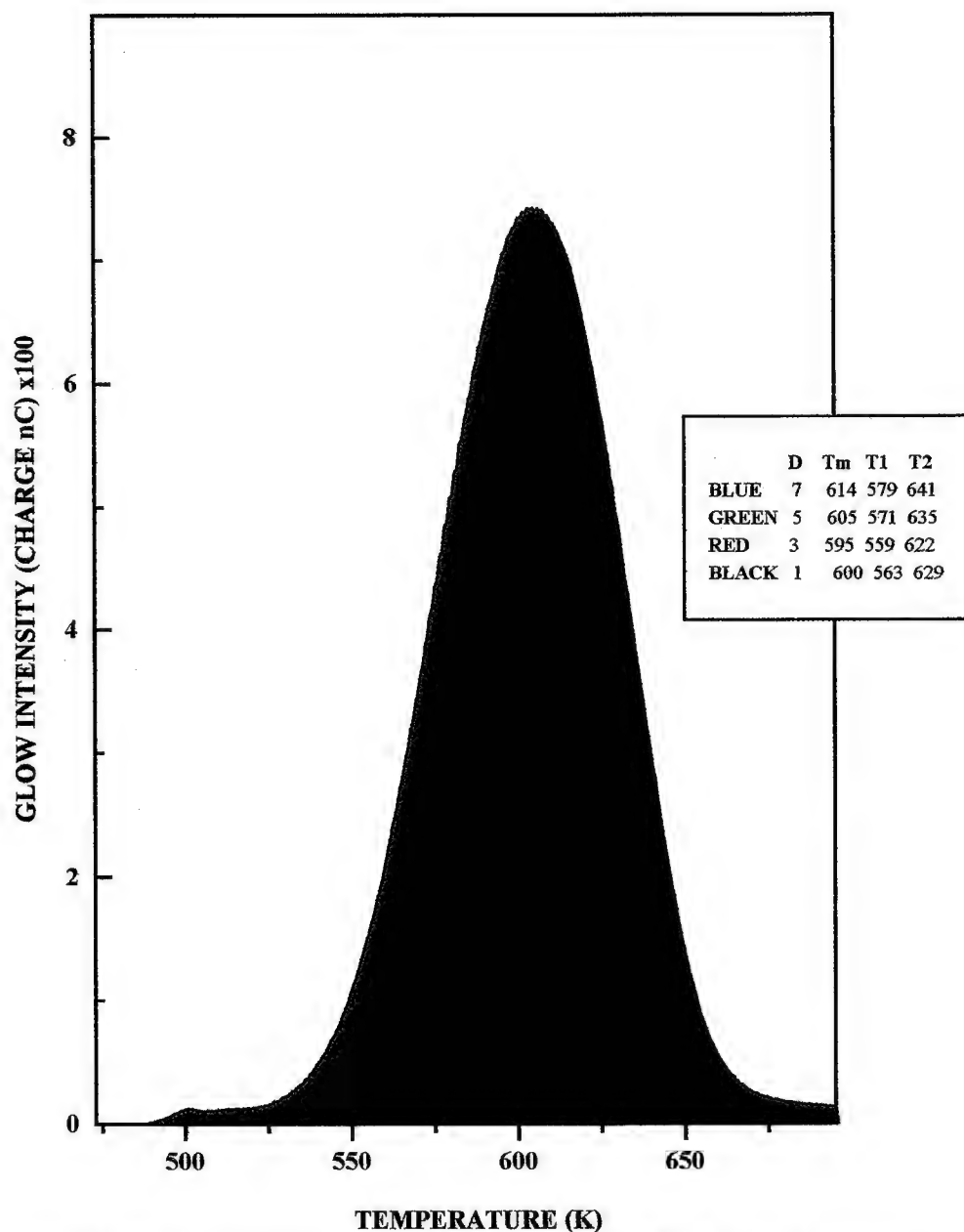


**Fig.3.6** Glow curves for a Victoreen Mn-doped Calcium Fluoride chip dosed with X-rays.

**D** Given dose in Gy.

**T<sub>m</sub>** Temp. of glow peak max intensity in (K).

**T<sub>1</sub>** Temp. of 50% intensity (rising side).

**T<sub>2</sub>** Temp. of 50% intensity (falling side).

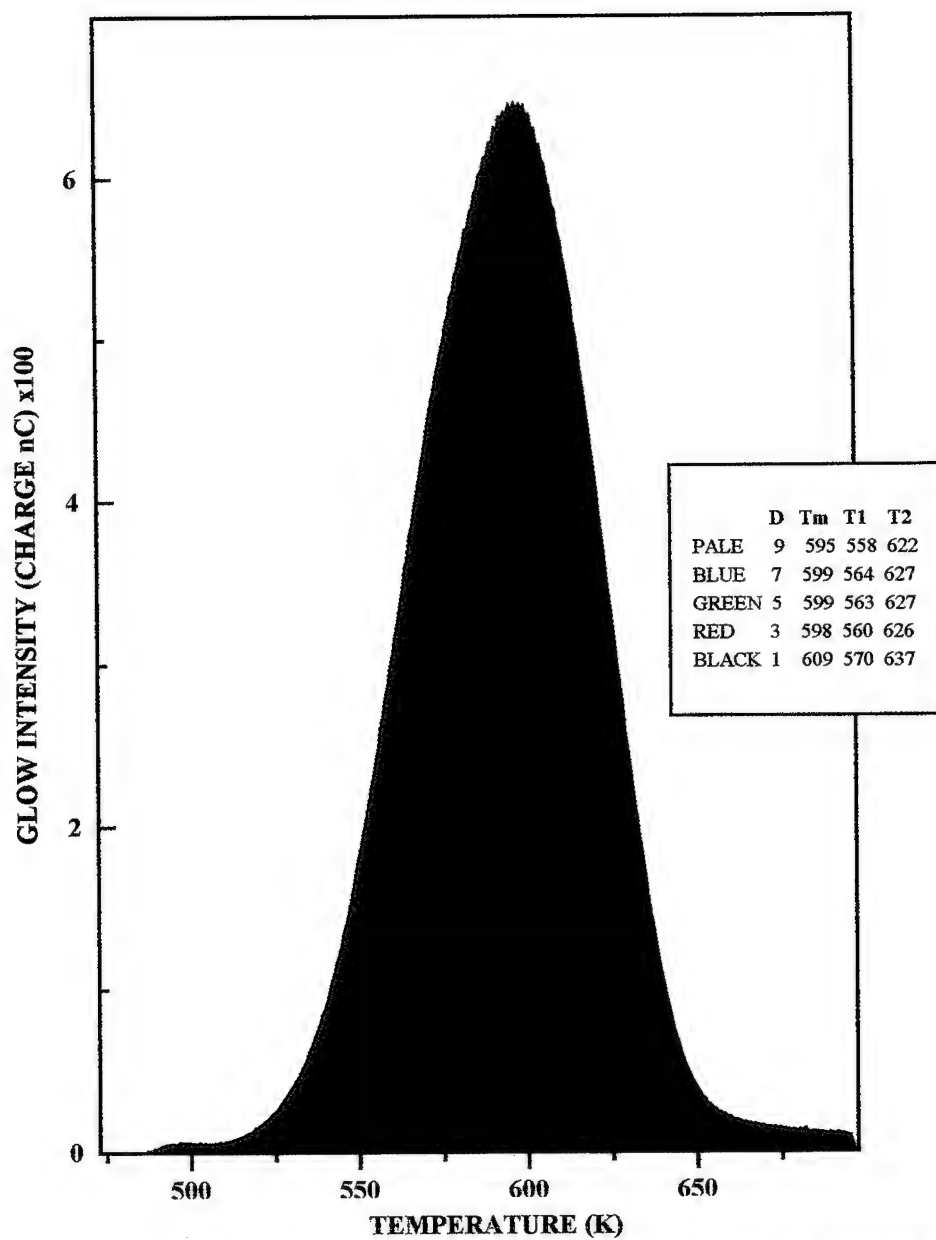


**Fig.3.7** Glow curves for a Victorecn Mn-doped Calcium Fluoride rod dosed with X-rays.

**D** Given dose in Gy.

**T<sub>m</sub>** Temp. of glow peak max intensity in (K).

**T<sub>1</sub>** Temp. of 50% intensity (rising side).

**T<sub>2</sub>** Temp. of 50% intensity (falling side).

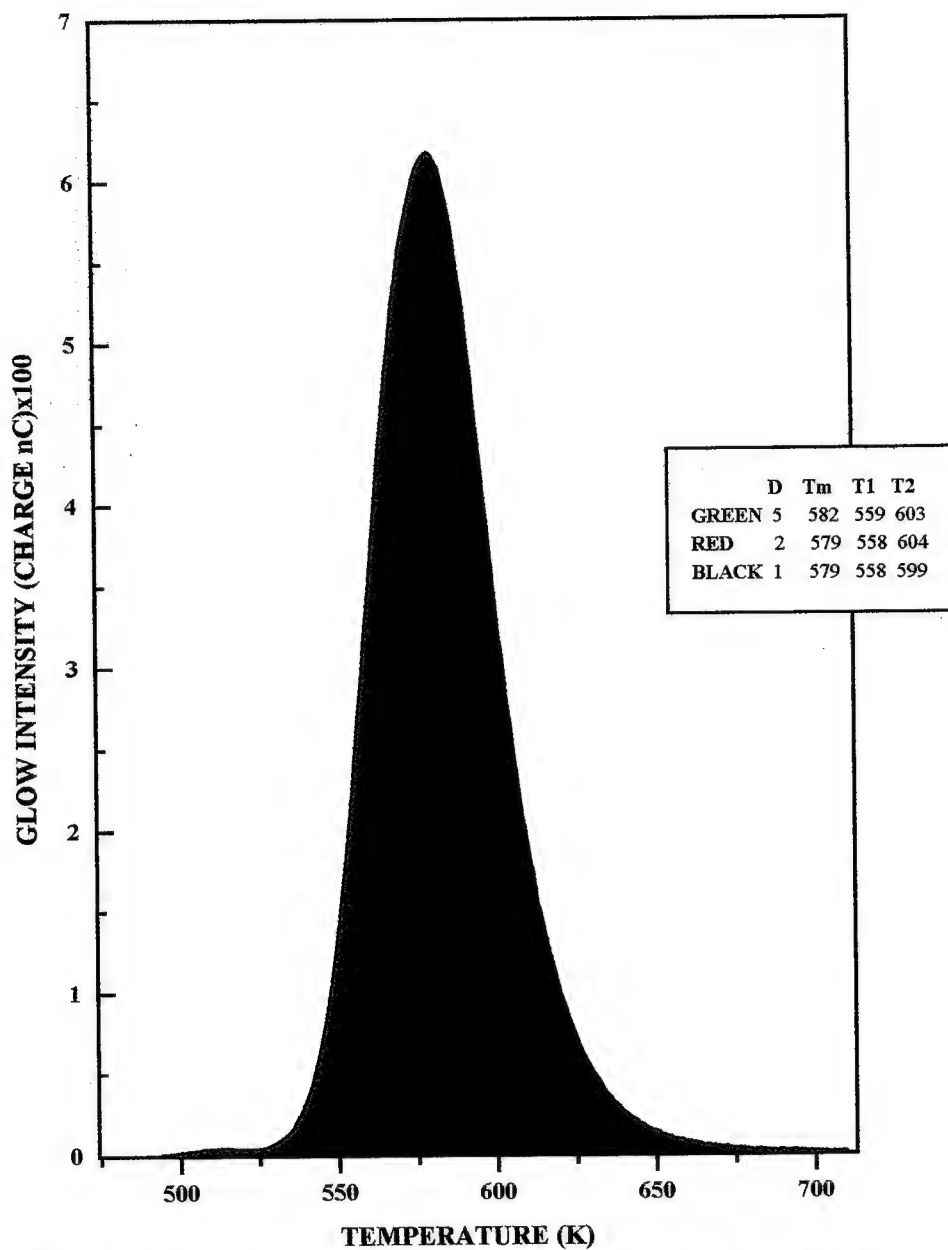


**Fig.3.8** Glow curves for a Victoreen Mn-doped Calcium Fluoride bulb dosed with X-rays.

**D** Given dose in Gy.

**T<sub>m</sub>** Temp. of glow peak max intensity in (K).

**T<sub>1</sub>** Temp. of 50% intensity (rising side).

**T<sub>2</sub>** Temp. of 50% intensity (falling side).



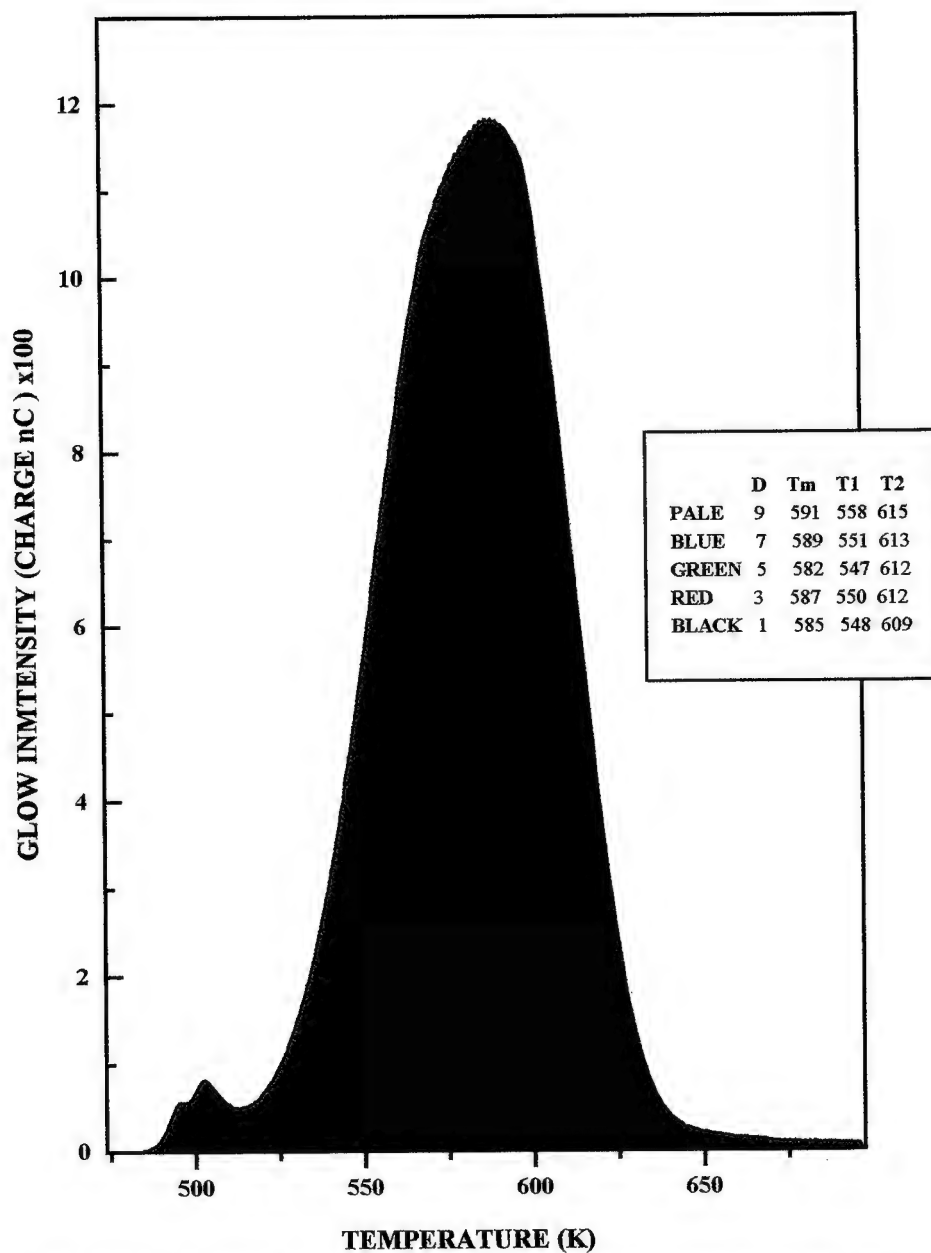


**Fig.3.9** Glow curves for a Harshaw Mn-doped Calcium Fluoride chip dosed with X-rays.

**D** Given dose in Gy.

**T<sub>m</sub>** Temp. of glow peak max intensity in (K).

**T<sub>1</sub>** Temp. of 50% intensity (rising side).

**T<sub>2</sub>** Temp. of 50% intensity (falling side).

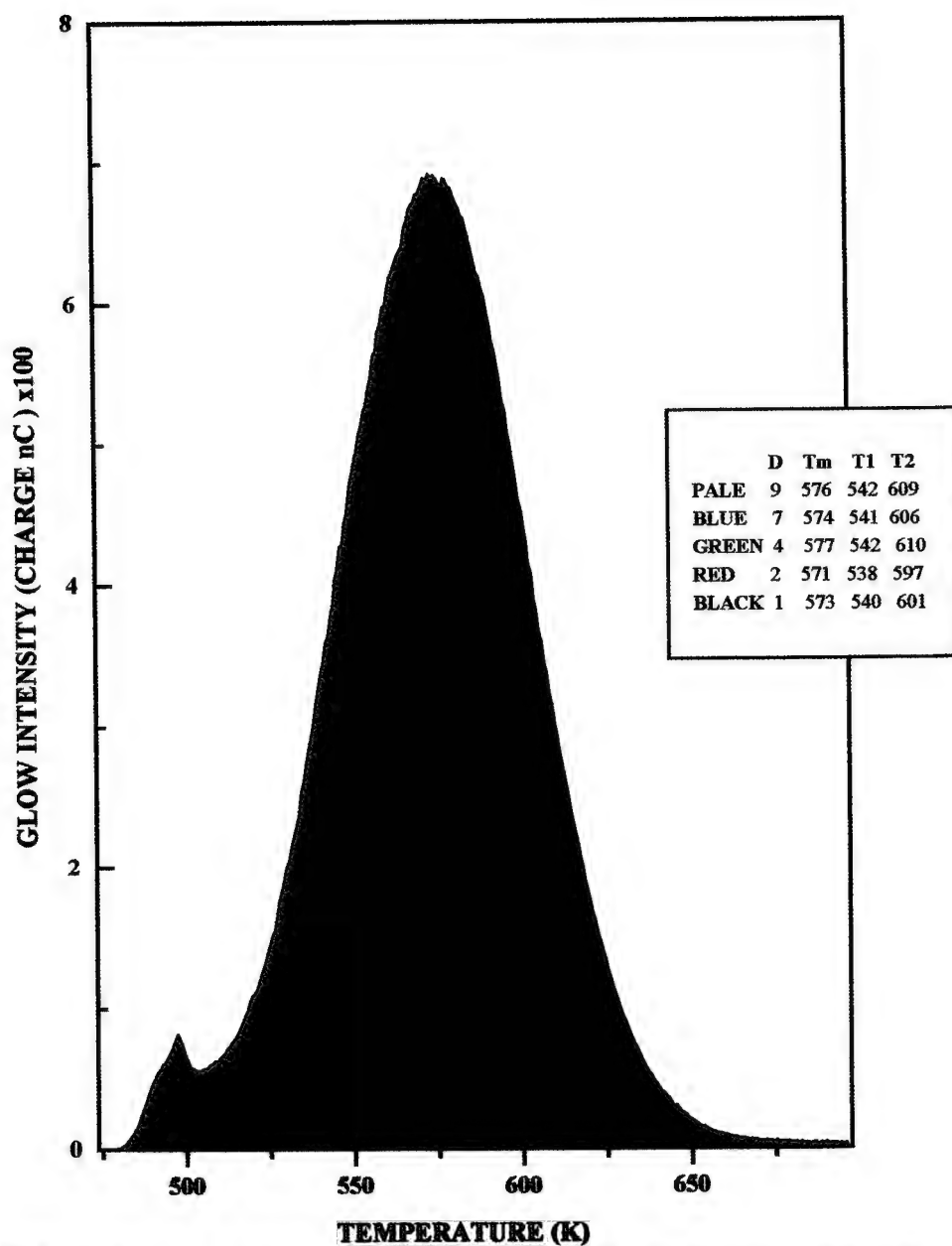


**Fig.3.10** Glow curves for a Harshaw Mn-doped Calcium Fluoride powder dosed with X-rays.

**D** Given dose in Gy.

**T<sub>m</sub>** Temp. of glow peak max intensity in (K).

**T<sub>1</sub>** Temp. of 50% intensity (rising side).

**T<sub>2</sub>** Temp. of 50% intensity (falling side).

broad peak evolved and the TL curve looks very nearly similar to the TL curves reported in the current work.

It is of interest to note that all Harshaw samples show peak temperatures  $T_m$  lower than those of the Victoreen chips or rods. The Victoreen bulb dosimeter, however, shows a peak temperature lower than those of rods and chips supplied by the same manufacturer. This could be due to the discoloration of the glass envelope by radiation. The irradiated glass envelope has been found to acquire a brown colour indicating a formation of colour centres. There is no doubt that the TL emitted by the glass during heating in the TL reader will interfere with the original TL signal of the dosimeter giving rise to a modified TL signal. For this reason, the use of  $\text{CaF}_2 : \text{Mn}$  bulbs in radiation dosimetry should be restricted to the mR range where discoloration of glass by radiation is negligible and does not pose any serious practical problem.

Before proceeding any further in discussing the TL of  $\text{CaF}_2 : \text{Mn}$ , it is important to point out some general principles and mechanisms by which energy from ionizing radiation is absorbed and stabilized by the dosimeter material; this energy being subsequently released in the form of light during sample heating.

It is well known that the processes governing the absorption of energy from ionizing radiation are energy dependent. Below about 15 KeV in most materials, the photoelectric effect dominates. For higher energies and in low effective atomic number materials, Compton scattering dominates up to about 10 MeV. For higher  $Z_{\text{eff}}$  materials, however, the photoelectric effect continues to dominate up to about 100 KeV. Stabilization of this absorbed energy takes place via two major processes namely electronic excitation and displacement damage, primary electrons liberated by photons may occasionally displace atoms from stable lattice sites by elastic collision giving rise to lattice vacancies and interstitials. Electronic excitation and atomic displacement result in damage of the material in the sense that radiation - induced defects are created or populated over and above the thermal defects and impurities already existing in the material since manufacture. A radiation -induced defect is usually defined as any non-equilibrium electronic or atomic species which exists in the material after irradiation but which was not present beforehand. Thus, an impure TLD material such as  $\text{CaF}_2$  intentionally doped with Mn may have localized electronic energy states existing within the material before irradiation, but only after irradiation do we find that some of these states are occupied by a

non-equilibrium concentration of electrons. The occupied states are radiation - induced defects; the unoccupied states, which existed at thermal equilibrium prior to radiation, are not. Additionally, one might find within the material host lattice atoms existing in interstitial positions after energy absorption. The interstitial atom and the vacancy it left behind are defects; the same atom in its original site is not. Defect creation by the process of electronic excitation and displacement damage has been the subject of research for decades and many detailed review articles exist concerning defect creation by radiation in several materials of interest to TLD researchers, including alkali halides (e.g. LiF [119-121]), alkaline earth halides (e.g. CaF<sub>2</sub> [122]) and oxides (e.g. MgO [123-125]). Calculations for photon irradiation show that defect formation caused by electronic excitation (ionization) dominates over non-ionizing displacement damage [126].

Energy storage via electronic excitation occurs via the processes of electron - hole pair production and exciton creation. These electron entities have wavefunctions which are not localized on any particular site within the sample and as a result significant energy migration can occur after absorption. Stabilization of the absorbed energy, therefore, requires a mechanism for localization of

these electronic species at lattice sites. For free electrons and holes, localization occurs via the processes of non-radiative charge trapping. Excitons are short-lived electron-hole pairs, bound by their coulombic field, but which are able to move through the lattice before annihilation occurs. Localization of these electronic entities can occur before annihilation via the process of "self-trapping". Various self-trapping configurations are possible, depending upon the host material [119-125].

It follows from the above discussion that lattice disorder, existing in the specimen before irradiation, enhances energy storage either by providing localized trapping states for free electrons and holes or by stabilizing interstitial atoms and vacancies. It is not surprising, therefore, to find that most sensitive TLD materials such as  $\text{CaF}_2:\text{Mn}$  are intentionally impure. However, this is not meant to imply that more defects necessarily means more TL since non-radiative sites and competing centres, for example, can decrease the luminescence yield per absorbed dose. Thus, the key to making a sensitive TLD material is to add controlled amounts of the desired dopants, such as manganese, in numbers in excess of the uncontrollable intrinsic defects and background impurities. Referring back to the TL curves of  $\text{CaF}_2:\text{Mn}$  shown in the previous

figures, it is now possible to discuss the origin of these peaks and the TL mechanism involved.

The small satellite glow peak appearing on the low temperature side of the main dosimetric peak is probably caused by the existence of trace quantities of background, rare earth impurities. Several authors[127,128] have noted the presence of such small, satellite peaks on either side of the main TL signal and were attributed to the same reason. In a detailed study by McMasters et al [129] it was shown how the glow curve from  $\text{CaF}_2\text{:Mn}$  evolves as the Mn content is increased. At low Mn levels, the TL (and optical spectra) are dominated by trace quantities of rare earths. As the Mn content increases competition effects take over, and the TL and absorption properties become characteristic of Mn; however, background effects due to rare earth impurities can still be discerned. It is important to remember in this context that, although doped during growth with 3 mol %  $\text{MnF}_2$  in the melt, only approximately 1.4 - 1.6 mol% Mn finds its way into the final  $\text{CaF}_2$  sample [129].

The effect of such background impurities on the dosimetry properties of this material is that they give rise to a certain amount of non-universality. Certainly one can expect batch-to-batch

variations in the TL sensitivity, overall shape and position of the main TL peak and the TL fading rate[130]. De Planque [131] compiles extensive data on the fading of TL from  $\text{CaF}_2\text{:Mn}$  and demonstrates an enormous spread in the observed fading rates obtained by different research groups. In many instances the samples used by these groups were from different manufacturers; or, if from the same manufacturer, they were almost certainly from different batches. Similarly, Horowitz [13] notes a wide variation in the observed LET response of  $\text{CaF}_2\text{:Mn}$  which led him to speculate that variation in the trace impurity content at the ppm level has a profound effect on the TL properties. One is led to conclude that it is the extreme sensitivity of TL to the presence of small quantities of impurities (the very property that makes TL an exciting dosimetric tool) that is causing problems with non-universality.

Several mechanisms have been suggested for the production of TL in  $\text{CaF}_2\text{:Mn}$ . Each mechanism results finally in the de-excitation of the  $\text{Mn}^{2+}$  ion to the ground state. The first model was proposed by Schulman [132] who envisioned the trapping of a hole by  $\text{Mn}^{2+}$  during irradiation to become  $\text{Mn}^{3+}$  with the compensating electron being trapped at unidentified sites elsewhere in the crystal. During TL readout, the electron is released to recombine with the



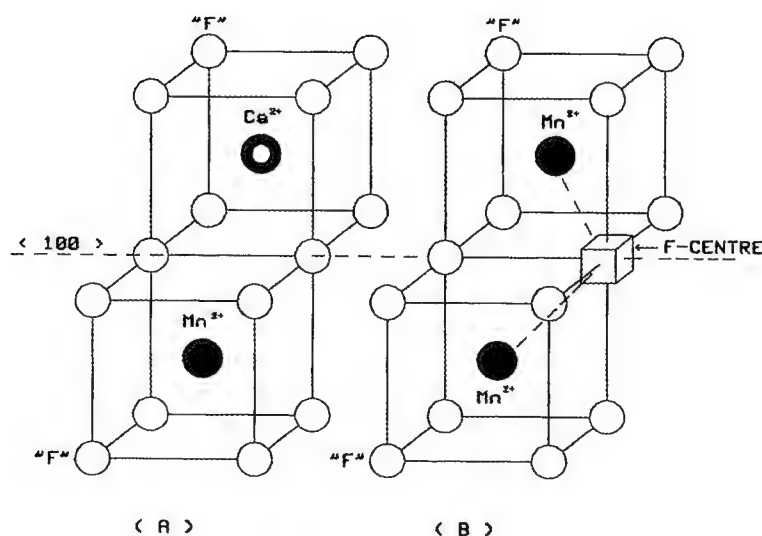
$\text{Mn}^{3+}$  centre to form  $\text{Mn}^{2+}$  in an excited state. Relaxation of the  $\text{Mn}^{2+}$  ion produces TL emission at 495 nm.

An alternative suggestion was given by Alcala et al [105,133] who proposed the trapping of an electron by the  $\text{Mn}^{2+}$  ion to become  $\text{Mn}^+$ , with holes being trapped elsewhere. Raising the temperature releases holes which recombine with trapped electrons, again resulting in  $\text{Mn}^{2+}$  in an excited state. However, a study of thermally stimulated exoemission (TSEE) in  $\text{CaF}_2 : \text{Mn}$  [134] did not reveal a TSEE peak which could be correlated with the TL peak and therefore, no evidence of electron release during the production of TL. On this evidence, one would have to rule out the mechanism suggested by Schulman.

Sunta [134] suggested a different model entirely. He presented a mechanism in which the luminescence from Mn is activated by the presence of background rare earth impurities, notably  $\text{Ce}^{3+}$  ions. In this process, the  $\text{Ce}^{3+}$  ions trap electrons, with holes trapped elsewhere at unspecified centres. Heating releases the holes which recombine at the  $\text{Ce}^{2+}$  site, producing  $\text{Ce}^{3+}$  in an excited state. Non-radiative relaxation of the excited  $\text{Ce}^{3+}$  ions then occurs via energy transfer to  $\text{Mn}^{2+}$ . Subsequent relaxation of the excited  $\text{Mn}^{2+}$  ions results in TL emission at 495 nm. However, detailed examination of

this possibility by Jassemnejad and colleagues [135, 136] led to the conclusion that rare earths, such as Ce, act as competitors to the production of TL from Mn, not as sensitisers. This fact gives  $\text{CaF}_2\text{:Mn}$  its high sensitivity to background traces of rare earth impurities.

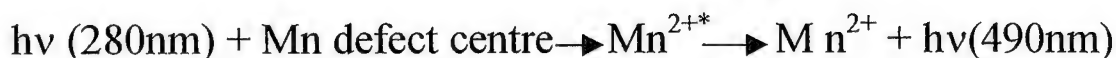
Studies of the optical properties of irradiated  $\text{CaF}_2\text{:Mn}$  by McKeever and colleagues [137, 138] suggest the production of perturbed F centres in the material following irradiation at room temperature with the complementary H centres being trapped elsewhere in the crystal. A ( $\text{Mn}^{2+}$  - F centre) complex is formed which consists of an  $\text{Mn}^{2+}$  ion substituting for  $\text{Ca}^{2+}$  ion and an F centre residing in a nearest fluorine site in a  $\langle 100 \rangle$  direction as shown below in the diagram where part (A) represents the crystal lattice of  $\text{CaF}_2\text{:Mn}$  before irradiation showing the substitutional site for Mn and the 8-fold coordination while part (B) shows the F-centre perturbed by two  $\text{Mn}^{2+}$  ions and formed after irradiation of the Mn-doped  $\text{CaF}_2$ .



Thus, a possible model consists of an  $[\text{Mn}^{2+} - \text{F} \text{ centre} - \text{Mn}^{2+}]$  complex termed as  $\text{F}_\text{A}$  centre, that is, an F centre perturbed by two  $\text{Mn}^{2+}$  ions as shown above. The TL process is supposed to involve an  $\text{F}_\text{A} - \text{H}_\text{A}$  recombination process, where  $\text{H}_\text{A}$  centre is an impurity stabilized H centre ( interstitial fluorine ion which has captured a hole; i.e.interstitial fluorine atom) . A similar mechanism of F centre and H centre recombination has been suggested before [139]. The  $\text{F}_\text{A} - \text{H}_\text{A}$  recombination produces light of 280 nm, which is subsequently reabsorbed by the defect centre resulting in an excited state of  $\text{Mn}^{2+}$  emitting 490 nm radiation. Thus, a possible TL mechanism can be represented as follows:



and:



Theoretical studies of Lewandowski [140] of the ( $\text{Mn}^{2+}$ -F centre -  $\text{Mn}^{2+}$ ) defect complex, however, do not support this model of  $F_A$  centre. According to their calculations, the Mn-perturbed F centre is not a stable configuration at room temperature and, therefore, the observed absorption bands cannot be attributed to transitions "within" the F - centre. Their work supports an alternative model of Mn ion perturbed by a vacancy, where the observed absorption may arise due to  $d \rightarrow d$  transitions within the Mn ion. In view of these two divergent results, one can stress the need for more investigations in order to understand the physical mechanism of TL in  $\text{CaF}_2 : \text{Mn}$ . It is amazing that after more than 40 years of research, the models describing the TL of this material can be only considered as part of the story.

### **3.2 Analysis Of The Main Dosimetric Peak Of $\text{CaF}_2:\text{Mn}$**

The characteristic TL curve of  $\text{CaF}_2 : \text{Mn}$  consists essentially of a main dosimetric peak. The behaviour of this peak led some authors to suggest first-order kinetics (e.g. Ref. 127). If we assume the validity of such monomolecular glow process, then it is easy to

calculate the activation energy , $E$ , (i.e. the trap depth) and the escape frequency factor,  $s$  , for the trapping states present . This can be done by any of the several methods available for this purpose. Two methods have been used in the present work: the first is due to Grossweiner [52] which makes use of the temperature ,  $T_1$ , of half-maximum TL intensity on the low temperature side of the peak while the second method is that suggested by Chen [42] which relies on the temperature ,  $T_2$ , of half-maximum intensity on the high temperature side of the peak. The resulting values are shown in tables (3.1) , (3.2) and (3.3) where ranges of the activation energy values and the escape frequency factors as well as the corresponding average values are given. Apparently, the two methods used yield slightly different values of  $E$  and  $s$ . Nevertheless, if we exclude the bulb dosimeter with its associated discoloration problem, the calculated values of the two parameters fall reasonably well within the range of values reported by other authors [11,84] ; published activation energy values varied from 0.95 eV to 1.4 eV while the frequency factors ranged from  $1.87 \times 10^7 \text{ s}^{-1}$  to  $2.8 \times 10^{12} \text{ s}^{-1}$ . The large scatter in reported values is being ascribed to differences in sample physical configuration, its origin of supply , the type of kinetics

assumed and the method adopted for calculation. This widespread in the  $E$  and  $s$  values led to the belief that the main dosimetric peak is caused by either several closely spaced (in energy) traps or results from a continuous distribution of traps. These notions were first expressed by some earlier researchers [141-143] based on annealing studies and were supported later by measurements of photo-transferred TL (PTTL) which gave a PTTL peak of a significantly different shape from that of the original TL peak. In fact, the PTTL data strongly suggest that the dosimetric peak of  $\text{CaF}_2\text{:Mn}$  is made up of at least two, closely overlapping, but discrete TL peaks, rather than a single peak caused by a continuous distribution of activation energies. Hornyak et al [127] analyzed the main dosimetric peak for kinetic behaviour and reported activation energy values ranging from 0.97 eV to 1.37 eV ; the highest value being obtained from the initial rise method [3]. Moreover, they showed the activation energy of the dosimetric peak to increase in value with increase in preheating temperature ; a result which indicated that the dosimetric peak may consist of several discrete overlapping peaks.

Table 3.1  
Calculated values of the trap depth (E)  
for the main TL peak (Co- 60 irradiation )

Name of supplier	Dosimeter type	Grossweiner's Method		Chen's Method	
		Range of E (eV)	Average E (eV)	Range of E (eV)	Average E (eV)
Victoreen	Chip	1.17 – 1.31	$1.24 \pm 0.06$	1.15 – 1.17	$1.17 \pm 0.01$
	Rod	1.14 – 1.26	$1.21 \pm 0.06$	1.13 – 1.24	$1.17 \pm 0.06$
	Bulb	1.82 – 2.01	$1.96 \pm 0.09$	1.66 – 1.37	$1.70 \pm 0.16$
Harshaw	Chip	1.12 – 1.55	$1.37 \pm 0.16$	1.15 – 1.56	$1.37 \pm 0.16$
	powder	1.13 – 1.37	$1.22 \pm 0.11$	1.16 – 1.23	$1.16 \pm 0.05$

Table 3.2  
Calculated values of the trap depth (E)  
for the main TL peak (X-ray irradiation )

Name of supplier	Dosimeter type	Grossweiner's Method		Chen's Method	
		Range of E (eV)	Average E (eV)	Range of E (eV)	Average E (eV)
Victoreen	Chip	1.19 – 1.31	$1.26 \pm 0.07$	1.18 – 1.32	$1.24 \pm 0.06$
	Rod	1.15 – 1.26	$1.19 \pm 0.05$	1.18 – 1.24	$1.21 \pm 0.03$
	Bulb	1.84 – 2.00	$1.95 \pm 0.09$	1.58 – 1.78	$1.68 \pm 0.10$
Harshaw	Chip	1.11 – 1.30	$1.17 \pm 0.08$	1.21 – 1.33	$1.22 \pm 0.07$
	powder	1.16 – 1.22	$1.20 \pm 0.03$	1.06 – 1.20	$1.12 \pm 0.06$



Table 3.3  
Calculated values of the escape frequency factor,  
 $s$  ( $\text{sec}^{-1}$ ), for the main TL peak

Radiation source	Name of supplier	Dosimeter type	Grossweiner's Method		Chen's Method	
			Range of $s$	Average $s$	Range of $s$	Average $s$
Co - 60	Victoreen	Chip	(0.30 - 5.55) E10*	(2.12)E10	(0.28 - 0.49) E9	(0.39)E9
		Rod	(0.16 - 2.42) E10	(1.26)E10	(0.20 - 1.68) E9	(0.71)E9
		Bulb	(0.05 - 1.98) E17	(1.43)E17	(2.07 - 9.93) E13	(6.56)E13
	Harshaw	Chip	(0.01 - 15.23) E12	(4.57)E12	(0.01 - 024.50) E11	(6.46)E11
		powder	(0.02 - 4.30) E11	(1.14)E11	(0.41 - 2.90) E9	16.19)E9
X-rays	Victoreen	Chip	(0.37 - 4.32) E10	(2.04)E10	(0.46 - 3.79) E10	(1.56)E10
		Rod	(0.14 - 1.50) E10	(0.56)E10	(0.43 - 1.38) E9	(0.80)E9
		Bulb	(0.6 - 1.84) E17	(1.24)E17	(0.04 - 2.37) E14	(0.88)E14
	Harshaw	Chip	(0.12 - 5.30) E10	(1.31)E10	(0.03 - 1.33) E10	(0.36)E10
		powder	(0.58 - 2.43) E10	(1.37)E10	(0.01 - 2.20) E9	(0.73)E9

\*E (X) =  $10^{(x)}$

Further evidence in support of the previous views is provided in the present work. We describe here the attempts made to construct a theoretical dosimetric peak from equation (1.5) using the tabulated values of  $E$  and  $s$  and assuming a monomolecular glow process; i.e. traps of a single energy depth. The resulting theoretical peak is then compared with the corresponding experimental peak to assess whether or not the latter is being due to the same specific traps. The theoretical calculations are performed as follows:

Starting with equation (1.5), it can be re-written as:

$$I = cn_0 s \cdot \exp \left[ - (s/\beta) \int_0^T \exp (-E / kT') dT' \right] \cdot \exp (-E / kT) \quad (3.1)$$

In order to evaluate the integral  $\left[ \int_0^T \exp (-E / kT') dT' \right]$ , let us consider the exponential function  $E_2(u)$  defined by :

$$E_2(u) = \int_1^\infty (dx/x^2) \cdot \exp (-ux) \quad (3.2)$$

If we let :  $y = ux$ ,

$$\text{then : } (dx/x^2) = u (dy/y^2) \quad (3.3)$$

$$\text{and : } \int_1^\infty (dx/x^2) \cdot \exp (-ux) = u \int_u^\infty (dy/y^2) \exp (-y) = E_2(u) \quad (3.4)$$

$$\text{Hence, } \int_u^\infty (dy/y^2) \exp (-y) = (1/u) E_2(u) \quad (3.5)$$

Now, consider the integral :  $\int_0^T \exp (-E / kT') dT'$  in equation (3.1),

$$\text{and let : } y = (E / kT') \quad (3.6)$$

$$\text{then : } dT' = - (k / E) T'^2 dy$$

$$= - (k / E) (E^2 / k^2 y^2) dy$$

$$= - (E / k) (dy / y^2) \quad (3.7)$$

From (3.6), when  $T' = 0$ , then  $y = \infty$ ; and when  $T'$  has any value other than zero, then :  $y = (E / kT')$ .

$$\text{Thus : } \int_0^{T'} \exp(-E / kT') dT' = - \int_{\infty}^{E/kT'} (E/k) \exp(-y) (dy/y^2) \quad (3.8)$$

$$\text{or : } \exp(-E / kT') dT' = \int_{E/kT'}^{\infty} (E/k) \cdot \{[\exp(-y)]/y^2\} \cdot dy \quad (3.9)$$

Now, by equation (3.6) above :

$$(E/k) \int_{E/kT'}^{\infty} \exp(-y) \cdot dy / y^2 \cdot dy = (E/k)^{-1} \cdot E_2(E/kT) \quad (3.10)$$

or :

$$(E/k) \int_{E/kT'}^{\infty} \exp(-y) \cdot dy / y^2 \cdot dy = T E_2(E/kT) \quad (3.11)$$

When  $(E/kT)$  is  $> 25$ , the exponential function  $E_2(E/kT)$  may be approximated with less than 10% error by the relationship:

$$E_2(E/kT) \cong \exp(-E/kT) / (E/kT) \quad (3.12)$$

Substituting (3.11) into (3.1) gives :

$$I = c n_0 s \cdot \exp[-\{(sT/\beta) \cdot E_2(E/kT) + (E/kT)\}] \quad (3.13)$$

Thus, by use of the approximation (3.12), equation (3.13) can be evaluated at various values of  $T$  and the theoretical TL peak can be

calculated. Since the values of the constants  $c$  and  $n_0$  are not known, the values of  $I$  obtained are relative rather than absolute and must be normalized for comparison with the experimental curve. This is done by equating the theoretical value of  $I$  at the TL peak maximum to the experimental value of  $I$  at the maximum. Normalized theoretical values of  $I$  at other temperatures are then obtained by simple proportion. The theoretical TL peaks are shown in figures (3.11) to (3.15); the normalized experimental peaks are included in the figures for comparison. It is evident that no agreement exists between the theoretical and experimental peaks of the same TLD sample. This result suggests that the experimental dosimetric peak is not caused by traps of a single energy depth. Indeed, this TL peak is made up of two components  $C_1$  and  $C_2$  which are obtained by simple subtraction.

Clearly, even now after more than 40 years of use, the simple TL curve of  $\text{CaF}_2:\text{Mn}$  is far from fully characterized. One may conclude by saying that an average activation energy of about 1.23 eV can be assigned to the TL emission from the material and that the TL curve appears to be made up of two, closely spaced, discrete TL peaks.

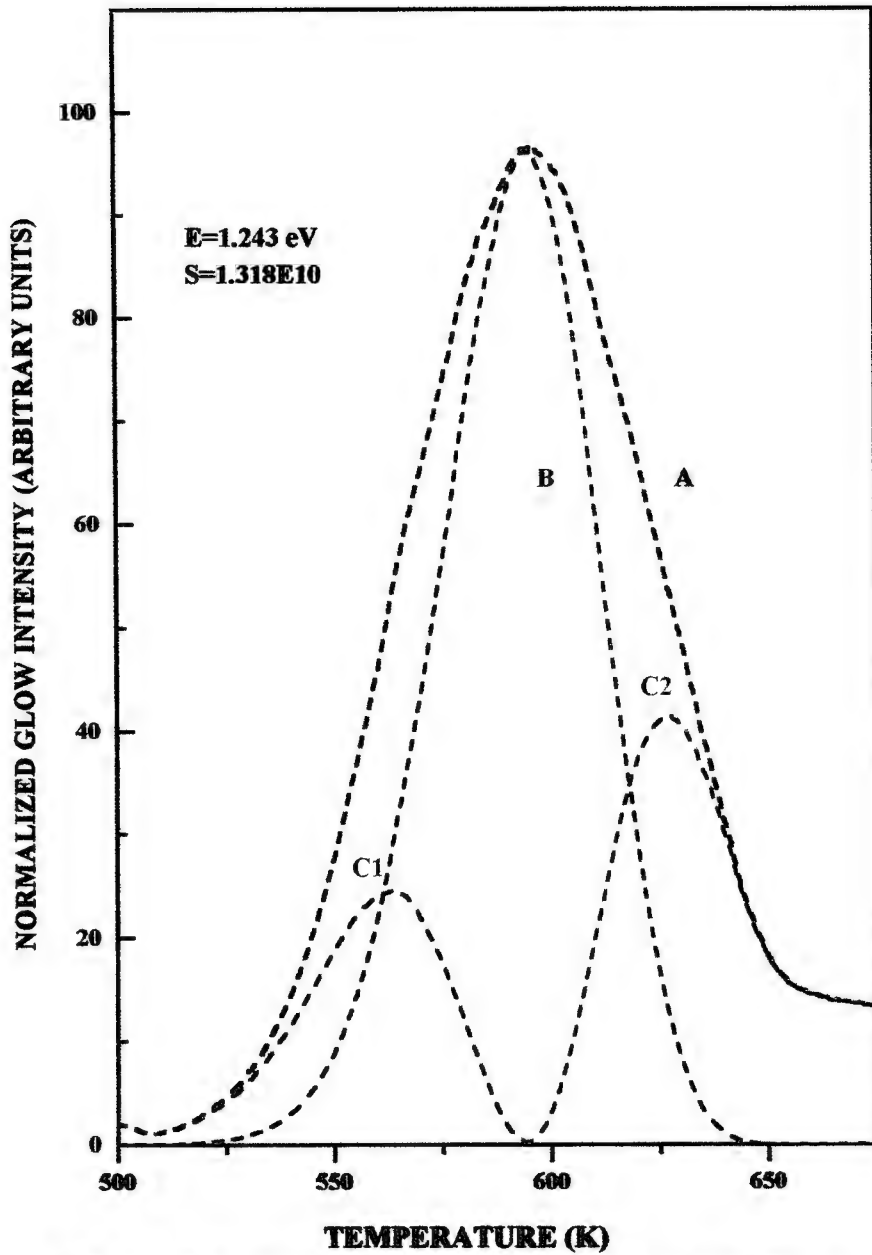


**Fig.3.11** The main glow peak for a Victoreen Mn-doped Calcium Fluoride chip dosed with 1 Gy Cobalt-60 gamma-rays. (A) Experimental (B) Theoretical (C) Components C1 and C2 of the experimental peak.

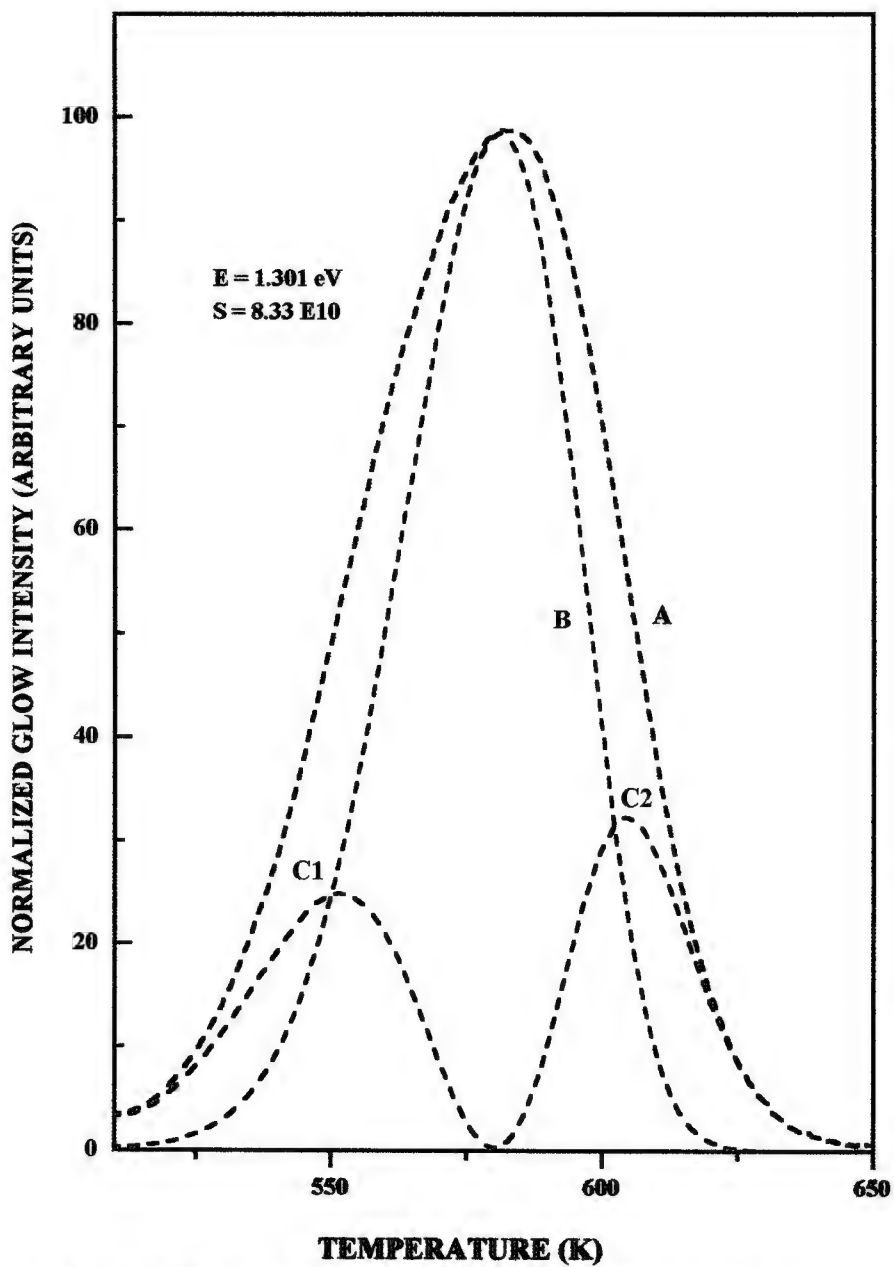


**Fig.3.12** The main glow peak for a Harshaw Mn-doped Calcium Fluoride chip dosed with 2 Gy Cobalt-60 gamma-rays. (A) Experimental (B) Theoretical (C) Components C1 and C2 of the experimental peak.

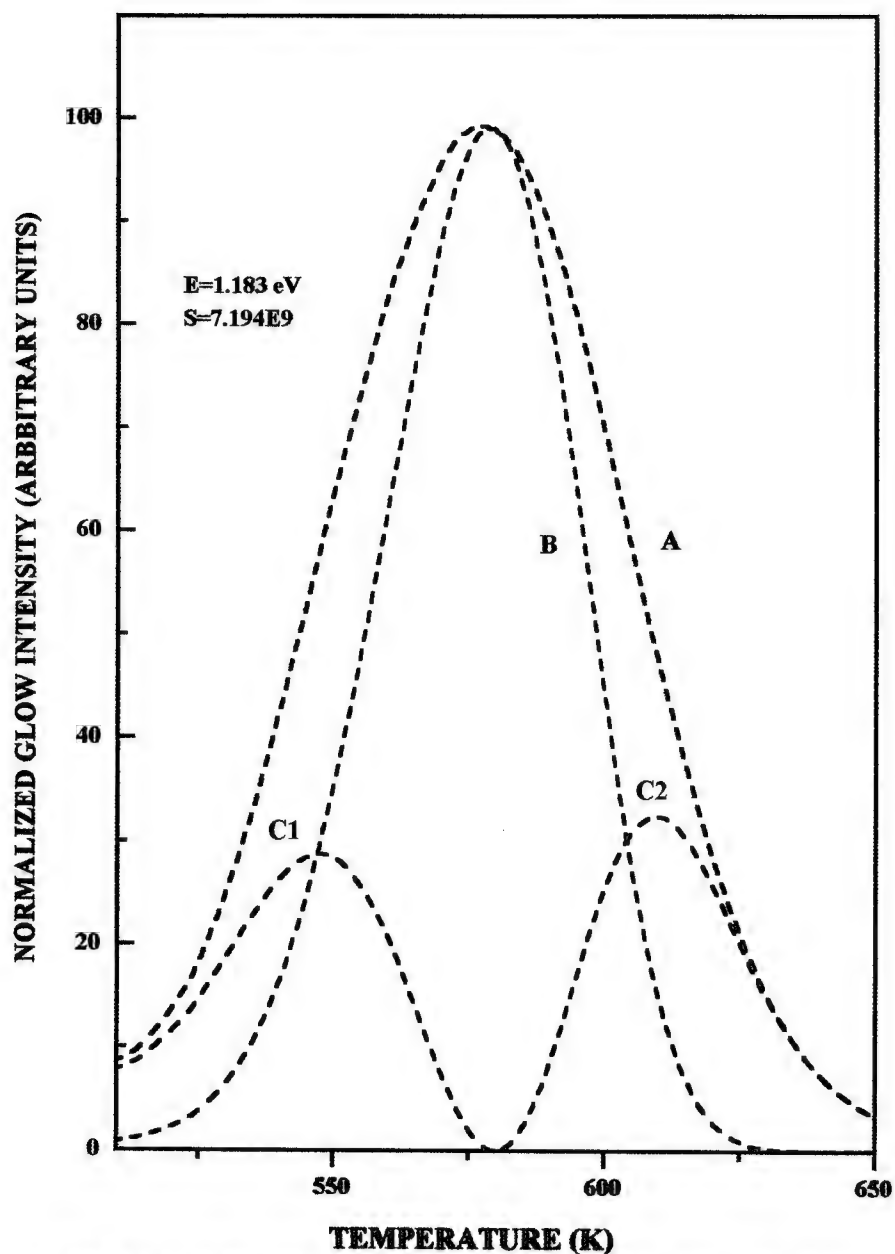


**Fig.3.13** The main glow peak for a Harshaw Mn-doped Calcium Fluoride powder dosed with 4 Gy X-rays.  
(A) Experimental (B) Theoretical (C) Components C1 and C2 of the experimental peak.

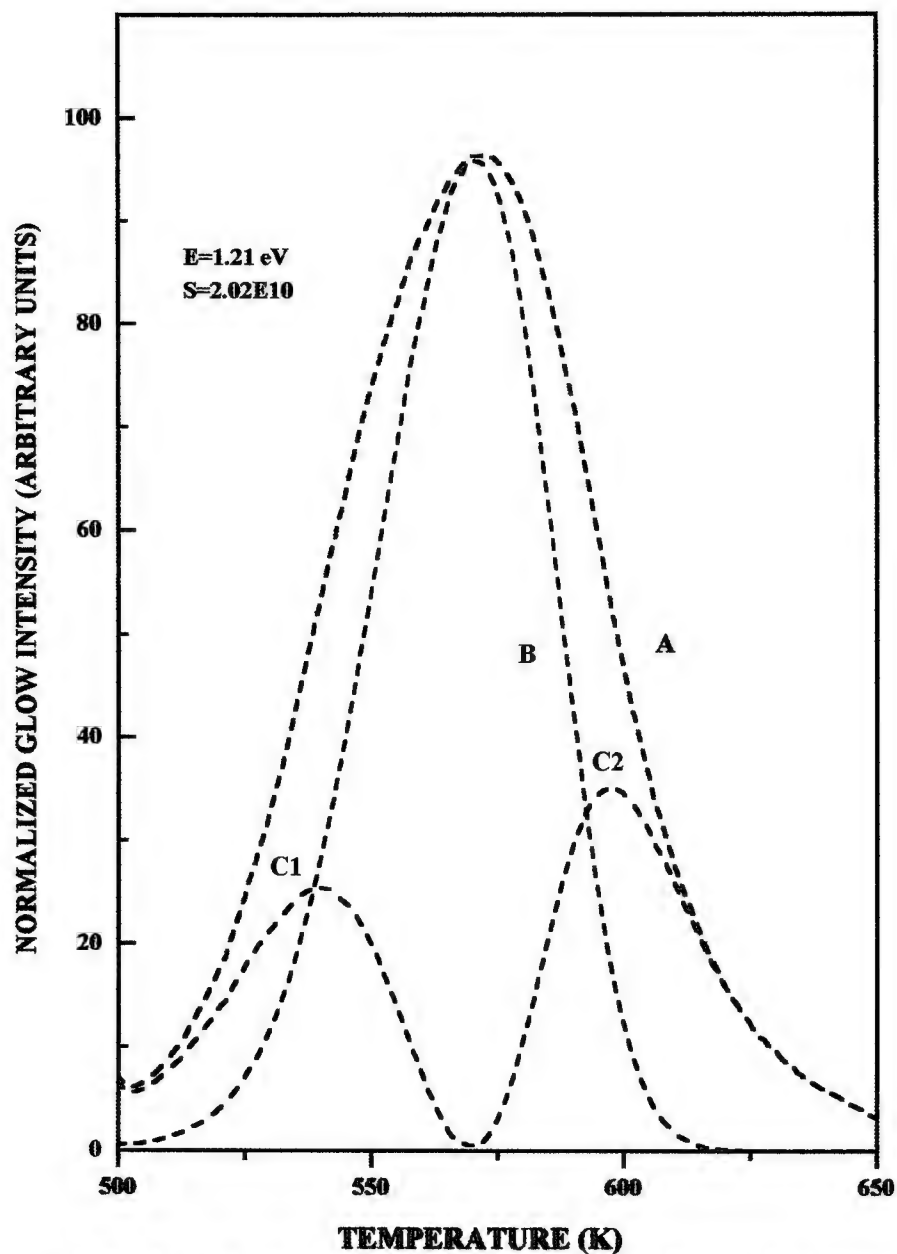


**Fig.3.14** The main glow peak for a Harshaw Mn-doped Calcium Fluoride powder dosed with 5 Gy Cobalt-60 gamma-rays. (A) Experimental (B) Theoretical (C) Components C1 and C2 of the experimental peak.



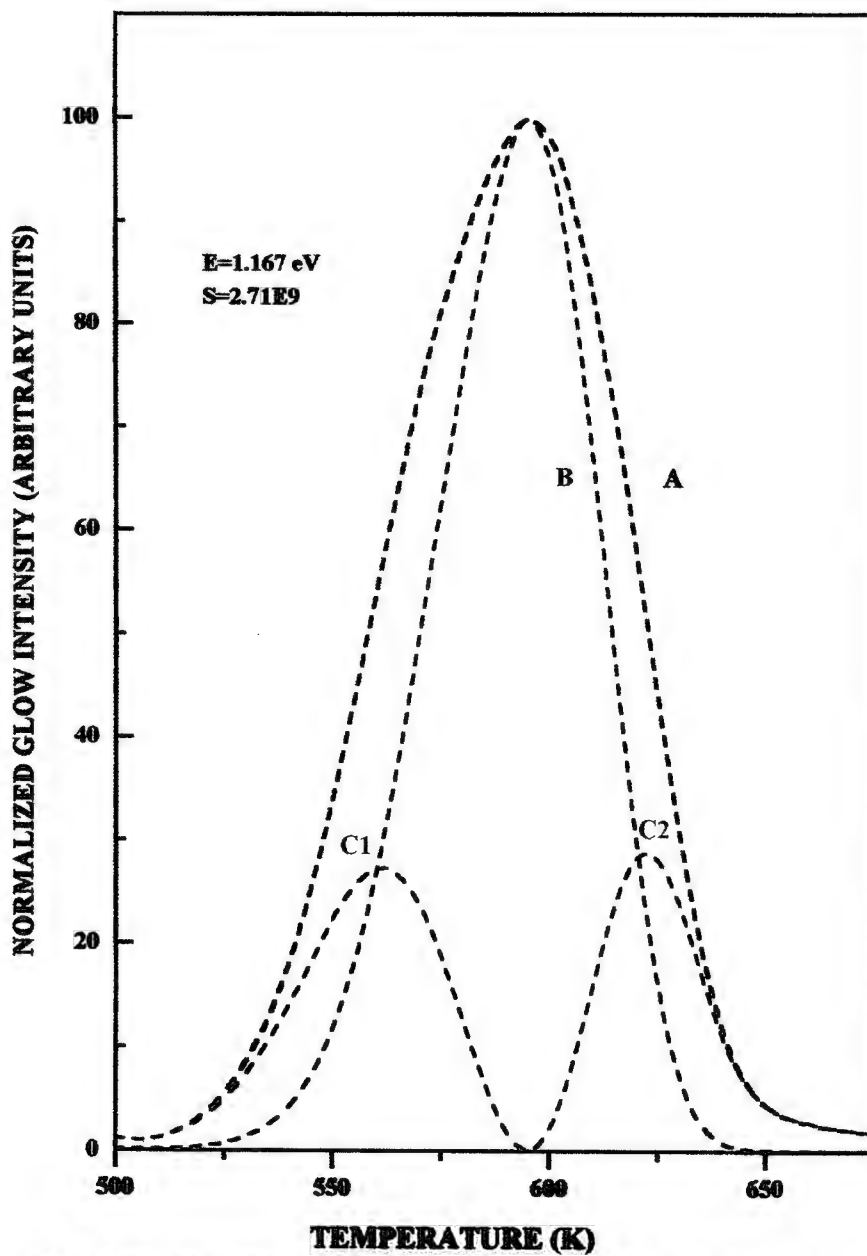


**Fig.3.15** The main glow peak for a Victoreen Mn-doped Calcium Fluoride rod dosed with 9 Gy X-rays.  
 (A) Experimental (B) Theoretical (C) Components C1 and C2 of the experimental peak.

### 3.3 Dosimetric Properties Of $\text{CaF}_2\text{:Mn}$

Synthetic manganese-doped calcium fluoride has been found to be a good material for dosimetry. The dosimeters proved to be rugged in the sense that the TL intensity remains unaffected by numerous exposure and heating cycles.

Irradiated  $\text{CaF}_2\text{:Mn}$  doped with 3 mol% of Mn concentrations exhibits a main broad TL peak appearing at temperatures very much higher than that of the room. An average value of 6 percent fading of the dose has been found for the Victoreen dosimeters during the first 24 hours of storage at room temperature (5% for chips, 7% for bulbs and 6% for rods). The rate of fading decreased with time and it was only about 12 percent for a storage period of one year. The Harshaw samples showed similar fading trends. Dekker [144] reported that most of the fading of  $\text{CaF}_2\text{:Mn}$  (about 5%) occurred during the first 24 hours and then it appeared to stabilize at 8% after two days. This anomalous initial fading rate has been examined by assuming that the apparent single dosimetric peak of  $\text{CaF}_2\text{ Mn}$  is in fact made up of traps having different degrees of thermal stability [145]. The data compiled by de Planque [131] show a widespread of fading rates for  $\text{CaF}_2\text{: Mn}$  by different research groups and point out to a degree of non- universality in the batch preparation.

The dose response of  $\text{CaF}_2:\text{Mn}$  to cobalt - 60 gamma radiation was investigated . The results are displayed in figures (3.16) and (3.17) for the Victoreen and Harshaw dosimeters respectively. The dose response is defined as the functional dependence of the intensity of the measured TL signal upon the absorbed dose. An ideal dosimeter would have a linear dose response over a wide dose range but unfortunately most TLD materials used in practical dosimetry display a variety of non - linear effects. The dose response figures show a linear dose response for all dosimeters over the dose ranges used. It should be noted that it was not possible in practice to exceed the upper dose limit of 30 Gy for the bulb dosimeter due to the under response observed which is attributed to the discoloration of the glass envelope. It is also of interest to observe the exact similarity in dose responses of the Victoreen and Harshaw chips but this is however expected because of the equal masses and thicknesses of these chips.

McKeever et al [17] defined a normalized dose response function as:

$$f(D) = [F(D) / D] / [F(D_1) / D_1] \quad (3.14)$$

where  $F(D)$  is the dose response at a dose  $D$  and  $F(D_1)$  is the dose

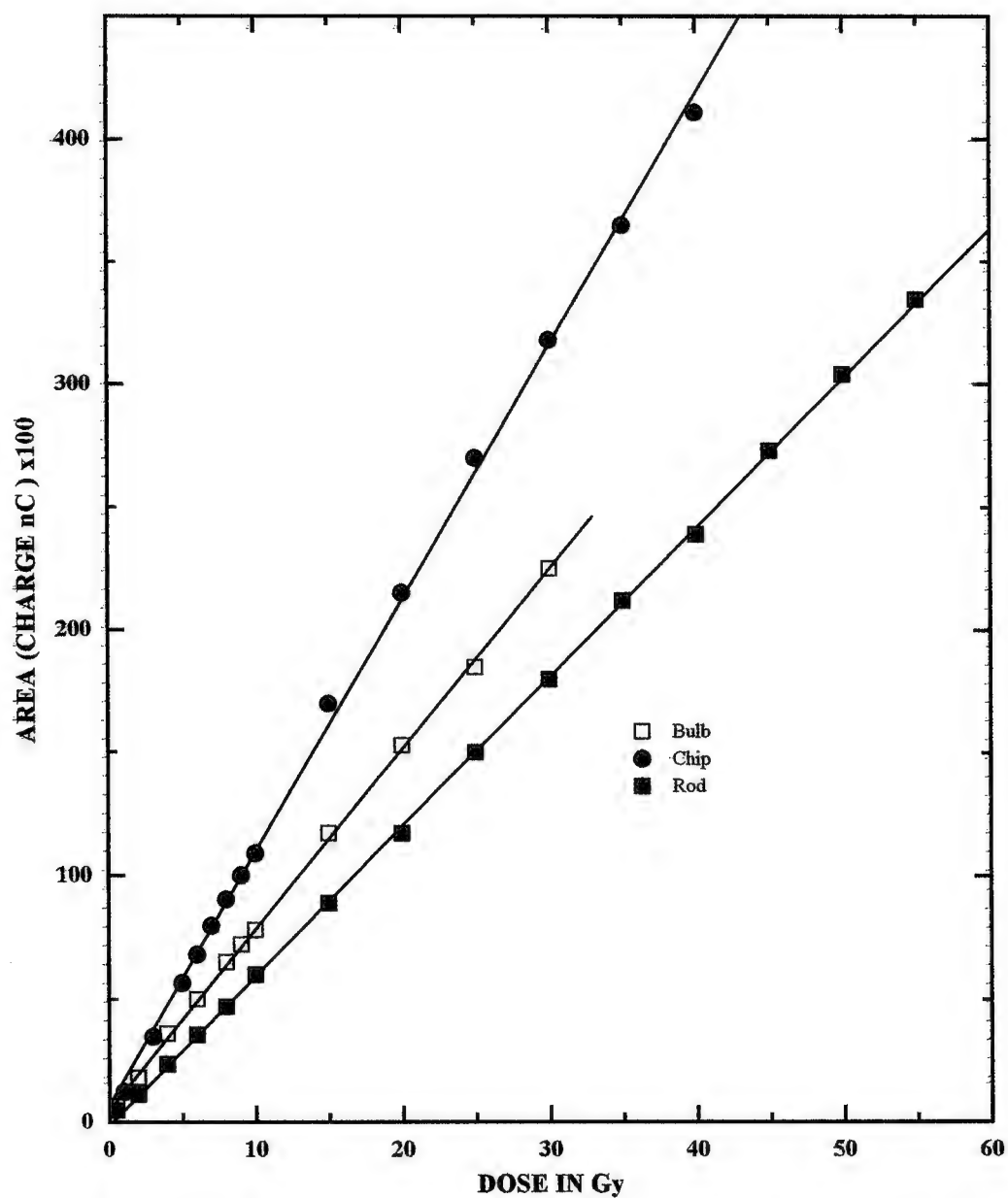
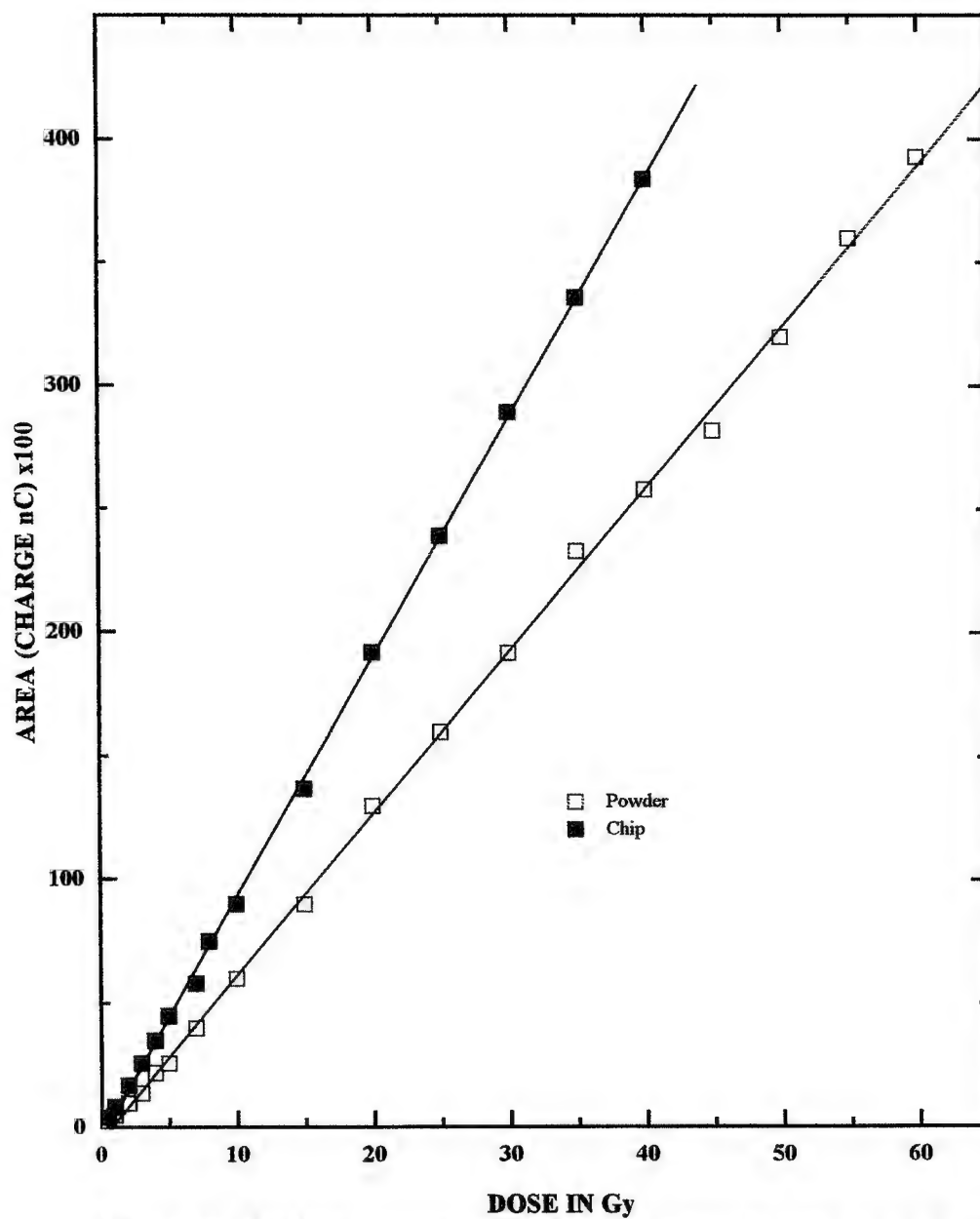


Fig. (3.16) The dose-response of Victoreen dosimeters exposed to cobalt-60 gamma-rays.



**Fig. (3.17)** The dose-response of Harshaw dosimeters exposed to cobalt-60 gamma-rays.

response at a dose  $D_1$  ;  $D_1$  being the lowest dose at which the dose response curve starts its linearity. Thus, an ideal dosimeter would satisfy  $f(D) = 1$  over a wide dose range up to several MGy. Unfortunately,  $f(D) = 1$  is found only over a narrow dose range in many TLD materials. Calculated values of the  $f(D)$  function for  $\text{CaF}_2:\text{Mn}$  showed all physical configurations of this material to give  $f(D)$  values very close to unity ( $\sim 0.98$ ) thus satisfying the requirement of the ideal dosimeter over the dose ranges studied.

The dose response curves of  $\text{CaF}_2:\text{Mn}$  irradiated with 70 KVp orthovoltage x-rays filtered by 1.1 mm aluminium are shown in figures (3.18) and (3.19). Evidently, all dosimeters show linear dose responses over the dose range from 0.5 to 12 Gy. It was not practically possible to increase the x - ray dose beyond 12 Gy due the excessive heat generated in the x - ray target which could cause its damage. Again, all dosimeter configurations gave calculated values for the normalized dose response function very close to unity ( $\sim 0.98$ ).

The sensitivity of a particular TLD material is formally defined as the TL signal strength per unit absorbed dose. Absolute sensitivity values for  $\text{CaF}_2 : \text{Mn}$  dosimeters have been calculated from the slope of the dose response curves ; the obtained values are listed in table (3.4).

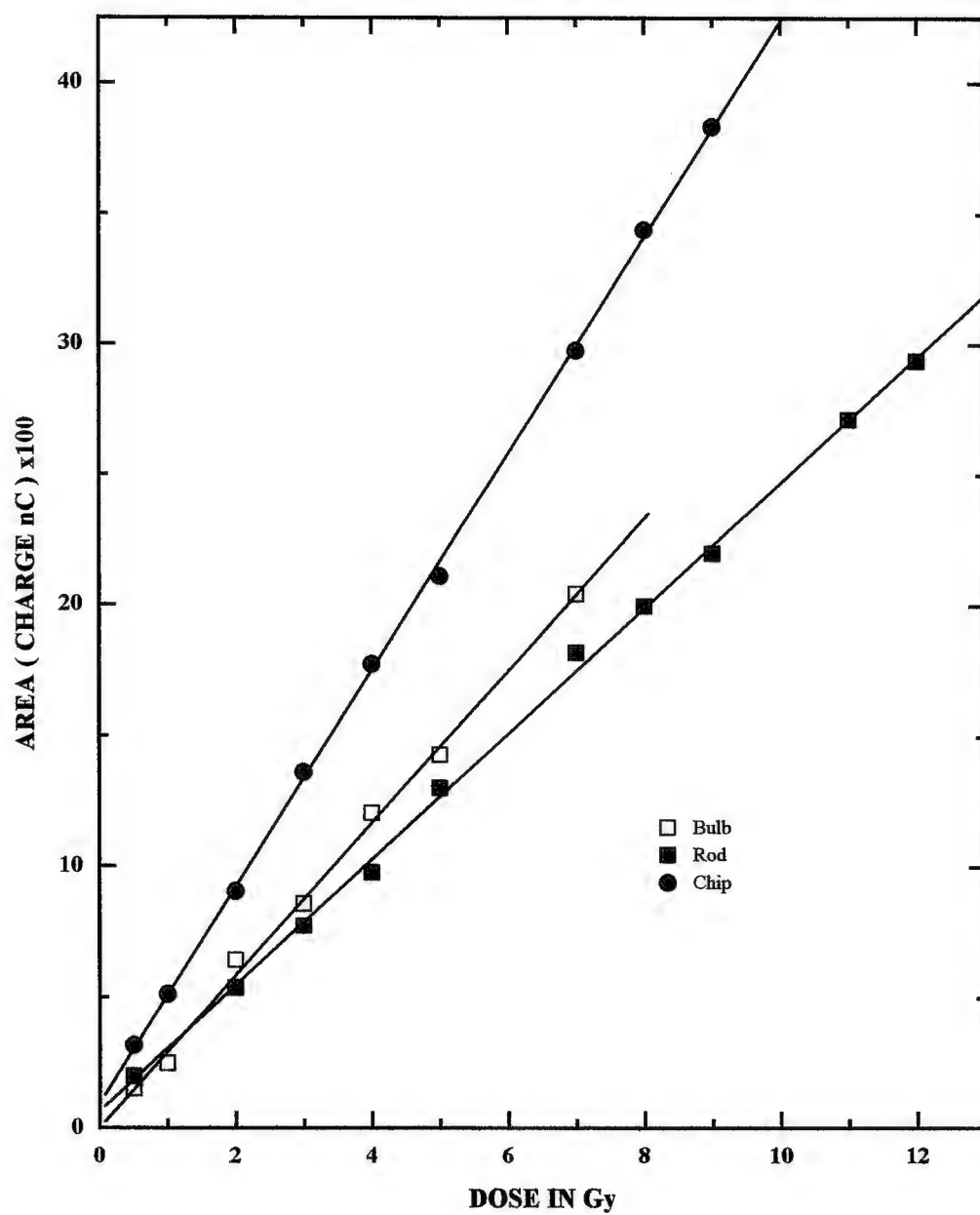


**Fig. (3.18)** The dose-response of Victoreen dosimeters exposed to 70 KV x-rays.

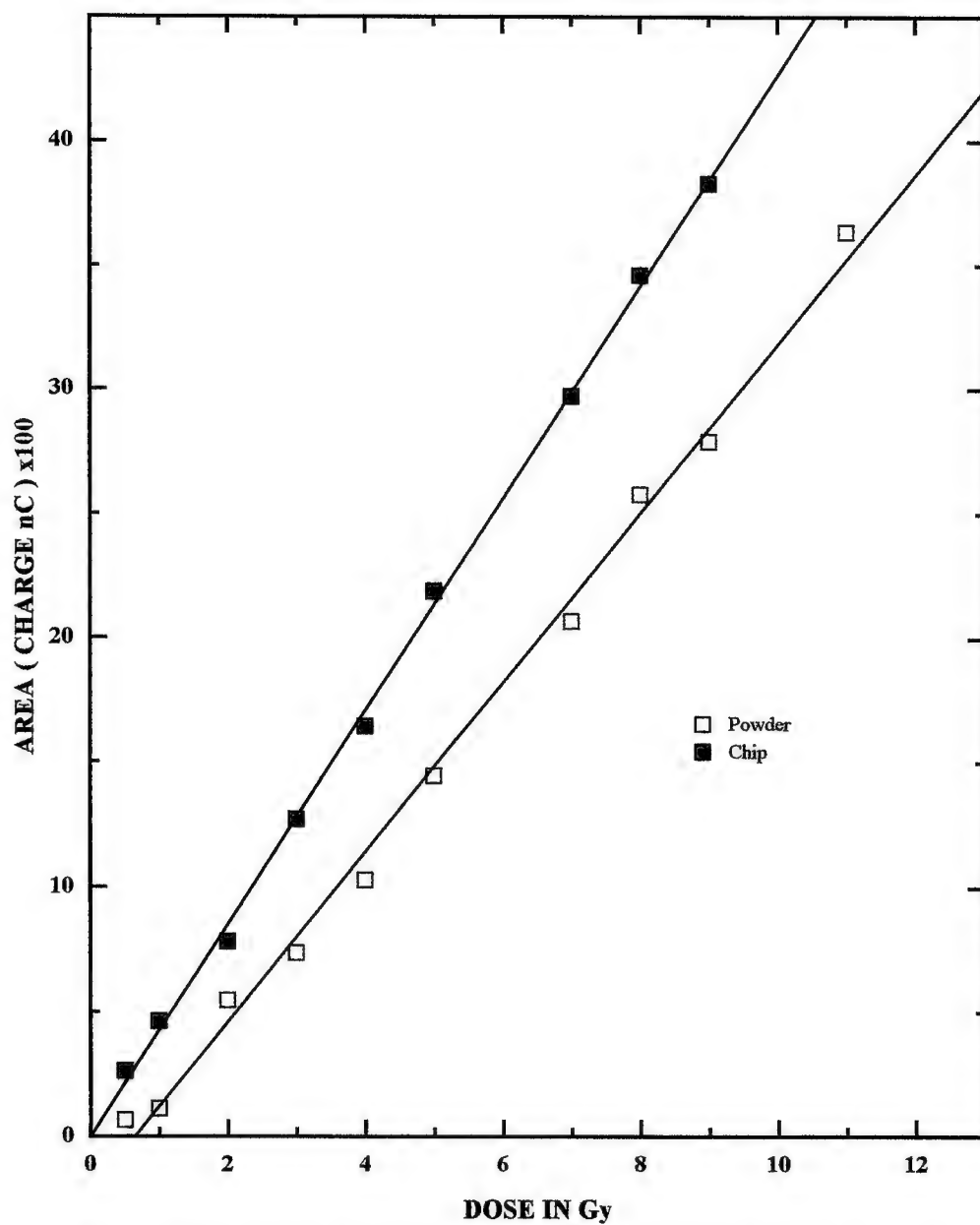


**Fig. (3.19)** The dose-response of Harshaw dosimeters exposed to 70 KV x-rays.



Table (3.4) Estimated sensitivities  
and relative sensitivities for  $\text{CaF}_2 : \text{Mn}$

Supplier	Dosimeter type	Gamma Irradiation (cobalt-60)	X-Irradiation (70 kVp)	Relative sensitivity
		Sensitivity (TL / Gy)	Sensitivity (TL / Gy)	
Victoreen	Chip	11.1	4.3	0.39
	Bulb	7.7	2.9	0.38
	Rod	6.0	2.5	0.42
Harshaw	Chip	11.2	4.2	0.38
	powder	5.2	2.9	0.56

Examination of table (3.4) shows  $\text{CaF}_2 : \text{Mn}$  chips as the most sensitive dosimeters to both gamma and x-ray irradiations ; the rods and powder samples being the least sensitive. Moreover, the sensitivities to x-rays are much lower than those to gamma - rays due to the attenuation of low-energy photons by the dosimeter material. A similar observation has been reported by Maiello et al [146] for LiF and attributed to the same reason.

The definition of sensitivity in an absolute sense , however, is difficult since this parameter also depends upon the TL readout system used in the measurement , the heating rate and the method of

measurement of the TL signal (usually glow curve area between two chosen temperature, or the height of a particular peak) . To overcome uncertainties associated with the absolute measurements of sensitivity, another parameter known as the relative sensitivity is used . This has been defined by many authors (e.g. Ref. 147) as the ratio of the TL emitted per Gy of absorbed dose from low-energy photons to that of cobalt - 60 photons of 1.25 MeV average energy. This ratio has been evaluated for all dosimeter configurations and the estimated values are displayed in table (3.4). It can be seen that all relative sensitivity values are less than unity ; the value of 1.0 is being reserved for the relative sensitivity to cobalt - 60 gamma radiation. The table also shows that although some differences exist in absolute sensitivities of the various forms of  $\text{CaF}_2:\text{Mn}$ ; differences in relative sensitivities are only slight. This agrees with the findings of other authors[146-148] who attributed these differences primarily to differences in the attenuation of low-energy photons by the TLD's due to their varying thicknesses. Thus, the primary concern in using these dosimeters for low- energy photon dosimetry is not the inherent sensitivity of the TLD but the thickness of the dosimeter.

## **CHAPTER IV**

### **SOME DOSIMETRIC APPLICATIONS OF $\text{CaF}_2 : \text{Mn}$**

This chapter is devoted to the attempts made to investigate the possible use of the TL bulb dosimeter to monitor radiation doses in two situations of important clinical applicational significance. Interest is focussed on the characterization of orthovoltage x-ray beams generated in the range from 60 to 150 KVp with added filtration, and the measurement of central-axis percentage depth doses of these beams in a solid tissue-equivalent phantom of Mix D.

#### **4.1 The Characterization Of X - Ray Beams**

In radiotherapy with x- rays, it is important to characterize the beams to be used in terms of their qualities in order to select the appropriate percentage depth dose data for treatment, to choose the dose/exposure conversion factor and to estimate the absorption in or the shielding by bone as well as the extra transmission by the lung [115].

In radiology, interest is focussed on the penetration of the x-ray beam into or through the patient, and it is logical to characterize the beam in terms of its ability to penetrate some material of known

composition; i.e. the quality of the beam. An ideal way to describe the quality of an x-ray beam is to specify its spectral distribution; i.e. the energy fluence in each energy interval. However, spectral distributions are difficult to measure and , furthermore, such a complete specification of the beam quality is not necessary in most clinical situations. Since the biological effects of x-rays are not very sensitive to the quality of the beam , in radiotherapy one is interested primarily in the penetration of the beam into the patient rather than its detailed energy spectrum . Thus, a crude but simpler specification of the beam quality is often used , namely the half-value layer (HVL)[149].

The HVL is the thickness of some standard material required to reduce the intensity of the x-ray beam to half its original value as measured by a device capable of reading exposure or dose such as an ionization chamber. The quality of the primary radiation incident on a patient is controlled by the applied kilovoltage of the x-ray machine and the filtration used (inherent or added). It has been found that the specification of the quality in terms of the HVL is usually sufficient for x-rays generated at voltages below 400 KVp [115]. Since the HVL used for the specification of % depth dose data is that for a narrow beam of radiation, only one determination

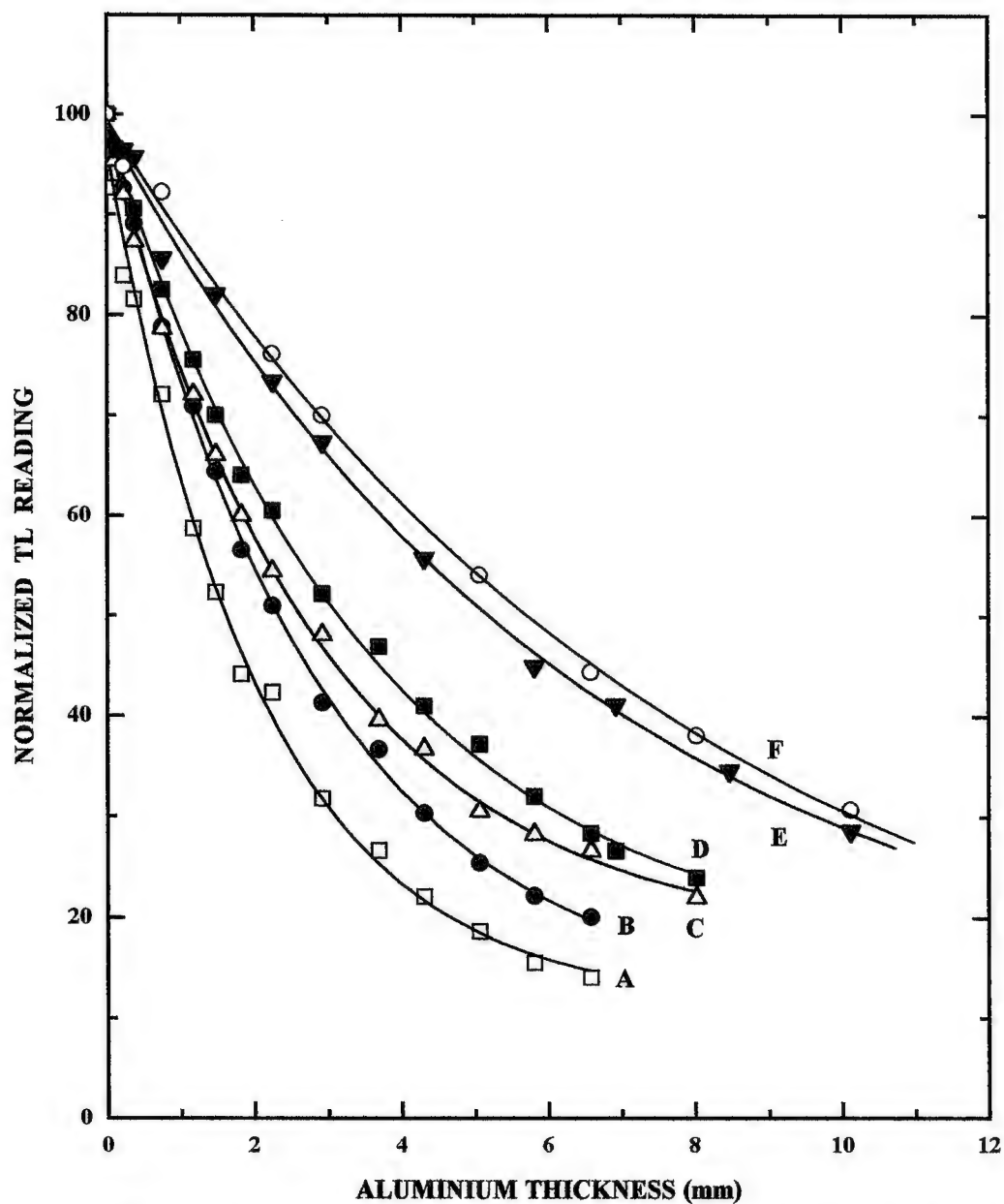
of HVL for each radiation quality ( i.e. KVp plus filtration ) used is needed. The HVL needs to be known only to an accuracy of about 0.2 mm [115], and measurements to this accuracy pose no serious experimental problems.

Figure (4.1) illustrates results of measurements of the attenuation of orthovoltage x-ray beams in aluminium ; the curves were obtained using a Victoreen TL bulb dosimeter and narrow beam geometry. It is of interest to mention that the majority of HVL measurements in the orthovoltage range relied mainly on ionization chambers and photographic films as radiation detectors [149-151].

To test the reliability of using TL dosimeters for this purpose, attenuation was also measured with an ionization chamber ; the results are displayed in figure (4.2) together with the corresponding curves obtained with the TL bulb dosimeter. The data used in plotting attenuation curves have been fitted by an equation of the form:

$$Y = Y_0 + A_1 \exp [ - (x - x_0) ] / t_1 \quad (4.1)$$

where  $Y_0$  ,  $A_1$  and  $t_1$  are fitting parameters and  $x_0 = 0$ . Values of the fitting parameters are collected in table (4.1). It is evident that a fairly good agreement exists between values of the fitting parameters for the TL bulb dosimeter and their corresponding values for the ionization chamber.



**Fig.(4.1)** Attenuation curves in aluminium for narrow x-ray beams obtained with TL bulb dosimeter.

(A) 60 KV ; filtration : 1.1 mm Al.

(B) 75 KV ; filtration : 1.1 mm Al.

(C) 90 KV ; filtration : 2.7 mm Al.

(D) 110 KV ; filtration : 2.7 mm Al.

(E) 130 KV ; filtration : 1.0 mm Al plus 0.23 mm Cu.

(F) 150 KV ; filtration : 1.0 mm Al plus 0.23 mm Cu.

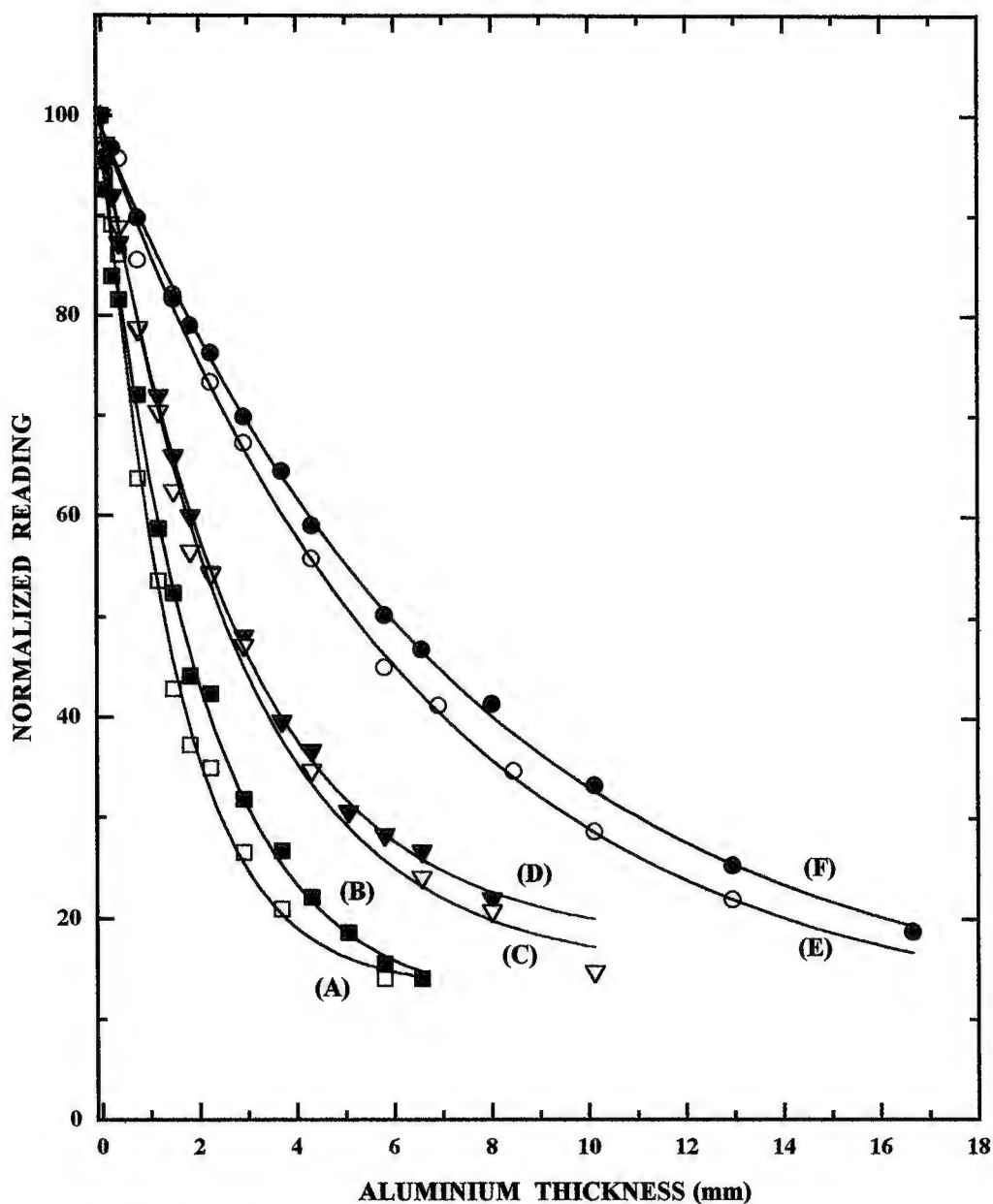


**Fig. (4.2)** Attenuation curves in aluminium for narrow x-ray beams:

- (A) 60 KV x-rays filtered by 1.1 mm Al ; detector : ionization chamber.
- (B) 60 KV x-rays filtered by 1.1 mm Al ; detector : TL bulb dosimeter.
- (C) 90 KV x-rays filtered by 2.7 mm Al ; detector : ionization chamber.
- (D) 90 KV x-rays filtered by 2.7 mm Al ; detector : TL bulb dosimeter.
- (E) 130 KV x-rays filtered by 0.23 mm Cu + 1.0 mm Al ; detector : TL bulb dosimeter.
- (F) 130 KV x - rays filtered by 0.23 mm Cu + 1.0 mm Al ; detector : ionization chamber.

Table (4.1)  
Values of the fitting parameter  $Y_0$  ,  $A_1$  and  $t_1$  .

Figure	Curve	Detector	$Y_0$	$A_1$	$t_1$
(4.1)	A	TL bulb	$11.29 \pm 1.68$	$85.27 \pm 1.68$	$2.05 \pm 0.12$
	B	TL bulb	$11.15 \pm 1.15$	$88.76 \pm 1.60$	$2.83 \pm 0.09$
	C	TL bulb	$17.61 \pm 1.08$	$80.62 \pm 1.01$	$2.89 \pm 0.10$
	D	TL bulb	$15.71 \pm 0.48$	$83.44 \pm 0.43$	$3.55 \pm 0.05$
	E	TL bulb	$9.99 \pm 2.97$	$89.04 \pm 2.97$	$6.50 \pm 0.45$
	F	TL bulb	$4.12 \pm 3.11$	$95.41 \pm 2.90$	$7.89 \pm 0.49$
(4.2)	B	Ion. chamber	$13.21 \pm 2.25$	$87.70 \pm 2.32$	$1.48 \pm 0.10$
	D	Ion. chamber	$14.84 \pm 1.58$	$84.24 \pm 1.63$	$2.85 \pm 0.15$
	F	Ion. chamber	$9.87 \pm 1.26$	$89.14 \pm 1.14$	$7.44 \pm 0.23$



Both figures (4.1) and (4.2) indicate that each added layer of aluminium acts very much like a filter and progressively changes the quality of the x-ray beam ; i.e. the beam becomes more penetrating. As it is well-known, a practical beam produced by an x-ray generator, however, consists of a spectrum of photon energies. Attenuation of such a beam is no longer quite exponential. This effect can be seen in the figures where the slope of the attenuation curve decreases with increasing absorber thickness, because the absorber or filter preferentially removes low energy photons. For such a heterogeneous beam, the first HVL is less than the second HVL; the latter being the thickness of attenuator required to reduce the dose rate to one quarter of the value of the unattenuated beam. As the absorber thickness increases, the average energy of the transmitted beam increases and the beam becomes increasingly harder. Thus, by increase of the filtration in such an x-ray beam , one increases the penetrating power or the half-value layer of the beam.

Estimated values of the first HVL , the second HVL , the homogeneity coefficient and the effective energy of the x-ray beams are quoted in table (4.2) .

Table (4.2)

HVL Values and homogeneity coefficients for x-ray beams

KVp	Filter mm	Detector	HVL (1) mm	HVL (2) mm	Homogeneity Coefficient	Effective Energy (keV)
60	1.1 Al	TLD	1.60	2.13	0.75	25
75	1.1 Al	TLD	2.35	2.84	0.83	28
90	2.7 Al	TLD	2.63	4.11	0.64	30
110	2.7 Al	TLD	3.14	4.56	0.69	32
130	1.0 Al + 0.23 Cu	TLD	5.18	6.28	0.83	40
150	1.0 Al + 0.23 Cu	TLD	5.73	6.15	0.93	43
60	1.1 Al	Ionization Chamber	1.29	1.68	0.77	23
90	2.7 Al	Ionization Chamber	2.48	3.72	0.67	29
130	1.0 Al + 0.23 Cu	Ionization Chamber	5.93	7.19	0.83	44

The homogeneity coefficient is defined as the ratio of the first HVL to the second HVL. Its importance arises in situations where additional information about the quality of radiation is needed. For example, when it is found that measured percentage depth dose data do not agree with published data for the same HVL; the difference may be accounted for by the radiations having different spectra in spite of their first HVL's being the same ; the value of the homogeneity coefficient will indicate whether this is so or not. The effective energy values of the x-ray beams were deduced from graphs relating the first HVL in aluminium to the effective energy of photons [152] ; the obtained values were found to agree with published effective energies based on mass attenuation coefficients of aluminium [149].

Examination of table (4.2) indicates that , for the same filtration used, values of all quality parameters tend to increase with increasing applied kilovoltage as a result of the increased penetrating power of the x-ray beam. The table also shows that under heavy filtration, softer components of the x-ray beams are removed and the radiation transmitted is more nearly monochromatic; thus higher HVL values are to be expected. A fairly good agreement exists between values of the homogeneity

coefficient obtained by the two detector types. It is of interest to note that the attenuation measured by the TL bulb dosimeter at small aluminium thicknesses agrees well with that measured by the fixed - volume ionization chamber ; deviations start to occur at large attenuator thicknesses. This could be due to a change in the energy response of one of the detectors. Since the TL dosimeter is reported to show a fairly flat response over the small effective KeV range used [108] , it is reasonable to assume that the fixed-volume ionization chamber used did show a slight energy-dependence in its response with increasing attenuator thickness.

#### **4.2 Central-Axis Percentage Depth Doses Of X-Ray Beams**

When radiation falls on a patient or a phantom , the absorbed dose varies with depth. This variation depends on many conditions such as beam energy, field size, distance from source and beam collimation system. Thus, the calculation of dose in the patient or phantom involves considerations in regard to these parameters as they affect depth dose distributions.

An essential step in the dose calculation system is to establish depth dose variation along the central axis of the radiation beam. A number of quantities has been defined for this purpose; the major

among these being percentage depth dose [115]. This quantity is usually derived from measurements made in water phantoms or any other water-equivalent phantom using small ionization chambers. Other dosimetry systems such as TLD , diodes and film have been very occasionally used particularly in the megavoltage range.

One way of characterizing the central axis dose distribution is to normalize dose at depth with respect to dose at a reference depth. The quantity percentage depth dose may be defined as the quotient , expressed as a percentage, of the absorbed dose at any depth  $d$  to the absorbed dose at a fixed reference depth  $d_0$  , along the central axis of the beam [149]. Percentage depth dose ( $P$ ) is thus:

$$P = ( D_d / D_{d_0} ) \times 100 \quad (4.2)$$

For orthovoltage (up to about 400 KVp ) and lower energy x-rays, the reference depth is usually the surface of the phantom (  $d_0 = 0$  ). For higher energies, the reference depth is taken as the position of the peak absorbed dose on the central axis (  $d_0 = d_m$  ).

Many sets of percentage depth dose tables are available in the literature and nearly all of them are essentially based on ionization chamber measurements. Although most of these tables can be regarded as acceptably accurate, the most comprehensive, consistent

and widely used ones are those contained in Supplement 10 of the British Journal of Radiology, 1953. The decision to use published data must be based on, at least, few measurements made on the user's equipment. The adoption of the 5 cm deep scheme minimizes any errors which result from the data used being not exactly correct. Two parameters need to be known before percentage depth dose tables can be selected; these are the source-to-surface distance (SSD) and the HVL of radiation. Using these two parameters, the appropriate set of tables can be selected but their validity should be experimentally examined. A number of parameters affects percentage depth dose distributions. These include beam quality or energy, depth, field size and source-to-surface distance. These parameters are investigated in the present work. All measurements were made in a water-equivalent Mix D phantom. Mix D has a density of  $0.99 \text{ g/cm}^3$ , an effective atomic number for photoelectric absorption of 7.05 and an electron density of  $3.41 \times 10^{23} \text{ electrons/g}$ ; the corresponding values for water being  $1.0 \text{ g/cm}^3$ , 7.05 and  $3.34 \times 10^{23} \text{ electrons/g}$  respectively [151]. The detector used was the Victoreen TLD Bulb. All results presented in this section relate to x-ray beams generated in the orthovoltage range.

The variation of percentage depth doses with depth along the central axis of the x-ray beam is shown in figure (4.3) for three different sets of operating conditions of the x-ray machine. All depth dose data were fitted by equation (4.1) and values of the fitting parameters are listed in table (4.3). It is evident from figure (4.3) that the depth below the surface of the phantom is the most important parameter which affects percentage depth dose at a point; and generally the greater the depth, the smaller is the value of the percentage depth dose. This is expected from the operation of the inverse square law and the increasing attenuation suffered by the x-ray beam due to the greater thickness it has to pass through Mix D. The estimated half-value thicknesses (HVT's), quoted in figure (4.3), are found to increase with increase in both applied  $KV_p$  and tube filtration. This can be attributed to the resulting increase in the penetration power of the x-ray beam. Mass attenuation coefficients ranging from  $11 \times 10^{-3} \text{ m}^2/\text{kg}$  to  $20 \times 10^{-3} \text{ m}^2/\text{kg}$  have been determined for Mix D. These values are found to agree reasonably well with published mass attenuation coefficients of water for similar irradiation conditions [149,151].

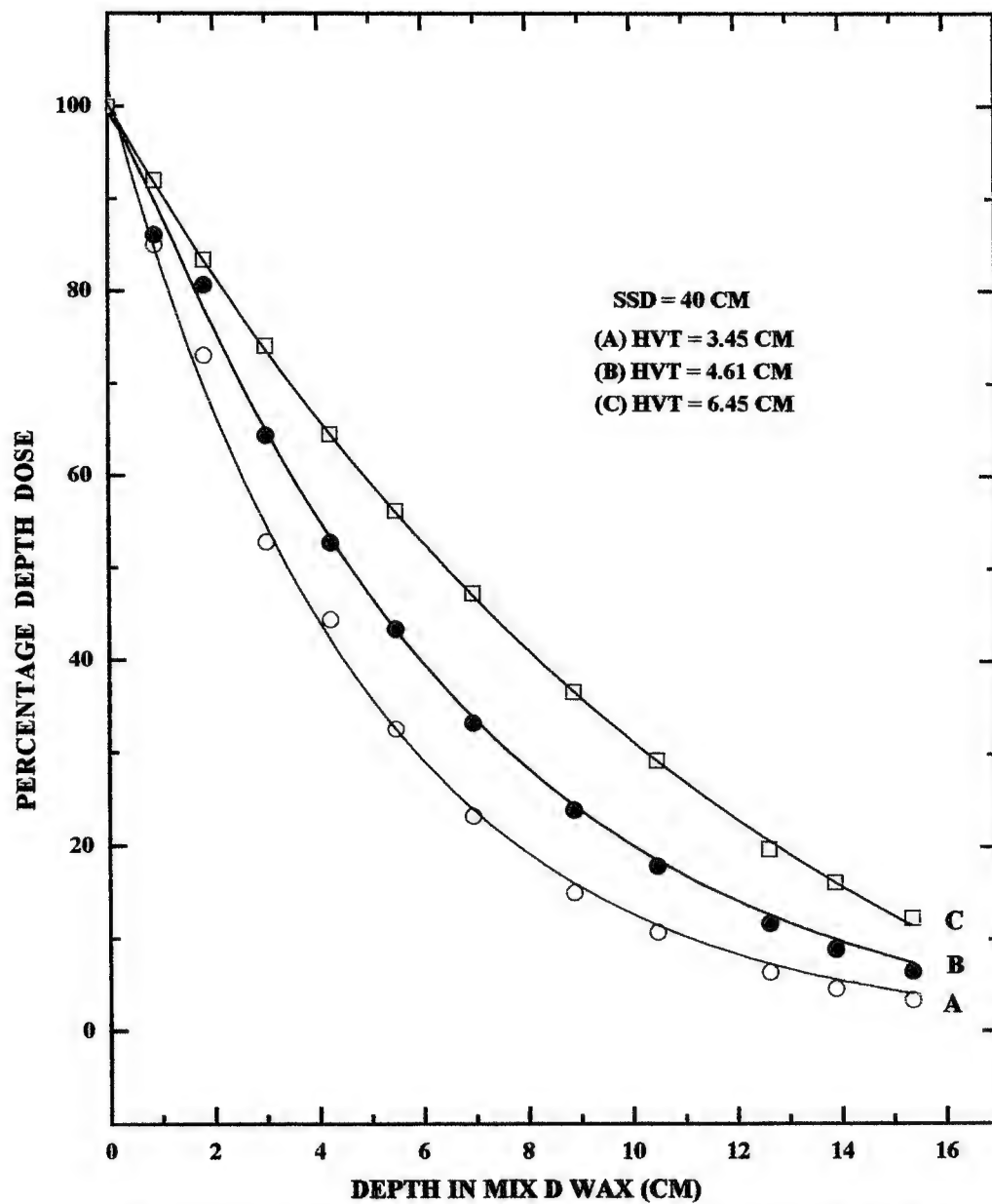


**Fig.(4.3)** Variation of central axis percentage depth dose with depth in Mix D wax for a circular X - ray beam 5 cm in diameter :

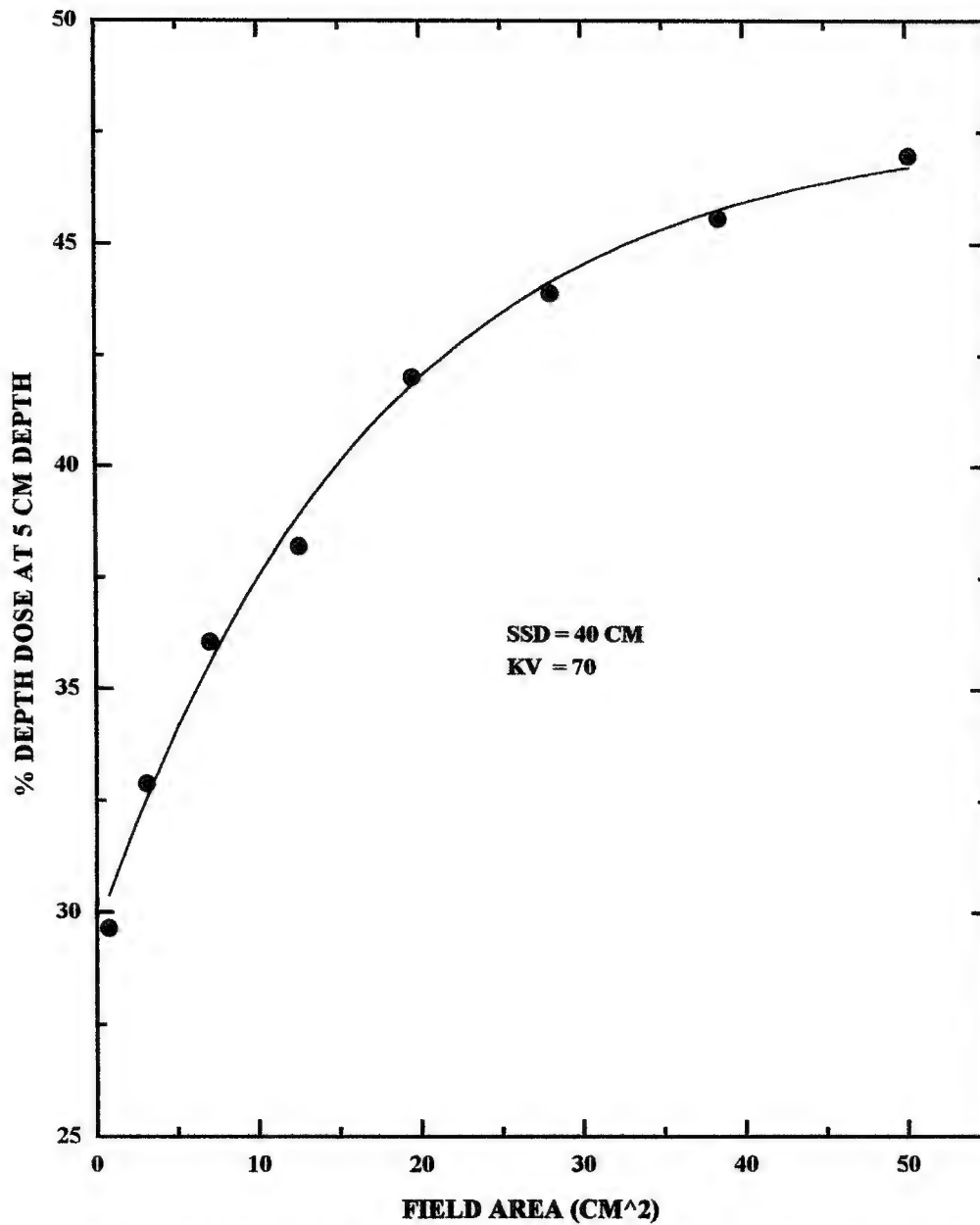
(A) 60 KV ; filtration : 1.1 mm Al.  
 (B) 90 KV ; filtration : 2.7 mm Al.  
 (C) 120 KV ; filtration : 1.0 mm Al plus 0.23 mm Cu.



Table (4.3)  
Values of the fitting parameters  $Y_o$ ,  $A_1$  and  $t_1$   
for the attenuation of x-rays in Mix D.

Curve No.	KV	Filter	$Y_o$	$A_1$	$t_1$
A	60	1.1 mm Al	$0.00 \pm 0.00$	$102.09 \pm 1.30$	$4.82 \pm 0.12$
B	90	2.7 mm Al	$6.59 \pm 0.00$	$97.06 \pm 2.70$	$5.26 \pm 0.28$
C	120	1.0mm Al + 0.23 mm Cu	$15.01 \pm 0.00$	$89.80 \pm 3.23$	$5.07 \pm 0.30$

Results of measurements made to investigate the dependence of central-axis percentage depth dose at 5 cm depth in Mix D on x-ray beam area (i.e. field size) are shown in figure (4.4). Percentage depth dose can be seen to increase steadily, though not linearly, as the beam area increases; a trend which is exactly similar to that based on ionization chamber measurements [149-151], and is due to the effect of scattered radiation. Not only at the surface, but everywhere in the irradiation zone, the exposure is made up of contributions from primary and scattered radiations; the former being independent of beam area, whereas the latter increases with beam size. For a sufficiently small field, one may assume that the percentage depth dose at a point in Mix D is effectively the result of



**Fig. (4.4)** Variation of central axis percentage depth dose at 5 cm depth in Mix D with x - ray beam area .

the primary radiation ; i.e. the photons which have traversed the overlying medium without interacting. The contribution of the scattered photons to the depth dose in this case is negligibly small or zero. But as the field size is increased, the contribution of scattered radiation to the absorbed dose increases. Since this increase in scattered dose is greater at large depths than at the reference depth  $d_0$  ( the surface of the phantom) the percentage depth dose increases with increasing field size.

The effect of changing the source-to-surface distance (SSD) on central- axis percentage depth dose at 5 cm depth in Mix D is shown in figure (4.5) for two different sets of operating conditions of the x-ray equipment. The figure illustrates clearly the general effect of increasing the SSD on percentage depth dose values causing them to increase. The reason for this increase can be explained by the following simple argument:

Let us assume two irradiation conditions which differ only in regard to SSD ; i.e. the field size on the phantom surface (  $r$  in diameter) and the depth  $d$  being the same for both conditions. Let  $P(d,r,f)$  be the percentage depth dose at depth  $d$  for  $SSD = f$  and a field size  $r$  . Since the variation in dose with depth is governed by three effects - inverse square law , exponential attenuation and

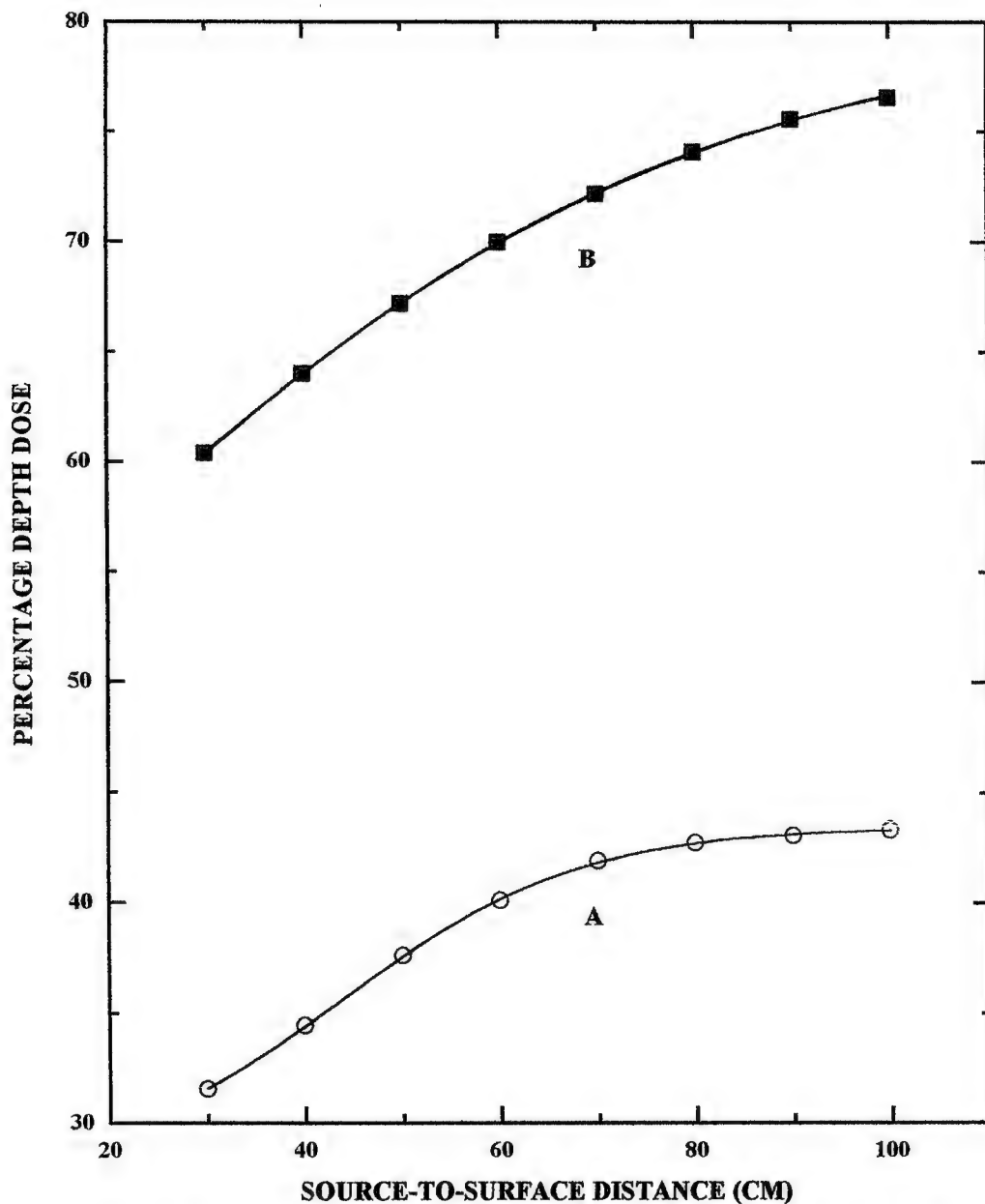


**Fig.(4.5)** Variation of central axis percentage depth dose at 5 cm depth in Mix D wax with SSD for a circular x-ray beam 5 cm in diameter.  
 (A) 60 KV ; filtration : 1.1 mm Al .  
 (B) 120 KV ; filtration : 1.0 mm Al plus 0.23 mm Cu .

scattering - then :

$$P(d, r, f_1) = 100 \left[ \frac{f_1 + d_0}{f_1 + d} \right]^2 \cdot e^{-(\mu d_0)} \cdot K_s \quad (4.3)$$

Where :  $\mu$  is the linear attenuation coefficient for the primary, and  $K_s$  is a function which accounts for the change in scattered dose. If we ignore the change in the value of  $K_s$  from one SSD to another then :

$$P(d, r, f_2) = 100 \left[ \frac{f_2 + d_0}{f_2 + d} \right]^2 \cdot e^{-(\mu d_0)} \cdot K_s \quad (4.4)$$

Dividing equation (4.4) by equation (4.3) gives :

$$\frac{P(d, r, f_2)}{P(d, r, f_1)} = F = \left[ \frac{f_2 + d_0}{f_1 + d_0} \right]^2 \cdot \left[ \frac{f_1 + d}{f_2 + d} \right]^2 \quad (4.5)$$

For orthovoltage beams,  $d_0 = 0$  , and the F factor becomes:

$$F = \left[ \frac{f_2}{f_1} \right]^2 \cdot \left[ \frac{f_1 + d}{f_2 + d} \right]^2 \quad (4.6)$$

Equation (4.6) shows that the F factor is greater than 1.0 for  $f_2 > f_1$  and less than 1.0 for  $f_2 < f_1$  . Thus, it may be restated that percentage depth dose increases with increase in SSD.

To confirm the validity of the above argument, let us compare the values of  $D_5$  at two different SSD values of 40 and 80 cm. Equation (4.3) gives the value of the fraction  $[f_1/(f_1 + d_5)]^2$  as 0.79 at 40 cm SSD ; while the corresponding value of the fraction at 80 cm SSD amounts to 0.89 . Since the value of  $[e^{-\mu d_5}]$  is the same in both cases ( 0.58 ) ; it would appear that an increase in SSD by 40 cm causes the %  $d_5$  to increase by almost 10% . It is of interest to note that figure (4.5) shows the same increase in the value of  $D_5$  when the SSD is increased from 40 to 80 cm.

Finally , the dependence of  $D_5$  , the percentage depth dose at 5 cm depth in Mix D , on radiation quality is illustrated in figure (4.6) where percentage  $D_5$  is plotted against the applied kilovoltage of the x-ray machine . As quality in radiology is an indication of the penetrating power of the x-ray beam, percentage depth doses are expected to increase with increasing HVL of the beam ; i.e. with increasing KVP . This trend is clearly observed in figure (4.6) and is similar to that reported in ionization chamber measurements [149-151]. The magnitude of the observed increase is not , however, as great as might be expected partly because of the influence of scattered radiation which contributes a considerable fraction of the total radiation dose at this depth , and which does not alter much

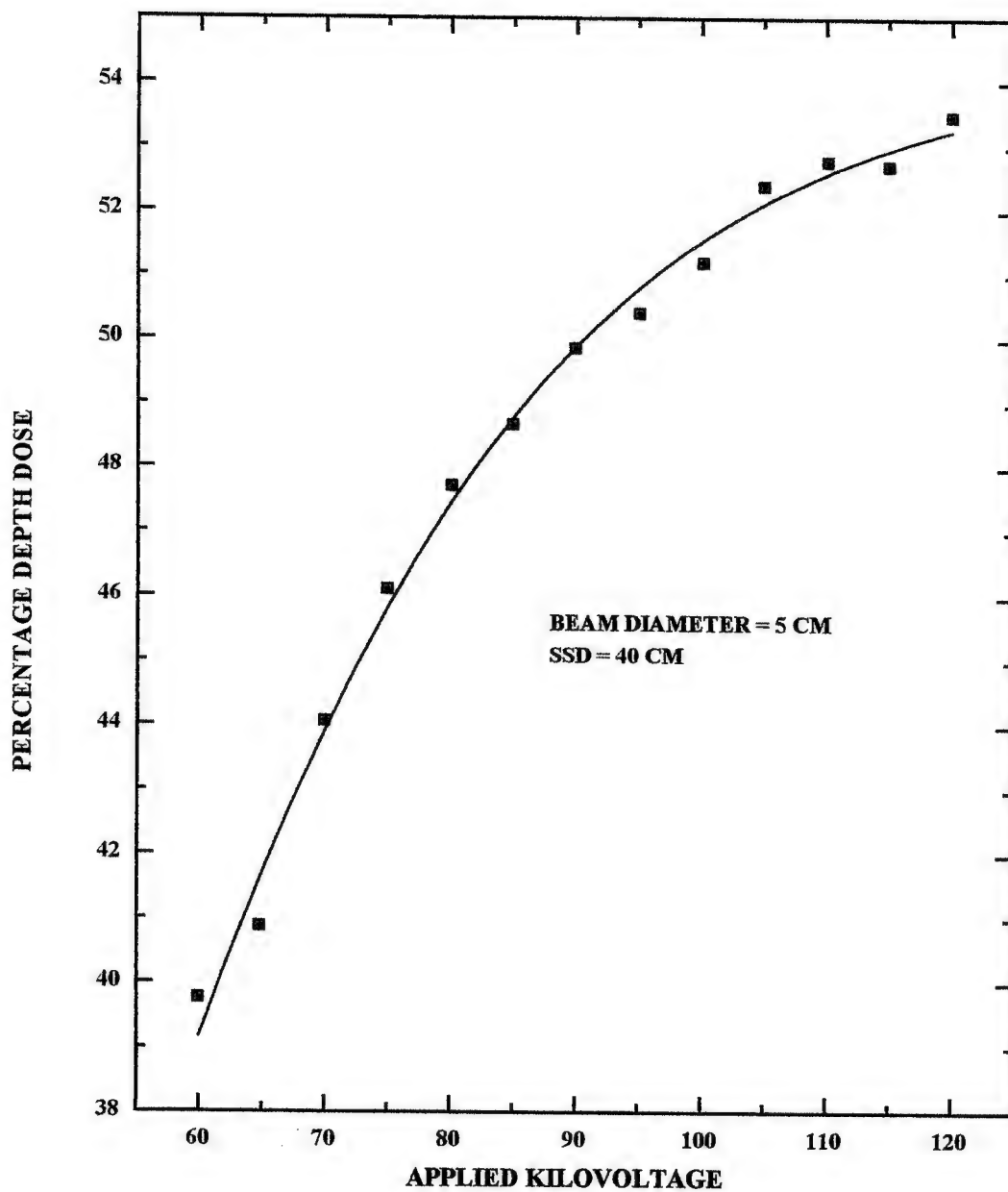


**Fig.(4.6)** Variation of central axis percentage depth dose at 5 cm depth in Mix D wax with the applied KV of the x - ray machine.

with quality changes [115] . Moreover, part of the fall of percentage depth dose with depth is due to the inverse square law and changes in quality (or KVp ) has no effect on this factor . Because of the influence of scattered radiation, changes in percentage depth dose with KVp should be more pronounced for small (where there is less scatter) than for large x-ray beams. Even so, as shown in the figure, a two-fold increase in the applied KVp only increases the percentage depth dose at 5 cm depth in Mix D by about 14% for the relatively small x-ray field used.



## CONCLUSIONS

The studies presented in this thesis represent an investigation into the dosimetric properties of  $\text{CaF}_2 : \text{Mn}$ . The following conclusions can be drawn :

(1) All X- or gamma - irradiated forms of  $\text{CaF}_2 : \text{Mn}$  exhibit thermoluminescence (TL) curves of the same general shape ; the shape being also independent of the given radiation dose. Increasing the dose , however, increases the area of the TL curve due to the increased population of traps by radiation.

(2) All forms of  $\text{CaF}_2 : \text{Mn}$  show glow curves consisting of a main dosimetric peak and a second small satellite peak appearing on the low temperature side of the main peak ; the small satellite peak being attributed to the existence of background rare earth impurities in  $\text{CaF}_2 : \text{Mn}$ .

(3) All models proposed to explain the TL mechanism in  $\text{CaF}_2 : \text{Mn}$  can be disputed and each of them results finally in the de-excitation of the  $\text{Mn}^{2+}$  ion to its ground state. However, the most promising model attributes the TL of the material to the recombinations of  $F_A - F_H$  centres but such a model still needs

further quantitative elaboration. The  $F_A$  centre is an F centre perturbed by two  $Mn^{2+}$  ions and the  $H_A$  centre is simply an interstitial fluorine atom.

(4) Theoretical analysis of the TL curve of  $CaF_2:Mn$  shows the apparent single dosimetric peak to be made up of two, closely spaced (in energy) discrete peaks. This view is supported by the observed anomalous initial fading rate of TL during the first 24 hours after irradiation; an observation which suggests that traps of different degrees of thermal stability are involved in the TL of this peak.

(5) The linear dose response of  $CaF_2:Mn$  to X- and gamma-radiations confirms its suitability for use in clinical dosimetry to monitor radiation doses over the dose ranges studied in this work. The absolute sensitivity (TL/Gy) of  $CaF_2:Mn$  chips, which far exceeds that of any other form of the material, indicates that preference should be given to these chips in dosimetry.

(6) The suitability of using  $CaF_2:Mn$  for the characterization of orthovoltage X-ray beams and the measurement of central-axis percentage depth doses of these beams has been confirmed. The results obtained with a  $CaF_2:Mn$  bulb dosimeter agree reasonably

well with those obtained by using a fixed- volume ionization chamber.

(7) Finally, one should emphasize that different preparations of  $\text{CaF}_2\text{:Mn}$  could lead to different TL characteristics. Even samples from the same batch can sometimes show some peculiarities. Each preparation should be therefore carefully examined and it is advisable not to rely heavily on results of other investigators, even for the same sample configuration. This is because of the numerous factors that can affect the TL characteristics such as the preparation conditions, natural and added impurities and annealing, as well as other instrumentation parameters which include the sensitivity of the photomultiplier used for detection of TL, the heating rate employed and its uniformity during the readout cycle.

## REFERENCES

- (1) Urbach, F. , Wiener Berichte , 139 (1930) 363.
- (2) Randall , J. T. and Wilkins, M.H. F, , Proc. Roy. Soc. , 184 (1945) 366 ; ibid p. 390.
- (3) Garlick, G.F.J. and Gibson, A. F., Proc. Phys. Soc. , 60 (1948) 574.
- (4) Daniels, F., Boyd, C.A. and Saunders, D.F. , Science, 117 (1953) 343.
- (5) Garlick, G.F.J. , Luminescent Materials, London : Oxford University press, 1948.
- (6) Curie, D. , Luminescence in Crystals, London : Methuen, 1960.
- (7) Cameron, J. R. Suntharalingam, N and Kenny, G.N, Thermoluminescence Dosimetry, Madison: University of Wisconsin Press, 1968.
- (8) McDougall,D.J. (Ed.) , Thermoluminescence of Geological Materials , London Academic Press, 1968.
- (9) Becker, K. , Solid State Dosimetry, Cleveland : CRS Press, 1973.
- (10) Braunlich, P. (Ed.), Thermally Stimulated Relaxation in Solids, Berlin : Springer-Verlage , 1979.

- (11) Chen , R. and Kirsh , Y. , Analysis of Thermally Stimulated Processes, Oxford : Pergamon Press, 1981.
- (12) Oberhofer, M. and Scharmann, A., Applied Thermoluminescence Dosimetry, Bristol : Adam Hilger, 1981.
- (13) Horowitz, Y. S. (Ed.), Thermoluminescence and Thermoluminescence Dosimetry Boca Raton, FL: CRC Press, 1984.
- (14) McKeever, S . W. S. , Thermoluminescence of Solids, Cambridge : Cambridge University Press, 1985.
- (15) Mahesh, K., Weng, P. S. and Furetta , C. , Thermoluminescence in Solids and its Applications, Ashford : Nuclear Technology Publishing, 1989.
- (16) Vij, D. R, (Ed.) , Thermoluminescence Materials, , Englewood Cliffs: Prentice Hall, 1993.
- (17) McKeever, S.W.S ., Moscovitch , M. and Townsend, P. D., Thermoluminescence Dosimetry Materials : Properties and Uses, Ashford: Nuclear Technology Publishing, 1995.
- (18) Attix, F.H. (Ed.), Proc. 1st Int. Conf. On luminescence Dosimetry , stanford, 1965.
- (19) Auxier, J.A., Becker, K. and Robinson, E.M. (Eds.), Proc. 2nd

Int. Conf. On Luminescence Dosimetry , Gatlinberg, 1968.

- (20) Majdahl, V., (Ed.) , Proc. 3<sup>rd</sup> Int. Conf. On Luminescence Dosimetry , Risa, Denmark, 1971.
- (21) Niewiadomski, T. (Ed.) , Proc. 4<sup>th</sup> Int. Conf. On Luminescence Dosimetry, Krakow, Poland, 1974.
- (22) Scharmann, A. (Ed.) , Proc. 5<sup>th</sup> Int. Conf. On Luminescence Dosimetry, Sao Paulo, Brazil, 1977.
- (23) Portal, G. (Ed.) , Proc. 6<sup>th</sup> Int. Conf. On Luminescence Dosimetry, Toulouse, France, 1980.
- (24) Stoebe, T.G. (Ed.) , Proc. 7<sup>th</sup> Int. Conf. On Luminescence Dosimetry, Ottawa, Canada, 1984.
- (25) Proc. 8<sup>th</sup> Int. Conf. On Solid State Dosimetry, Oxford, 1986.
- (26) Proc. 9<sup>th</sup> Int. Conf. On Solid State Dosimetry, Vienna, 1989.
- (27) Garlick, G.F.J., Handbuch der Physik, Vol. XXVI, (Ed. S. Flugge), Berlin : Springer-Verlag, 1958.
- (28) Johnson, R.P., J. Opt. Soc. Amer., 29 (1939) 682.
- (29) Schon, M.Z., Physik., 119 (1942) 463.
- (30) Klasens, H.A., Nature, 158 (1946) 306.
- (31) Halperin, A. and Braner, A.A., Phys. Rev., 117 (1960) 408.
- (32) Braunlich, P. and Scharmann, A., Phys. Stat. Soli., 18 (1966) 307.
- (33) Town, P.D., Ahmed, K., Chandler, P.J., McKeever, S.W.S. and

whitlow, H.J., Radiat. Effects, 72 (1983) 245.

(34) Shockley, W. and Read, W.T., Phys. Rev. 87 (1952) 835.

(35) Prener, J.S. and Williams, F.E., J. Electrochem. Soc., 103 (1956) 342.

(36) Lambe, J. and Klick, C.C., Phys. Rev., 98 (1955) 909.

(37) Klasens, H.A., J. Electrochem. Soc., 100 (1953) 72.

(38) Bohn, M. and Scharmann, A., Phys. Stat. Soli., (A) 4 (1971) 99.

(39) Braunlich, P., J. Appl. Phys., 38 (1967) 1221.

(40) Nicholas, K.H. and Woods, J., Brit. J. Appl. Phys., 15 (1964) 783.

(41) Braunlich, P., Ref. 8, p. 61.

(42) Chen, R., J. Appl. Phys., 40 (1969) 570.

(43) Chen, R., J. Mat. Sci., 11 (1976) 1521.

(44) Sathyamoorthy, A., Bhalla, K.C. and Luthra, J.M.J. Lumin., 11 (1976) 35.

(45) Aramu, F., Maxia, V. and Ruscci, A., J. Lumin., 10 (1975) 277.

(46) Kivits, P. and Kagebeuk, H. J. L., J. Lumin., 15 (1977) 1.

(47) Luthra, J.M., Defect and Diffusion Forum, 62/63 (1989) 183.

(48) Chistodoulides, C., Phys. Stat. Soli., (a) 118 (1990) 205.

(49) Arizon, J., Guillerrez, A and Martinez, C. G., Radiat. Effects, 84 (1985) 3.

(50) Nagpal, J. S., Int. J. Appl. Rad. Isotopes, 31 (1980) 333.

- (51) Christodoulides, C. , J. Phys. D: Appl. Phys. , 18 (1985) 1501.
- (52) Grossweiner, D. I. ,J. Appl. Phys. , 24 (1953) 1306.
- (53) Lushchik, C. B. , Sov. Phys. JETP, 3 (1956). 390.
- (54) Keating, P. N. , Proc. Phys. Soc. , 78 (1961) 1408.
- (55) Booth, A. H. , Can. J. Chem. 32 (1954) 214.
- (56) Braunlich, P. and Scharmann, A. , Z. Phys. , 177 (1964) 320.
- (57) Pradham, A. S. and bhatt, R. C. , Nucl. Instr. Meth. , 166 (1979) 497.
- (58) Trousil, J. and Kokta, L. , Rad. Prot. Dosim. , 2 (1982) 169.
- (59) Bahbout, S. and Furetta, C. Rad. Prot. Dosim. , 3 (1983) 43.
- (60) Piesch, E. , Ref. 12, P. 197.
- (61) Proc. National Symp. On Thermoluminescence and its Applications, Kalpakkam, Madras, India, (1975).
- (62) Aitken, M. J. and Fleming, S. J. , In: Topics in Radiation Dosimetry ( Ed. A. F. Attix), New York: Academic Press (1979).
- (63) Wintle, A. G. and Huntley, D. J. , Quaternary Sci. Rev. , 1 (1982) 31.
- (64) Mejdahl, V. and Aitken ( Eds.), Proc. Second Specialist Seminar on TL Dating, Oxford, PACT, 6 (1980).



- (65) Mijdah, V. Bowman, S. G. E. , Wintle, A. G. and Aitken, M. J. (Eds. ), Proc. Third Specialist Seminar on TL Dating and Electron Spin Resonance, Helsingor, PACT, 6 (1982).
- (66) Fleming, S. J. , Thermoluminescence Techniques in Archeology, Oxford: Clarendon Press (1979).
- (67) Aitken, M. J. , Thermoluminescence Dating, Academic Press (1984).
- (68) Darlymple, G. B. and Doell, R. R. , Science, 167 (1970) 713.
- (69) Edgington J. A. and Blair, I. M. , Science, 167 (1970) 715.
- (70) Sears D. W. , Grossman, J. N. , Melcher, C. L. Ross, L. M. and Mills, A. A. , Nature, 287 (1980) 791.
- (71) Sears, D. M. , Nucl. Tracks Radiat. Meas. , Int. J. Radiat. Appl Instrum. , Part D, 14 (1988) 5.
- (72) Moorhead, F. F. and Daniels, F. , J. Phys. Chem. 57 (1952) 546.
- (73) Rutherford, E. , Radioactive Substances and Their Radiations, Cambridge University Press (1913).
- (74) Curie, M., Radioactive Substances ( English translation of doctoral thesis ), Faculty of Science, Paris: Greenwood Press, Westpoint (1961).
- (75) Lind, S. C. and Bardwell, D. C. , J. Franklin Inst. , 196 (1923) 357.

- (76) Wick, F. G., and Gleason, J. M. , J. Opt. Soc. Am. , 9 (1924) 639.
- (77) Wick, F. G. Phys. Rev. , 24 (1924) 272.
- (78) Wick, F. G. and Slattery, M. K. , J. Opt. Soc. Am. , 14 (1927) 125; 16 (1928) 398.
- (79) Lyman, T., Phys. Rev. 48 (1935) 149.
- (80) Weidmann, E. and Schmidt, G. C. , Ann. Phys. Chem. , Neue Folge, 54 (1895) 604.
- (81) Watanabe, S. , Phys. Rev. , 83 (1951) 785.
- (82) Trowbridge, J. and Burbank, J. E. , Am. J. Sci. Ser. 4, 5 (1898) 55.
- (83) Schayes, R. , Brooke, C. , Kozlowitz, I. And L' Hereux, M. , In: Proc. 1<sup>st</sup> Int. Conf. On Luminescence Dosimetry, Stanford: Springfield, (1965) P. 138.
- (84) Daniels, F. and Saunders, D. F. , Science, 111. (1950) 461.
- (85) Cameron, J. R. and Kenney, G. N. , Radiat. Res. , 19 (1963) 199.
- (86) Rieke, J. F. and Daniels, F. , J. Phys. Chem. , 61 (1957) 629.
- (87) Daniels, F. and Rieman, W. P. , University of Wisconsin, Final Report No. 7 (1954).
- (88) Moore, L. E. , J. Phys. Chem. , 61 (1957) 636.
- (89) Ginther, R. J. and Kirk, R. D. , J. Electrochem. Soc. , 104 (1957) 365.

- (90) Karaysnaya, A. R. , Nosenko, G. M. , Revzin, L. S. and Yasolko, V. , At. Energ. , 10 (1961) 630.
- (91) Schulaman, J. H., Kirk, R. D. and West, E. J. , In: Proc. 1 st Int. Conf. On Luminescence Dosimetry, Standford, (1965) P. 113.
- (92) Binder, W. , Disterhoft, S. and Cameron, J. R. , In: Proc. 2 nd Int. conf. On Luminescence Dosimetry, Gatlinberg. (1968) P. 53.
- (93) Yamashita, T., Nada, N., Onishi, H. and Kitamur, S. In: Proc. 2 nd Int. Conf. On Luminescence Dosimetry, Gatlinberg, (1968) P. 4.
- (94) Kozlowitz, I. And L'Hereux, M. , In: Proc. 1 st Int. Conf. on Luminescence Dosimetry, Stanford, (1965) P. 138.
- (95) Janas, R. and Hubner, K. , Isotopenpraxis, 12 ( 1976) 342.
- (96) Mehta, S. K. and Sengubta, S. , Health Phys. , 31 (1976) 176.
- (97) Lucas, A. C. and Kapsar, B. , In: Proc. 5 th Int. conf. on Luminescsnce Dosimetry, Sao Paulo, (1977) P. 131.
- (98) Takenaga, M. , Yamamoto, O. and Yamashita, T., Nucl. Instrum. Methods, 175 (1980) 77.
- (99) Prokic, M. , Nucl. Instrum. Methods, 175 (1980) 83.
- (100) Prokic, M. Radiat. Prot. Dosim. , 47 (1993) 191.
- (101) Nakajima, T. , Murayama, Y., Matsuzawa, T. and Koyano, A. , Nucl. Instrum. Methods, 157 (1978) 155.

- (102) Wang, S. , Chen, G., Wu, F., Li, Y. , Zha, Z. and Zhu, J. Radiat. Prot. Dosim. , 14 (1986) 223.
- (103) Akselrod, M. , Kortrov, V. S., Kravetsky, D. J. and Gotlib, V. L. , Rad. Prot. Dosim. , 32 ( 1990) 15.
- (104) Ginther, R. J. , J. Electrochem. Soc. , 101 (1954) 248.
- (105) Alcala, R., Alonso, R. J. Lalinde, G. and Carretero, A. , Phys. Stat. Solidi (b) 98 (1980) 315.
- (106) Rhodes, J. F. , Abbundi, R. J., Cooke, D. W. , Mathur, V. K. and Brown, M. D. , Phys. Rev. , 31 (1985) 5393.
- (107) Schulman, J. H. , Ginther, R. J. , Gorbics, S. G. , Nash, A. E. , West, E. J. and Attix, F. H. , Int. J. Appl. Rad. Isotopes, 20 (1969) 523.
- (108) EG & G Commercial papers. Thermoluminescent Dosimeter System, Bedford, MA (1964).
- (109) Parker, C. V. , Blake, K. R. and Nelson, J. B. , Proc. 2<sup>nd</sup> International Conference on Dosimetry, Gatlinburg, TN (1968) P. 438.
- (110) Gessel, T. F. and de Planque, G. , Nucl. Instr. Meth. , 175 (1980) 196.
- (111) Henniger, J. , Horlbeck, B. , Hubner, K. and Prokert, K. , Nucl. Instr. Meth. , 204 (1982) 209.

- (112) Schulman, J. H. , Ginther, R. J. , Kirk, R. D. and Garand, H. S. ,  
Nucleonics, 18 (1960) 92.
- (113) Hart, E. J. and Fricke, M. , Chemical Dosimetry, In: Radiation  
Dosimetry (Eds. Attix, I. H. and Roesch, W. C.), Chapter 4,  
Academic Press (1967).
- (114) Annual Book of ASTM Standards, Part 35, (1972).
- (115) Massey, J. R. , Manual of Dosimetry in Radiotherapy,  
Technical Reports Series No. 110, IAEA, Vienna, (1970).
- (116) Jones, D. E. and Raine, H. C. , Brit. J. Radiol. , 8 (1949) 549.
- (117) Walinder, G. , Acta Phys. Radiol. , 48 (1957) 68.
- (118) Jones, E. , Mallard, J. R. and Elmanharawy, M. S. , Phys. Med.  
Biol. , 8 (1963) 59.
- (119) Itoh, N. , In: Defects in Insulating Crystals ( Eds. Tuchkevich,  
V. M. and Shavarts, K. K. ), Springer - Verlag, Berlin (1981), p.  
343.
- (120) Itoh, N. , Radiat. Effects, 64 (1982) 161.
- (121) Itoh, N. , Adv. Phys. , 31 (1982) 491.
- (122) Hayes, W. and Stoneham, A. M. , In: Crystals with the Fluorite  
structure (Ed. Hayes, W. ) , Clarendon Press, Oxford (1974) p  
185.
- (123) Henderson, B. , Radiat. Effects, 64 (1982) 35.
- (124) Crawford, J. H. , J. Nucl. Mater. , 108/109 (1982) 644.

- (125) Fowler, W. B. , Semicond. Insul. , 5 (1989) 583.
- (126) Devine, R. A. B. , Phys. Rev. Letts. , 62 (1989) 340.
- (127) Hornyak, W. F. , Levy, P. W. and Kierstead, J. A. , Nucl. Tracks, 10 (1985) 557.
- (128) Lucas, A. C. and Kapsar, B. M. , Health Phys. , 27 (1968) 397.
- (129) McMasters, D. W. , Jassemnejad, B. and McKeever, S. W. S. , J. Phys. D: Appl. Phys. , 20 (1987) 1182.
- (130) McKeever, S. W. S. , Radiat. Prot. Dosim. , 33 (1990) 19.
- (131) De Planque, E. G. , US Department of Energy Report EML - 418 (1984).
- (132) Schulman , J. H. , In: Solid State and Chemical Radiation Dosimetry in Medicine and Biology, ST1/PuB/138 ( IAEA, Vienna ), (1967) p. 3.
- (133) Alonso, P. J. and Alcala, R. , J. Lumin. , 21 (1980) 147.
- (134) Sunta, C. M. , Rad. Prot. Dosim. , 8 (1984) 25.
- (135) Jassemnejad, B. , Abbundi, R. J. , Brown, M. D. and McKeever, S. W. S. , Phys. Stat. Solidi, a 108 (1988) 753.

- (136) McKeever, S. W. S. , Jassemnejad, B. , Brown, M. D. , Mathur, V. K. , Abbundi, R. J. and Chan, H. , Radiat. Effects, 99 (1986) 15.
- (137) McKeever, S. W. S. , Jassemnejad, B. , Landreth, J. F. and Brown, M. D. , J. Appl. Phys. , 60 (1986) 1124.
- (138) Mathur, V. K. , Abbundi, R. J. , Brown, M. D. and McKeever, S. W. S. , Rad. Effects, 99 (1986) 10.
- (139) Townsend, P. W. , Nucl. Instrum. Meth. Res. , 197 (1982) 9.
- (140) Lewandowski, A. C. , Ph. D. Thesis, Oklahoma State University (1993).
- (141) Lucas, A. C. and Kapsar, B. M. , Health Phys. , 27 (1974) 600.
- (142) Puite, K. J. , Int. J. Appl. Radiat. Isotopes, 19 (1968) 397.
- (143) Allen, P. and McKeever, S. W. S. , Radiat. Prot. Dosim. , 33 (1990) 19.
- (144) Dekker, H. , Health Phys. , 30 (1976) 339.
- (145) Gorbics, S. G. , Attix, F. H. and Pfaff, J. A., Int. J. Appl. Radiat. Isotopes, 18 (1968) 625.
- (146) Maiello, M. L. , Rosenthal, F. and Harely, N. H. , Health Phys. , 50 (1986) 287.

- (147) Jayachandran, C. A. , Phys. Med. Biol. , 15 (1970) 325.
- (148) Worley, R. D. , Health Phys. , 43 (1982) 422.
- (149) Johns, H. E. and Cunningham, J. R. , The Physics of Radiology, Charles Thoms (1984).
- (150) Meredith, W. J. and Massey, J. B. , Fundamental Physics of Radiology, John Wright (1977).
- (151) Khan, F. M. , The Physics of Radiation Therapy, Williams and Wilkins (1994).
- (152) Radiological Health Handbook, US Department of Health, Education and Welfare, US Government Printing Office, Washington D. C. (1970).